Dosimetric Investigation of Electron Arc Therapy Delivered Using Siemens Electron Arc Applicator with a Trapezoidal Aperture

A thesis

submitted in partial fulfilment

of the requirements for the Degree

of

Master in Medical Physics

in the

University of Canterbury

by

Aitang Xing

University of Canterbury

2007

Abstract

This study investigated the delivery of electron arc treatment with a trapezoidal aperture. The aim of the investigation is to reduce the nonuniformity of the dose distribution, which is caused by the variation of the patient contour from superior to inferior. The characteristics of static electron beam were first investigated. Then a measurement-based algorithm was developed and implemented as a computer program called EarcMU to calculate the monitor units required for delivering the prescribed dose with a trapezoidal aperture. The central axis percentage depth dose was found to be independent of source-to-surface distance (SSD) and the width of the aperture. The inplane profiles of a trapezoidal aperture show that the dose decreases longitudinally from the wide to the narrow end of the trapezoidal aperture. The EarcMU program was verified using two cylindrical water phantoms. The measured dose and the dose calculated by the program agreed within 2.1% in the typical clinical conditions. A simple method was also proposed for determining the trapezoidal aperture for an individual patient. Under the same conditions, the trapezoidal apertures calculated by this method along with the open aperture were used to deliver treatments to several conical phantoms. Significant improvement in the uniformity of dose distribution was observed. On average, the flatness index of the longitudinal dose distribution from superior to inferior decreases dramatically from 8% for open aperture down to 0.58% for trapezoidal aperture. The results are clinically significant, indicating that delivering the electron arc treatment using a trapezoidal aperture can bring more uniform dose to the patient regardless of the change of patient contour from superior to inferior.

Acknowledgements

I would like to thank all who encouraged me in many different ways during the course of doing my project and my clinical training. Very special thanks go to my supervisor Prof. Lou Reinisch. As a dean of the college of science in the University of Canterbury and the director of the medical physics research group, he always has time and is patient and ready to answer my questions through his visits to the hospital and e-mail. I am grateful to him for helping me go through the hard time and resolve the problems encountered during my graduate study.

I am greatly indebted to Keith Croft, the chief physicist of physics department. I really appreciate that he gave me a chance to enter the wonderful world of the clinical medical physics I have been enjoying so much. He has always advocated a commonsense but intelligent approach to any physics problem. He was always approachable, despite his best attempts to appear otherwise, and he always had the best interest of the physics registrar in mind. Without his guidance, brilliant ideas and numerous discussions, this thesis would not be possible.

I would also like to thank John Sutcliffe for his proof reading and support for my clinical training. As an editorial advisor of the Journal "Physics in Medicine and Biology", he has a tremendous(uncanny even) talent for proof reading. His correction of the shaky parts and rewording of the less intelligible parts of my thesis is most appreciated. He has been more than willing to help any problems I encountered.

I can not thank Dilli Banjade enough for his assistance throughout the year. He is always sharing his practical and valuable knowledge on the medical physics and how to do research. His help was crucial to finish research and my thesis work.

I would like to express my great appreciation to Tania Groudeva for her help and support for my clinical training and research. I always thank her from the bottom of my heart for training me on the job always with the sweetest smile in

the world.

I would like to deeply thank Tim O'brien for his numerous support and help for my clinical training and doing my project. His door has always been open to me and he is always willing to answer my questions.

I would like to thank my labmates Riaan Mounton and Iordan Kostourkov. They always discuss the serious topics of medical physics in a humorous way with me. They have been bringing me not only the clinical experience and knowledge but also the great enjoyment.

I would also like to thank Richard for his help for my project. He made all the phantoms I used for the research. Without his support, I could not imagine I would be able to finish my project and my thesis.

There are many other staffs in the department who deserve recognition for their help and support: the managers Joanne Anson and Dianne Feck, Dr. Nick Nedev, Aaron Phillips, Lisa Te Paiho, Joan Arcs and all other radiation therapists.

Finally, I would like to thank my parents who respected, encouraged and supported their son. I thank all my family, especially my wife, Wang Dongqing, who sacrificed so much for taking care of our daughter and my parents. I would like to dedicate this thesis to my lovely daughter, Xing Yue. Her smile always gives me the hope for the future and helps me go through the hard time.

Aitang Xing

August, 2007

Contents

List of Figures

List of Tables

Chapter 1

Introduction

1.1 Literature review

1.1.1 Electron arc therapy

Radiotherapy uses ionizing radiation to kill cancer cells by delivering uniform dose to the target volume while minimizing the dose to the healthy tissues around the tumor. The commonly used ionizing radiations are photon and electron beams[96].

Electron beam has been an important modality for over 50 years for treating the tumor underlying skin by a few centimeters while sparing the deeper tissues and structures[30]. For most patients treated with electron beam therapy, a single or multiple static electron beams are often used. This is typically used for the tumor volume with a limited surface. If the area of the superficial tumor is very large and curved, electron dose can be delivered by continually moving electron beam over a certain range of arc angle to cover the target volume. This technique is called electron arc therapy[48].

Electron arc therapy was first described by Becker and Weitzel in 1956[10]. At that time, the technique was also known as telecentric shell irradiation or telecentric pendulum therapy[11]. In 1970s, Rassow, at the Essen Radiotherapy Clinic in Germany, had tried this treatment technique in some clinical applications such as treating the carcinoma of the bladder, gynecologic tumors, kidney tumors and post-mastectomy chest wall treatments[82]. Since then, more than 40 years have passed. However, electron arc therapy did not gain wide acceptance. It is largely due to the fact that electron arc therapy is much more complicated

than conventional static electron beam therapy in terms of treatment delivery and planning techniques[102].

1.1.2 Delivery of electron arc therapy

Treatment machine

In early days, most high energy machines did not provide the capability for electron arc beam therapy. The machines were often modified by users for delivering electron arc therapy. Even for modern linear accelerators, they usually only provide standard photon arc mode. In order to deliver electron arc therapy to patients, Lam et al.[52] and Leavitt et al.[59] modified a Varian machine to permit the arc with electron mode and allowed the machine to recognize a special mechanical accessory electron mount. In the middle of 1970s, some of the facilities with high energy accelerators, in particular those with Brown Boveri betatrons, investigated the potential use of electron arc therapy[37, 86]. Khan and his colleagues also reported on the use of electron arc therapy with a Toshiba linear accelerator[47].

Many of the newly available linear accelerators have electron arc capability. In recent years, there has been a growing interest for the use of this modality[8, 17, 21, 56, 81]. Through a review of recent literature, it was found that the electron arc therapy is being used as a routine clinical modality at a few centers: Hospital Mainsonneuve-Rosemount [22] and Toronto-Sunnybrook Regional cancer center[106] in Canada, University of Utah in USA[28] and one regional cancer center in Germany[29].

Delivery techniques

The basic techniques and principles involved in electron arc therapy are discussed in detail by Paliwal[74]. The implementation and delivery of an electron arc depend on the specific linear accelerators used and may differ from center to center. However, in terms of how electron beams are distributed over a range of arc angle, the delivery techniques can be classified as true electron arc[8, 22, 87]

and pseudo-electron arc[14, 78].

During the treatment using true electron arc therapy, the electron beam starts from the beginning of arc and continually travels through to the end of arc without stopping. This technique requires the linear accelerators to have the capability of delivering arc therapy in electron mode, which is either implemented by manufacturers or customers[22, 52, 59].

Pseudo-arc technique uses a series of static electron fields to achieve the homogenous arc dose distribution. As illustrated in Fig. 1.1, these static fields are usually narrow rectangular fields positioned over the arc with an inter-field angle, which is defined by the central-axis of each field. Because the technique uses a single standard electron field as a building block, it is much simpler than the true arc technique and is suitable for the linear accelerators with or without electron arc mode. Pseudo arc was first discussed by Boyer in 1974[14, 15]. Recently, Pla and his colleagues did a series of investigations on this technique [78, 79, 80].

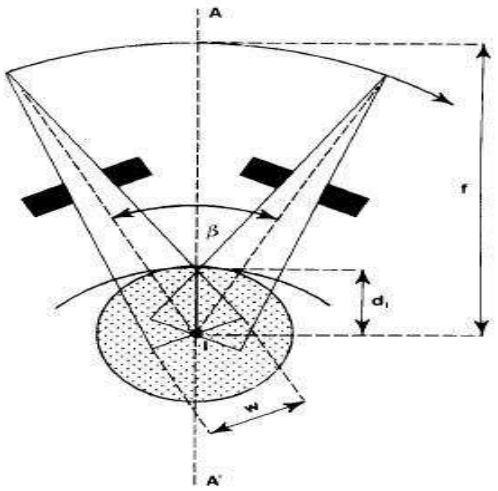

Figure 1.1: Definition of β angle. f is the distance between the virtual source and isocenter. w is the nominal field width at isocenter and d_i the depth of isocenter(from [77]).

Collimation of electron arc beam

For fixed field electron beam therapy, the distance between the patient surface and the end of applicator is very short. Electron arc therapy requires considerable clearance between the patient and the collimator of the treatment unit. A special collimation system is usually employed.

This system consists of three-level collimation. The first level is provided by the x-ray field defining jaws. Leavitt et al.[59] found that the electron dose profile and dose rate depend strongly on the position of these jaws. They are held in a fixed position.

The second level of collimation is located between the x-ray jaws and the isocenter at a distance, which usually provides 20 to 26 cm of clearance to the isocenter. The function of this second level collimation is to define the scanning slot width and to shape the longitudinal dimension of the slot, since for many applications the sides of collimator are not parallel[66]. The second collimator is either custom made or provided by the manufacturers of linear accelerators. Lam et al.[52] made a 4 cm thick aluminum collimator with an opening of 2.5 cm wide by 20 cm long, which could slide into the accessory tray holder of Varian Clinac 20. A dedicated electron arc applicator provided with Elekta SL25 was used by Duchesne et al.[22] for their electron arc investigation. The large air gap between applicator and patient leads to the unsharp boundaries due to in-air and edge scattering unless a third level of collimation is employed.

The third level of collimation is located on the surface or in close proximity to the surface of patient. Fig. 1.2 shows an example of this level collimation. Its purpose is threefold. First, it clearly defines the edge of the target treatment area. Second, it protects out-of-field tissues from the scattered electron dose. Third, it provides a starting and stopping area. This tertiary collimator is customized for each patient. Its fabrication is time consuming and complicated[102]. The techniques for making tertiary collimation were described in details by Keith[42], Leavitt et al.[54] and Thomadsen[100], respectively.

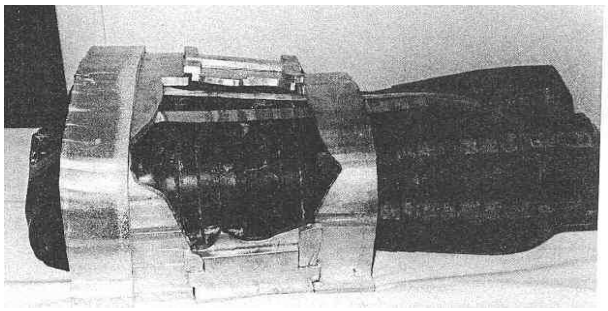

Figure 1.2: An example of custom-made tertiary collimation system (from[100]).

1.1.3 Treatment planning techniques for electron arc therapy

Once electron arc therapy is considered by the oncologists to be an optimal method for treating a patient[63, 76, 106], treatment planning starts. Compared with the treatment planning for static electron beam[35], the planning for electron arc therapy has some specific requirements related to this modality[14, 44, 53, 75, 102]. The procedure for electron arc planning usually includes the computerized tomography(CT) simulation, the choice of proper algorithms, calculation of isodose distribution and finding a reproducible treatment position.

CT simulation for electron arc patient

For electron arc patients, the CT images of transverse sections are first acquired with a CT simulator. They are used not only for defining the tumor volume and finding a reproducible setup position for treatment[34], but also for determining the chest wall thickness, lung density and the change in patient outline in transverse and sagittal sections. These data provide the critical information for choosing beam energy and the location of isocenter in patient.

The choice of beam energy for electron arc therapy needs first to consider the variation of chest wall thickness. A multiple-segment arc may be planned, each segment using different beam energy [12, 59]. Another consideration is to minimize the dose in lung when choosing the beam energy. Photon contamination is a well-known problem for electron arc therapy[15, 80].

The location of the isocenter within patient is determined by considering how to deliver a more uniform dose to the large treated area[38]. Previous research

showed that the change of dose rate with effective source-surface distance(SSD) follows the inverse square law[47, 59]. The patient contours always vary within and between transverse sections, causing a variation of SDD during the beam rotation. As a result, the dose distribution is not uniform across the treated area. Therefore, the location should be chosen at a depth approximately equi-distance from the surface for all beam angles[52]. In addition, the depth of isocenter must be greater than the maximum range of the electrons so that the electron dose at the isocenter does not become significant.

Algorithms for electron arc therapy

For electron beam therapy using a single or multiple static fields, the electron dose in the treated volume can be accurately calculated using the electron pencil beam algorithm[33, 64]. It was a state-of-art algorithm for electron dose calculation and implemented into most commercial treatment planing systems like CMS Xio[88]. However, there is no such a gold standard algorithm for electron arc therapy. Different centers developed their own algorithms[17, 18, 32, 52, 59]. These algorithms fall into two categories: the measurement-based algorithms and the physics model-based algorithms.

The pencil beam algorithm developed in 1981[33] does not model either the skin collimation or the air-scattering in the large air gap between the final collimator and patient. Skin collimation and a big air gap are typical scenarios for electron arc treatment and not used in treatment with static electron beams[16]. To tackle these problems, Hogstrom developed an algorithm based on the electron pencil beam algorithm for electron arc therapy[16, 17, 32]. Basically, the electron arc dose distribution in patients is calculated by modeling the arced beam as a single broad beam defined on the irradiated patient surface. The broad beam is modeled as a collection of strip beams, each strip beam being a linear array of pencil beams.

Because these algorithms are based on the physics model of electron pencil beam, there are several unique advantages compared with the measurement-based algorithms. Firstly, commissioning the algorithm requires a small amount of

measurements. The fundamental dosimetry data required for a particular beam energy are the central-axis depth dose, the major-axes beam profile at the depth of maximum dose and major-axes beam profiles just beyond the practical range for a single field setup. Secondly, the algorithm is able to calculate the electron arc dose distribution in the treated volume for an arbitrary location of the isocenter, limits of arc rotation, secondary collimation shape, skin collimation and patient geometry. The results from measurements showed agreement with the calculated arc dose to within 2 mm in the high dose region and 3% in low dose region[16, 17]. Thirdly, it can accurately predict the depth of dose maximum, d_{max}, and the dose at d_{max} on the central axis of the mid-arc plane, which is required to calculate the monitor units for delivering the desired electron arc dose to the patient. It is able to calculate the mid-arc depth dose($< 3\%$) in the buildup region and dose output($\leq 4\%$)[9, 51]. Overall, the electron arc pencil beam algorithm is adequate for clinically planning electron arc therapy. The only drawback is that it has not been implemented into most commercial treatment planning systems (TPS), making it unavailable to other centers. Therefore, the measurement-based algorithm is used by most of centers.

The common feature of the measurement-based algorithms is to measure a series of central-axis depth dose curves and profiles for a static electron beam. The dose rate per unit angle of arc is also required for different SSD. These dosimetric data act as the algorithm commissioning data and are usually measured beneath a flat water surface under a range of typical treatment conditions. Then these data are stored on computational grid in the form of tables[68]. The distribution of electron arc dose in patients can be calculated through directly interpolating or extrapolating from the stored tables. In most situations, a simple mathematical model is established based on either the fitting of experimental data or the observation from a large number of measurements. In the latter case, the mathematical formula uses the measured data to calculate dose at any point in the treated volume. For convenience, this mathematical procedure is often implemented as a computer program.

A typical example for the former case is the method used by Lam et al.[52]

for electron arc treatment planning. Only two central-axis depth dose curves at two typical SSDs and one off-axis profile at one SSD were measured. These data were manipulated to get the dose distribution with the method developed by Milan and Bently[68]. This is probably the simplest method for electron arc planning.

By contrast, the empirical-formula based methods are more complicated. Leavitt et al.[59] derived several mathematical expressions for central axis depth dose and off-axis profiles. Based on these formulas, a treatment planning program was implemented for aiding in the visualization and optimization of a dose distribution.

Another well-known empirical model is called the angle β concept which is used for the pseudo-arc technique[77]. As shown in Fig. 1.1, the angle β is the angle between two adjacent static arc fields. This angle is uniquely defined by the nominal field width at isocenter, the depth of the isocenter and the effective source-axis distance (SAD). The latter is defined by the distance between the isocenter and the position of electron virtual source. It was found experimentally that, for a constant effective SAD, the electrons beam with the same β exhibit a similar percentage depth dose for different combination of field width and depth of isocenter. This characteristic of static electron beam is used for electron arc treatment planning through determination of radial depth doses for a series of surface points in the treatment volume[49, 78, 80].

These measurement-based methods may appear different, but they have the same disadvantages. A significant amount of measured data needs to be acquired, which is time-consuming and impractical in most radiation therapy clinics. An additional shortcoming of the data-driven algorithms is their inability to accurately correct for the patient contour and tissue inhomogeneities[53]. These algorithms lack the ability of the pencil-beam or more sophisticated transport algorithms to model the three-dimensional (3D) transport of the electrons in patients[32]. Nevertheless, as long as the desired configuration can be interpolated or extrapolated from the tabulated data, the measurement-based algorithm can provide accurate dose results[52, 59].

Calculation of isodose distribution

There are three options which can be used for calculating the isodose distribution for electron arc therapy. The first option is to directly use the electron arc pencil beam algorithm[51]. Unfortunately, it is not accessible to commercial TPS users[16]. The measurement-based methods developed by different centers can also be employed for the isodose calculations[52, 77].

As a third option, the dose distribution from an arced electron beam can be calculated by summing the dose distribution from a series of fixed electron beams. These beams are placed over the arc at very small angular increment. For each of them, the electron dose distribution can be accurately determined using either an electron pencil beam algorithm[33], an electron pencil beam redefinition algorithm[13, 92] or a Monte Carlo (MC) algorithm[18, 55]. The summation approach is essentially an application of the pseudo-arc technique in treatment planning.

The summation option is reasonably straightforward. Most centers can use this method to do treatment planning for electron arc therapy, provided that the TPS they are using has Hogstrom's pencil beam algorithm installed for electron dose calculation. In addition, the option also allows for the modeling of a more sophisticated delivery of arc therapy, such as the dynamic shaping of the secondary collimator during the arc rotation[57, 58]

1.2 Electron arc therapy in Palmerston North Hospital

1.2.1 Rationale

Breast cancer is the most common cancer in women and second leading cause of cancer deaths in women in New Zealand. The risk of women in New Zealand developing cancer is very high, approximately one in ten[26]. Following potentially curative mastectomy, failure to control breast cancer on the chest wall or in regional nodes is the major cause of morbidity. There are three common chest wall irradiation techniques used in post-mastectomy radiation therapy: tangential photon beam, appositional electron beam and electron arc[106].

The large areas of chest wall post-mastectomy could be treated with the use of multiple abutted electron cone fields. However, when one abuts electron fields, overdosing or underdosing is introduced at the field junctures[99]. For a curved surface like the chest wall, the gap between the cone and the patient's skin varies, leading to a variable SSD and oblique beam incidence[45, 72]. Therefore, small alignment errors hold the potential for exacerbating the degree of heterogeneity already present. Often, the internal mammary nodes must be treated either with photons or with higher energy electron beams, again resulting in field abutment inhomogeneities.

With the high energy photon tangential method, the dose tolerance of lung imposes a practical limit to field extent over the chest wall posteriorly and contralateral to the anterior midline. If the internal mammary nodes are included in the tangential fields, an excessive volume of lung or heart may lie within the high-dose region. Usually, a separate internal mammary node field is added to reduce the lung irradiation at the expense of dose homogeneity of skin and subcutaneous tissue in the abutment region.

Except for these general limitations of fixed field techniques, there are several patient-specific factors that complicate these approaches. The location and extent of the tumor, length and placement of scars, and location of drain sites can create the need for an exceptionally large, irregularly-shaped target volume. The occasional patient with simultaneous bilateral primary cancers in need of postoperative radiation represents a special case of a large target volume. Large medially placed tumors with scant surgical margins may result in the match line of abutment coinciding with an internal mammary node field lying at the precise area of highest risk for recurrence. An angular chest wall shape in some women results in large volumes of lung lying in the high-dose region, particulary if other factors dictate an especially large surface target area.

By contrast, there are a number of advantages of electron arc technique over the fixed photon and electron technique. The electron arc technique has been employed when electron arc capability was available with a linear accelerator or a betatron[47, 86]. A feature that have been demonstrated is the excellent dose

uniformity along a curved superficial volume that can be achieved by an electron arc treatment. In addition, reduction of lung volume exposure to a damaging dose of radiation has potentially great clinical significance. Detailed lung dose-volume analysis has shown that electron arc therapy results in a statistically significant superior dose distribution as compared to tangential photon techniques[67].

Electron arc therapy has been used by the University of Utah Health Center for treating breast cancer after mastectomy since 1981. A series of patients were treated with advanced local-regional breast cancer and no known residual disease following mastectomy. Clinical results show that local control has been achieved in 96%[66]. Only 4% local failure rate in such a group of patients is comparable to other methods of adjuvant irradiation post-mastectomy[25, 27].

1.2.2 Clinical application

Because of these advantages of electron arc therapy over the other two modalities for treating the chest wall after mastectomy, the oncology department in Palmerston North Hospital clinically implemented this technique and treated patients in 2004.

Electron arc implementation

Electron arc is delivered with the Siemens Primus linear accelerator (linac). For the description of the linac and its electron arc collimation system in detail, see Section 2.2.1 in chapter 2.

The department uses the commercial treatment planning system, CMS Xio, as a planning tool for all treatment including intensity modulated radiation therapy (IMRT) and three-dimension conformal radiation therapy (3DCRT). CMS Xio has an electron pencil algorithm installed, but it dose not support electron arc. The electron arc is simulated by placing a series of static beams over the arc with inter-field angle less than 5 degree. A protocol was made to provide a guideline for radiation therapists (RT) on how to chose the isocenter depth and determine the start and end angles[41].

The commissioning of electron arc static beam is accomplished by treating

electron arc applicator as a normal electron cone and following the standard procedure provided by CMS Xio manual. The commissioning data, such as the percentage depth dose (PDD) and in-plane and cross-plane profiles, were measured at zero gantry and collimator angles. Thorough verification was done after commissioning. Details of electron arc commissioning and verification were described by Keith[40]. In general the commissioning procedure consists of matching the measured percentage depth dose and beam profiles by adjusting the beam model parameters. The commissioning results showed that the agreement between the measured and calculated PDDs and profiles are within 2% and 2 mm[40], which meets the criteria for commissioning a treatment planning system[23, 2].

Dose inhomogeneity from superior to inferior

In 2004, ten patients were treated using electron arc technique in Palmerston North Hospital. Each patient was carefully selected to ensure minimum variation of patient curvature in traverse and sagittal planes. The change of patient curvature causes the variation of SSD when the electron arc applicator sweeps through an arc, resulting in the dose inhomogeneities[44]. The ideal patient shape for electron arc is a cylinder positioned perpendicular to the arc cone. In this instance, the radius is the same through the arc travel. As a result, the dose distribution is uniformly distributed.

However, the reality is that the actual patient contour largely differs from an ideal cylinder although some patients may be close to it. Most patient's curvatures change, especially in the direction along the midline from superior to inferior. Therefore, thermoluminescent dosimeters (TLD) were used for monitoring the dose during treatment. Specifically, as shown in Fig. 1.3, nine sites were chosen within the treated area on the chest wall, representing one superior transverse section, the mid-arc transverse section and one inferior transverse section. Three TLD chips (LiF) were taped on each site. TLD dose verification was carried out on the first and second day of treatment. After applying a super-linearity correction, the results were recorded.

Table 1.1 shows the measured dose for ten patients treated at Palmerston

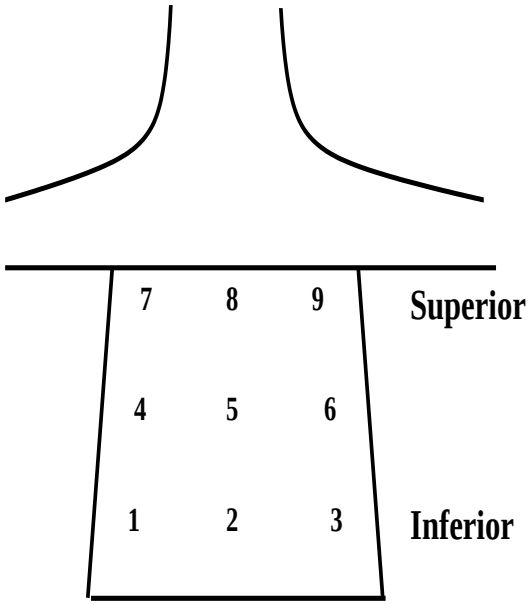

Figure 1.3: The sketch of the sites where TLDs were placed on patient skin for monitoring dose during electron arc treatment.

Hospital. For the confidentiality, the patient named was suppressed and replaced by letter P. The superior dose was the averaged value of the TLD dose from sites 7, 8 and 9 and the inferior dose from sites 1, 2 and 3. Although they are averaged point doses, the results indicate that for most of the treated patients the uniformity of dose distribution from superior to inferior was not good. The dose difference between superior and inferior, on average, was 10%. Only two patients were under 5%. The difference for others ranged from 5.7% to 18.5%.

Table 1.1: The difference between superior and inferior in-vivo dose measured during the electron arc treatment.

Patient name	P1	P2	P3	P4	P5	P6	P7	P8	P9	P10
Superior(cGy)	5.19	1.96	1.69	1.87	1.72	1.91	1.66	1.91	1.99	1.65
Inferior(cGy)	5.96	2.36	2.36	2.29	1.83	1.94	1.83	1.99	2.29	1.88
Difference(%)	12.9	16.9	13.6	18.4	5.7	1.52	9.04	4.14	13	11.97

Techniques developed for improving dose uniformity

The dose inhomogeneity caused by the variation of the curvature of patient has been a well-known issue for electron arc therapy since the early days of this technique[12]. It is a problem of delivery technique but not of the algorithm used for calculating electron arc dose. The dose distribution calculated even with a simple measurement-based method agrees very well with the dose delivered to a cylindrical pseudo-patient[52].

Various techniques have been developed to improve the uniformity of the dose distribution in a patient, especially along the direction from superior to inferior. The simple solution is to shape the apertures of the secondary electron arc collimator according to the variation of the radius of the patient contour. As the aperture is customized to conform to the curvature of an individual patient, the dose homogeneities can be improved greatly. Blackburn[12] and Leavitt et al.[59] implemented clinically shaped apertures, which improved the dose uniformity across the entire treatment surface. Blackburn implemented a trapezoidal shaped aperture, whereas Leavitt developed the customized cerrobend collimators. The shape of the aperture was determined specific to each patient based on the dose calculation using the patient contours in multiple sections superior and inferior to the central calculation plane.

However, in both cases, a single aperture was shaped as a compromise across the entire limits of the arc. A further improvement in dose uniformity was achieved by dividing the electron arc into several segments with a different customized collimator aperture used for each arc segment. This technique is usually called multiple arc segment technique. The aperture for each arc can be changed manually by entering into the treatment room or automatically. For example, Leavitt designed and constructed a computer-controlled multi-vane collimator for electron arc therapy[57]. The collimator consisted of 18 independently controlled vanes and was inserted into the standard accessory mount assembly of a linear accelerator, in the same fashion as standard field shaping blocks. The electron multileaf collimator (eMLC) appears to be another promising option in future for

delivering electron arc therapy and electron beam modulated therapy[31, 62].

1.3 Aim of thesis

Although the trapezoidal aperture was employed by other centers and proved to be an effective way to improve dose homogeneity in the sagittal plane, the beam characteristics and electron arc dose distribution are closely associated with a specific electron arc beam collimation system. For example, Blackburn[12] and Leavitt et al.[59] used an electron cutout with a trapezoidal aperture to collimate the electron beam for electron arc treatment. The electron cutouts were inserted into the block tray. However, our implementation of electron arc therapy employs a dedicated electron arc applicator designed and provided by Siemens.

The goal of this thesis is to dosimetrically investigate the delivery of electron arc treatment using the electron arc applicator with a trapezoidal aperture. This is a preclinical study, aiming to solve the problem of inhomogeneity of dose distribution from superior to inferior that was found in electron arc treatment.

Before clinically using a trapezoidal aperture aperture to treat patients, there are three questions that need to be answered. First, what are the characteristics of a static electron beam collimated by an electron arc applicator with its aperture shaped into a trapezoidal aperture? This is the basic information that the medical physicist should provide to help the oncologist make a decision on whether to treat a patient with a trapezoidal aperture or not. Second, once the oncologists decide to use this technique and prescribe the dose to a reference point, then next questions is: how does one calculate the number of monitor units required to deliver the prescribed dose with a trapezoidal aperture? Finally, the most important issue is how to customize the trapezoidal aperture for each patient based on the contour information of chest wall? The variation in chest wall contour from patient to patient causes the in-vivo results to show a variety of dose percentage differences for each individual patient. A specific trapezoidal aperture needs to be made for an individual patient.

These three questions are investigated in Chapter 2, Chapter 3 and Chapter

4, respectively. In Chapter 5, the main results of the thesis are summarized and suggestions for the future work are also briefly discussed.

Chapter 2

Physical characteristics of static electron beam

2.1 Introduction

The physical characteristics of a static electron beam are determined by the the specific implementation of electron arc therapy. An understanding of the physical characteristics of an accelerator as well as an understanding of common features of static electron beam is necessary for arc irradiation.

In this chapter, the features of a static electron beam, which are specific to our collimation system and linear accelerator, were investigated. The purpose of this study is twofold: first, to investigate the effect of various beam parameters on the central axis depth dose distribution, and second, to study the influence of trapezoidal and rectangular apertures on the inplane and crossplane profiles.

2.2 Materials and methods

2.2.1 Linear accelerator

Siemens Primus

The Siemens Primus linear accelerator is a dual energy standing wave accelerator that produces electron beams of 6, 9, 12, 15 and 18 MeV in addition to 6 and 15 MV x-rays[94]. The electron beams operate at the dose rate of 300 MU/min. Table 2.1 describes the characteristics of electron beams available on this unit. These data are taken from the data measured for monthly quality control(QC),

averaged over last three years.

Table 2.1: Siemens Primus electron beam parameters for 10 cm × 10 cm electron applicator at 100 cm SSD.

Nominal Energy E (MeV)	6	9	12	15	18
Mean surface energy $\bar{E}_0$ (MeV)	5.68	8.35	11.19	14.13	17.34
Practical range R (mm)	29.3	43.8	58.7	74.1	91.2
Beam quality R_{50} (mm)	23.8	35.9	48.6	61.3	76.7
Depth to 100 % dose d_{max}(mm)	13	20	26	26	20

The Siemens Primus has the intrinsic capability of delivering rotational therapy in electron arc mode. 6 MeV and 9 MeV electron beams were commissioned on this machine for delivering electron arc therapy. The electron beams are collimated by a dedicated electron arc applicator specially designed by Siemens. After commissioning, the machine can deliver arc therapy through the gantry angle range from -180 to 180 degree either in the clockwise or anti-clockwise direction. Fig. 2.1(A) shows a photo of the machine with electron arc applicator installed.

Collimation of electron beam

The collimation system specific to our implementation is illustrated in Fig. 2.1(B). Beam limitation is provided first by the upper photon collimators(y jaws) and lower photon multi-leaf collimator (MLC), and then by the electron arc applicator. Once the electron arc applicator is inserted into the gantry head, the y jaws and the MLC open automatically 30 cm and 10 cm wide, respectively. When electron beam passes through the arc applicator, it is collimated by two apertures as shown

in Fig. 2.2.

The upstream aperture is a rectangular aperture in a steel plate. The plate is a 35 cm-by-35 cm square. The thickness of plate is 0.5 cm. The leakages outside the body of the electron arc applicator and the electron field were verified to be less than 0.1% as specified by Siemens[93]. The upstream rectangular aperture is 14 cm long and 3.5 cm wide. The downstream aperture is also a rectangular but slightly larger than the upper aperture. Its dimension is 17.2 cm long and 4 cm wide. The lower aperture is also inside a steel plate with the thickness of 1 cm. The lower aperture is attached to the upper one by four spring loaded steel rods. If the nearest end is pushed up, it can move up a few centimeter to avoid physical contact with patients. The projected light field of the applicator at isocenter is 23.8 cm by 5.8 cm.

Compared with normal electron applicators, the electron arc applicator has the following special features: (1)It is relatively short. The source-axis distance(SAD) is 100 cm. The nominal distance from the target to the end of applicator is only 72.5 cm. The virtual source position is much lower than the focal spot. The distance from the virtual source to isocenter, denoted as f, is 58.8 cm for 6 MeV and 68.8 cm for 9 MeV. The virtual source positions were determined using the method described by Ostwald et al.[71] and Roback et al.[85]. (2)The distance between the two apertures is 18 cm. There is no steel wall between two apertures. In contrast, the normal electron arc applicator has a solid wall between upper and lower limiting aperture, which also plays an important role in collimating the electron beam. (3)The distance between the end of applicator and the patient skin surface is only a few centimeters. For instance, if the radius of patient chest wall is 16 cm, this distance is 9 cm.

Shaping the aperture of electron arc applicator

To change the field size and shape, a simple special device called an aperture shaper was designed and fabricated. As shown in Fig. 2.3(A), it is a narrow steel rectangular plate. Its width and length are 4.5 cm and 24 cm, respectively. There are three screws on the plate. The aperture shaper can slide into the downstream

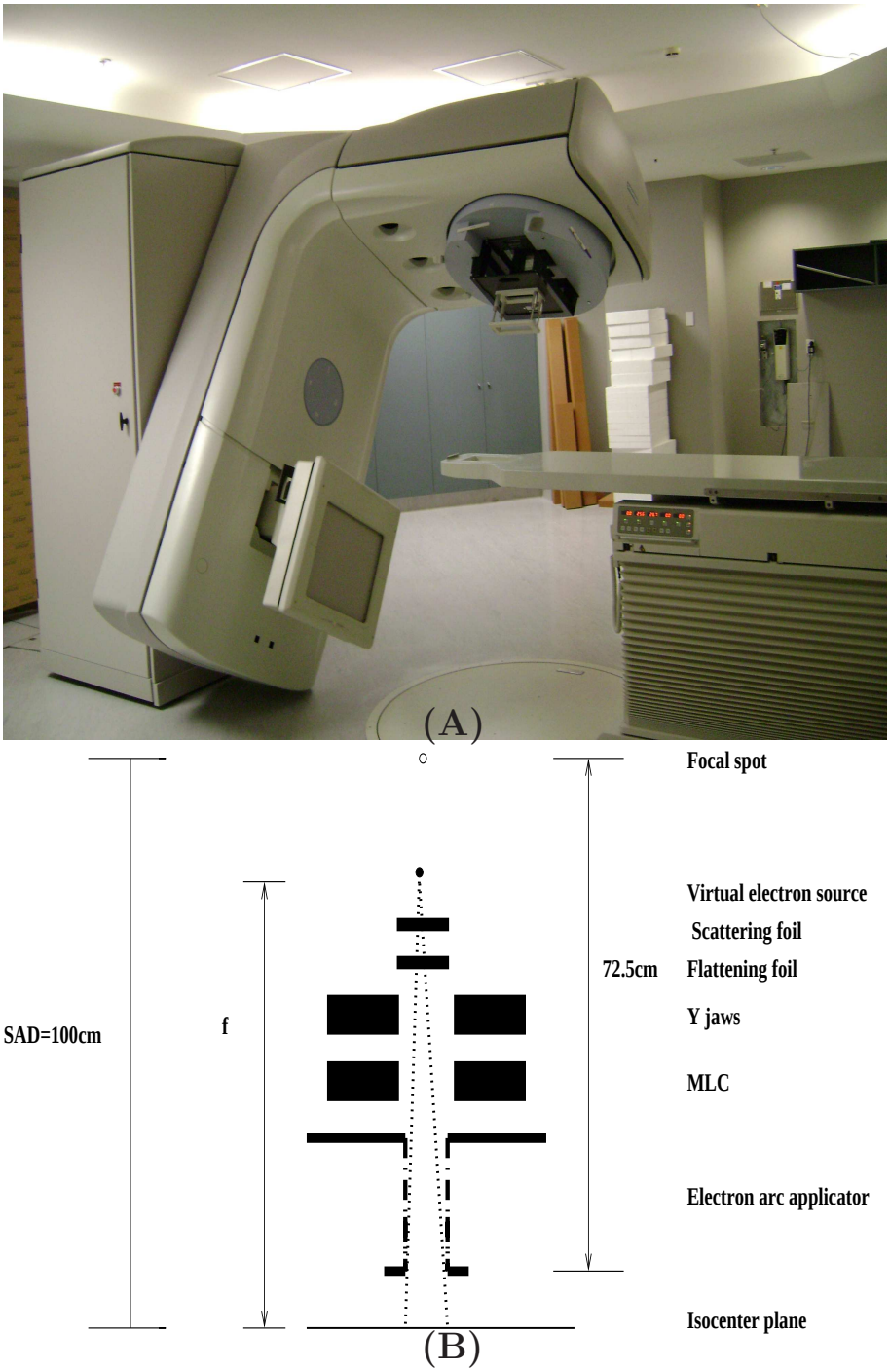

Figure 2.1: (A) Siemens Primus linear accelerator with an electron arc applicator inserted into the gantry head. (B) Schematic diagram of the collimation system for an electron arc beam.

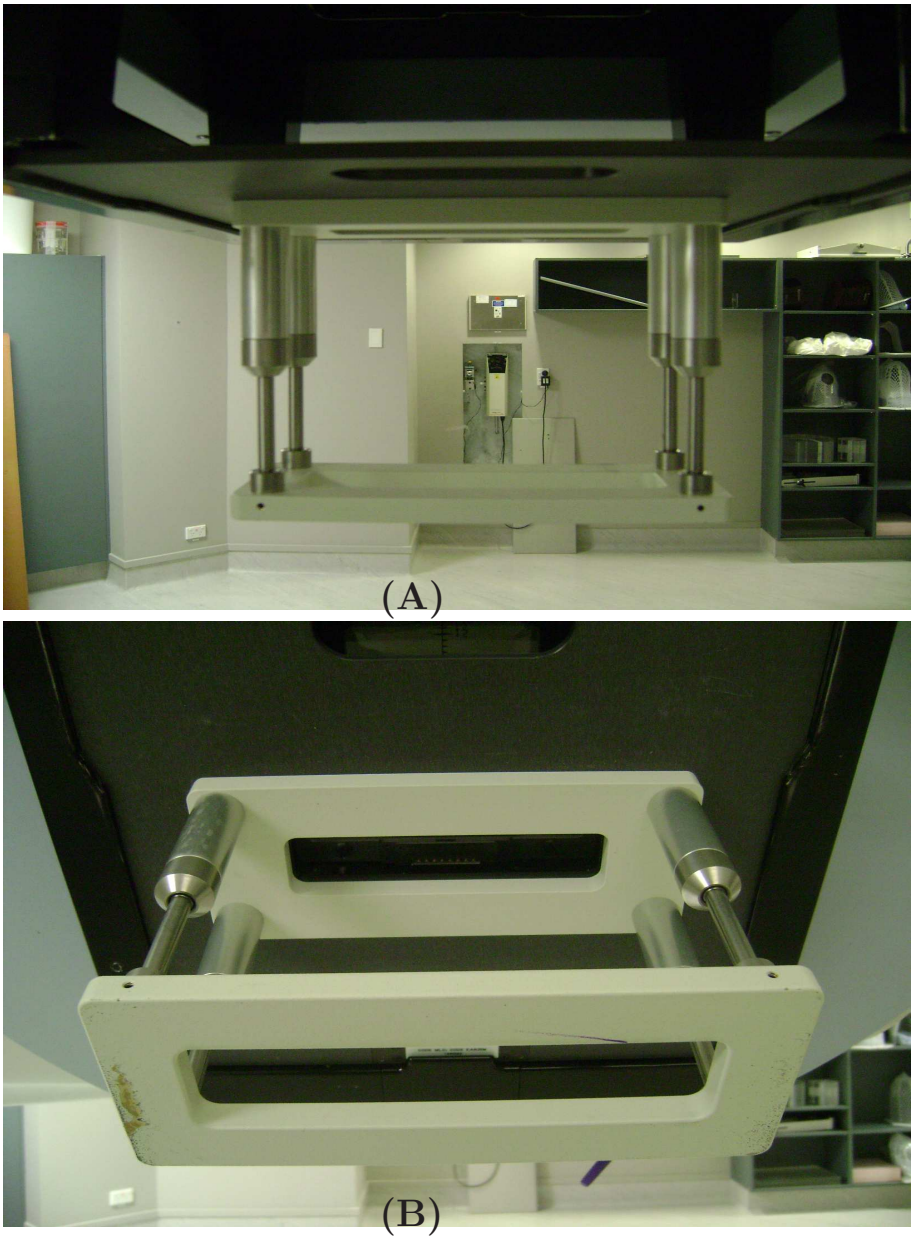

Figure 2.2: The structure of the electron arc applicator viewed from (A) the side and (B) the bottom.

aperture to block the part of aperture. Two screws are used to fix one end of the shaper plate to the steel plate of the downstream aperture and the third screw to determine the narrow end of the trapezoidal aperture.

As shown in Fig. 2.3, two types of shapes can be made using the aperture shaper: trapezoidal aperture and rectangular aperture. For the trapezoidal aperture and rectangular aperture used in the investigation, the length of aperture is fixed and always kept at 17.2 cm. For short, the trapezoidal aperture is simply denoted using the short and long end edges of trapezoid. Similarly, the rectangular aperture is denoted only using the width of aperture. For example, as shown in Fig. 2.3(B), the Ws cm-by-Wi cm trapezoidal aperture refers to a trapezoid with two edges of Ws cm and Wi cm and the height of 17.2 cm. A rectangular aperture with dimension Wc cm is a rectangle, whose width and length are Wc cm and 17.2 cm, respectively.

To keep consistent and clear, several terms regarding to the apertures are defined and used in the rest of thesis. The term "open field" or "open aperture" always refers to the unshaped downstream aperture, namely a rectangle of 17.2 cm long and 4 cm wide. The term "the aperture width at field center for a trapezoidal aperture " is defined as the physical width of the aperture at its center and is simply expressed as (Ws+Wi)/2 cm for the trapezoidal aperture shown in Fig. 2.3(B).

2.2.2 Phantoms and dosimeters

The aperture of the electron arc applicator can be shaped into an arbitrary trapezoid or rectangle. Our investigation did not cover all the shapes of apertures and it is also not necessary. The following eight apertures were chosen for the measurement:(1)rectangular apertures: open, 3.5 cm, 3 cm, 2.5 cm, 2 cm, and (2) trapezoidal apertures: 4 cm-by-3 cm, 4 cm-by-2 cm, 4 cm-by-1 cm. For each combination of beam energy and aperture, the percentage depth dose(PDD) and profiles are measured at 80 cm, 82 cm, 84 cm, 85 cm, 86 cm, 88 cm and 90 cm SSD. For each field size, the profiles along the field length(inplane) and the field width(crossplane) through the central axis of were measured at the depth

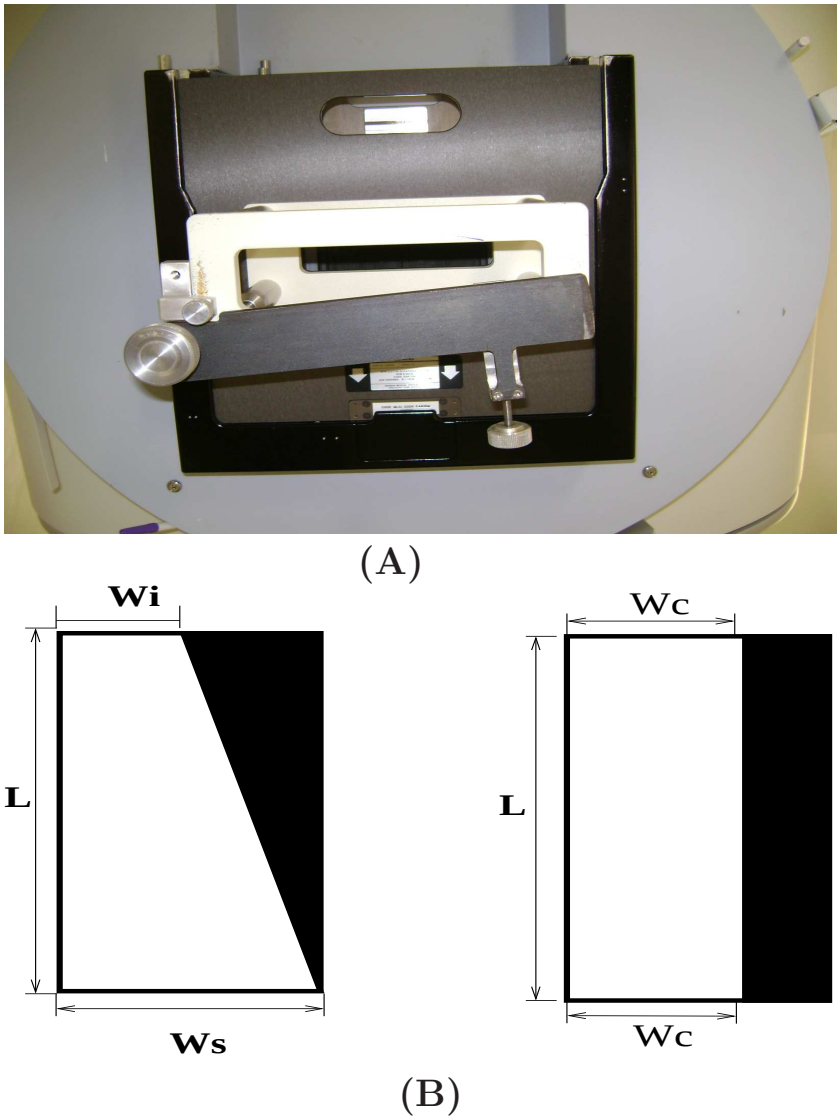

Figure 2.3: (A) A photo of electron arc applicator with the open aperture shaped into a trapezoidal aperture. (B) Two shaped apertures are denoted as Ws cm-by Wi cm trapezoidal aperture and Wc cm rectangular aperture, respectively. The length of the aperture, L, is neglected for short as it is always kept at 17.2 cm .

of maximum dose. A scanning water tank system(RFA300, Scanditronix Medical AB)with Omni Pro 6 software was used to measure the PDDs and profiles with gantry and collimator at zero degree.

The dosimeter chosen for measuring PDDs and profiles is a Scanditronix p-tpye silicon diode(EFD SN:DEB12-3035). The electron diode has the following advantages over a parallel chamber:(1)Its physical size is very small. The diode's diameter is 2.5 mm and the thickness of the silicon chip is only 0.5 mm. The effective thickness of the measuring volume is 60 μm. Such a small physical size provides very high spatial resolution, which is required for measuring the dose in region where the dose gradient is very high, for example, the penumbra region of profile and the falling portion of electron PDD curve; (2)The electron diode was preirradiated to 8 kGy using a 10 MeV electron beam by the manufacturer. It is considered to be dose-rate independent[83, 84];(3)The pure signal from diode detector signal is directly proportional to the absorbed dose in water. There is no need to convert the ionization signal to dose because the stopping power ratio of water to silicon varies slowly with depth especially for low electron energies[50].

Before any measurement, as suggested by the dosimetry protocol[5], the electron diode was verified by comparing the PDD with one measured with a parallel chamber. The chamber used was the one developed by the Nordic Association of Clinical Physicists (NACP) [65]. Its narrow air gap(2 mm) and carefully designed guard ring minimize the perturbation effects. The thin(< 0.1 mm) collecting electrode is mounted on a thin(< 0.3 mm)insulating layer, yielding negligible polarity effect. The thin(0.5 mm) graphite wall makes it approximately water equivalent. The chamber is enclosed in a waterproof housing that can be directly attached to the positioner of RFA300 water tank, enabling one to perform ionization measurements in water under the conditions of well-defined chamber position and phantom geometry. The variation of the overall perturbation factor with the depth is considered to be negligible for this type of chamber[6, 3, 4]. The relative depth ionization was measured using the NACP chamber and then converted to the depth dose using stopping-power ratio from IAEA TRS-398[5].

The smallest electron applicator available is a circular cone with the diameter

of 5 cm. This cone was used to compare the PDDs measured with the NACP chamber and electron diode for 6 MeV and 9 MeV electron beams. The SSD was set to be 100 cm. It was found the PDDs measured with two dosimeters agree to each other very well.

As an example, the results for the 6 MeV electron beam are shown in Fig. 2.4(A). To convert the ionization reading of the NACP chamber to dose, the stopping power ratio of water to air for 6 MeV electron energy was taken from the protocol[3]. The ratios were input into Excel and plotted against depth in Fig. 2.4(B). The data was fitted using the second-order polynomial, which fits the data quiet well with the confidence level of 99%. The fitting equation is used to calculate the stopping power ratio for each measurement depth.

2.2.3 Measurement procedure

For the measurement of central-axis percentage depth dose, the effective point of measurement for the NACP chamber was taken as the center of the inner side of the entrance window, i.e. 0.5 mm behind the entrance plane. A second small thimble chamber, the RK-type 8305, was placed in the corner of the radiation field as a reference monitor chamber for each set of measurements. The chamber was placed at a bias of -100 V and ionization readings were obtained through the standard RFA300 electronics. The measurements were always performed in the same manner with the chamber moved towards the surface in order to eliminate any backlash.

The diode is encapsulated in an epoxy cylinder such that its sensitive volume is located parallel to one face of the housing, 0.5 mm below the surface. The effective point of measurement for this diode was taken as 0.5 mm under the front surface toward the beam. The diode was also attached to the RFA300 positioner and data were obtained as with the NACP chamber above, with one exception that a second reference diode detector was used for monitoring the electron fluence instead of an ionization chamber.

The profiles were obtained using the silicon electron diode, which was also used for commissioning electron arc therapy for 6 MeV and 9 MeV[40]. One

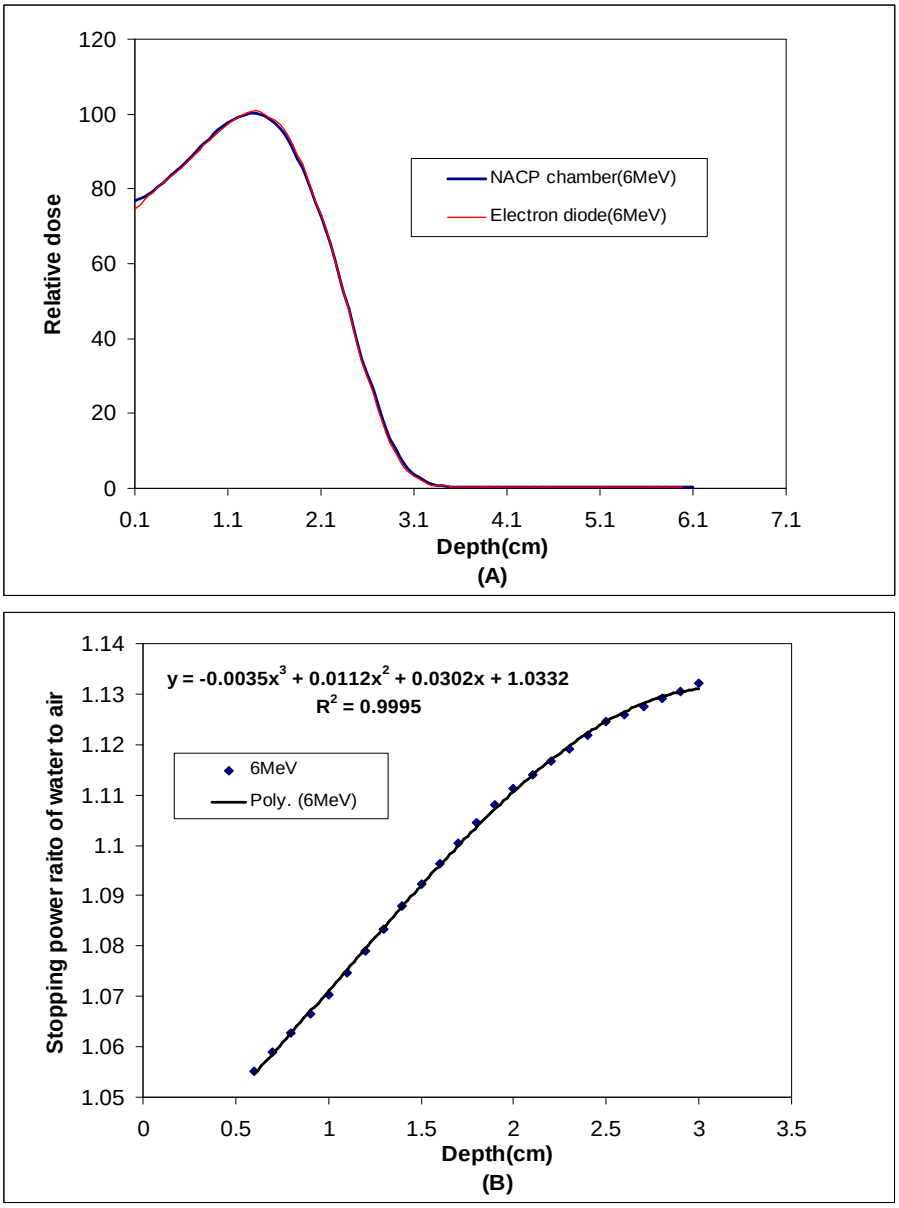

Figure 2.4: (A) Comparison of central axis percentage depth doses measured with a parallel plate chamber(NACP chamber) and a Scanditronix electron diode for 6 MeV electron beam. The PDDs were measured in water at 100 cm SSD using the circular electron cone with 5 cm diameter. (B) The polynomial fitting of the stopping power ratio of water to air for 6 MeV electron beam.

cross-plane profile passing the central axis of the beam was scanned at d_{max} for each field size and SSD. The scan was extended to ±90 mm on either side of the origin. For the inplane profile, the scanning limits were ±150 mm on either side of the origin. The scanning origin was redefined for each field, ensuring that the effective point of measurement of the diode was aligned with the center of the field on the central axis of the beam. The scanning was also set to be in the precision mode with the 1mm scanning step and the lowest scanning speed.

2.3 Results and discussion

2.3.1 Central axis percentage depth dose

Fig. 2.5 and Fig. 2.6 show the central-axis percentage depth dose curves for the open aperture and the 4 cm-by-2 cm trapezoidal aperture, respectively. The depth dose curved were measured at 80 cm, 85 cm and 90 cm SSD. The minimum and maximum limits of SSD range were 80 cm and 90 cm. It can be seen clearly that the PDDs do not change with SSD for open and trapezoidal apertures. The difference shown at shallow depth(less than 0.5 mm)is caused by the uncertainty during the redefining of the origin for each field.

The independence of PDD on the SSD can be explained as follows: The electron beam is scattered by collimator blades and by successive apertures and consequently became an extended source of radiation. Hence it will no longer obey the inverse square law with distance and the change of SSD has no effect on PDD curves.

The effect of the trapezoidal and rectangular apertures on the PDD was also investigated. Fig. 2.7 shows a typical result. The PDDs for open field and trapezoidal fields were measured at 85 cm SSD. The trapezoids were chosen to represent the typical range of apertures that may be encountered in clinical situation. It was found that, for both energies, the steeply falling portions of PDDs are unchanged for various apertures. However, in the build-up region, the PDD curves are quite different from aperture to aperture. This is very pronounced for the 9 MeV electron beam. For the 6 MeV beam, the dose difference in the

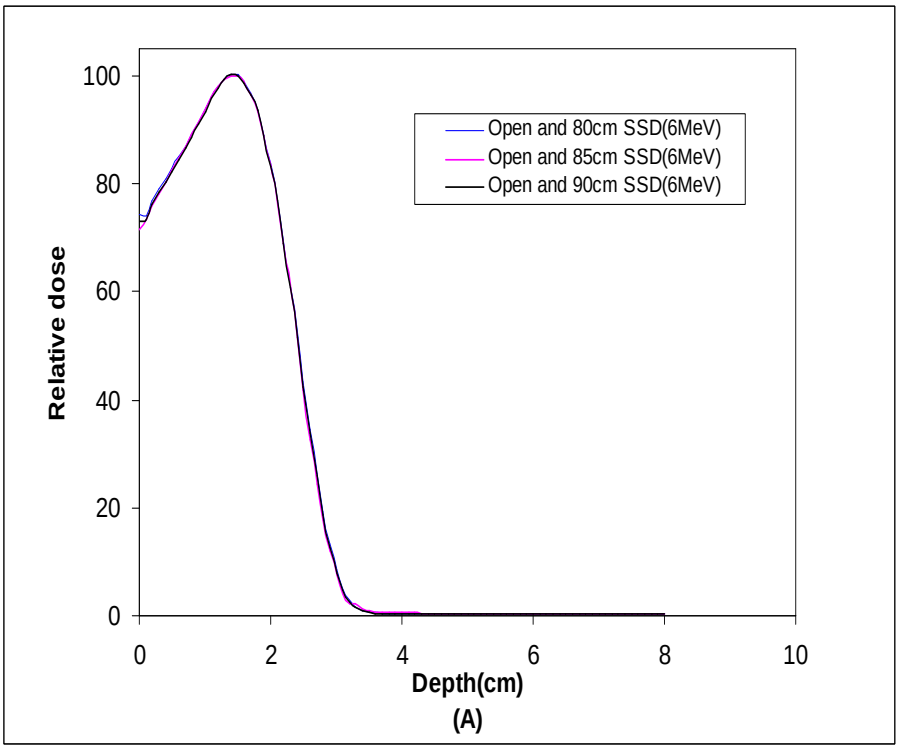

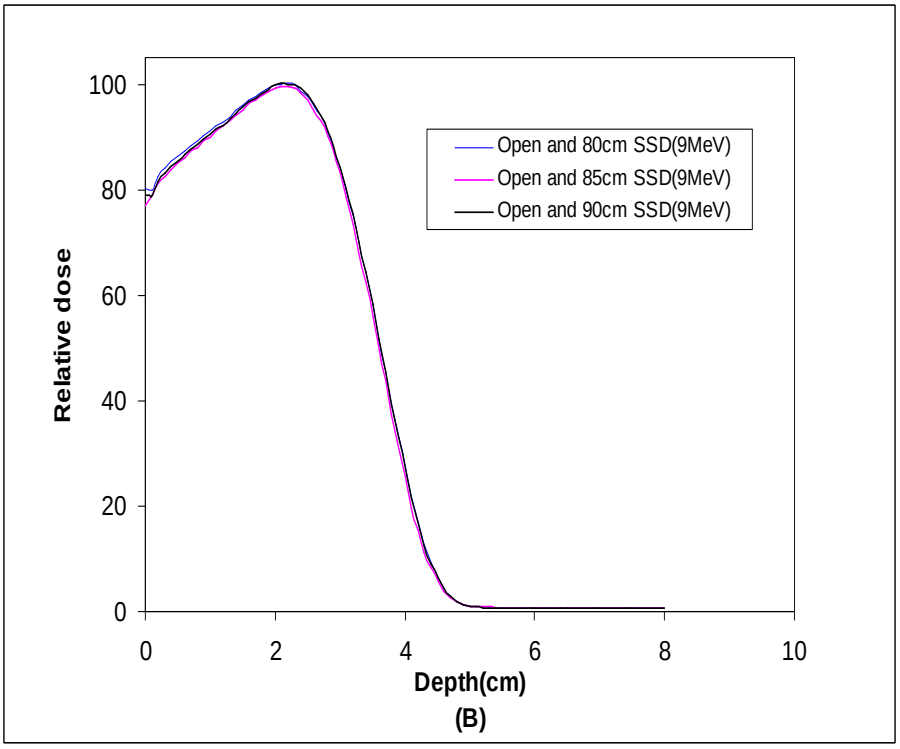

Figure 2.5: The central axis percentage depth dose of the static electron beam measured at different SSDs with open aperture for (A) 6 MeV (B)9 MeV.

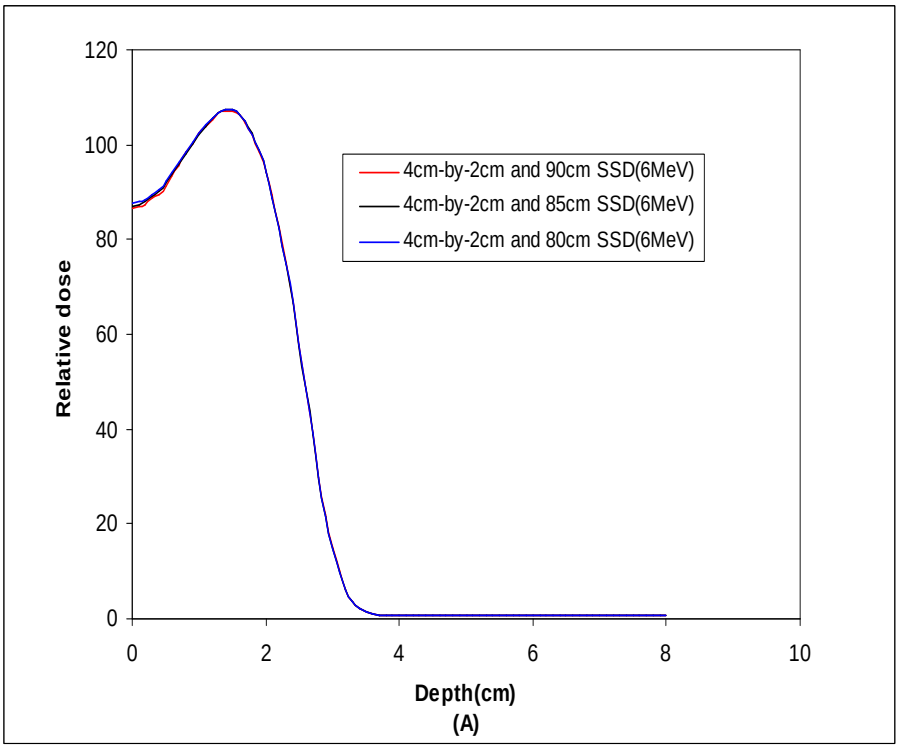

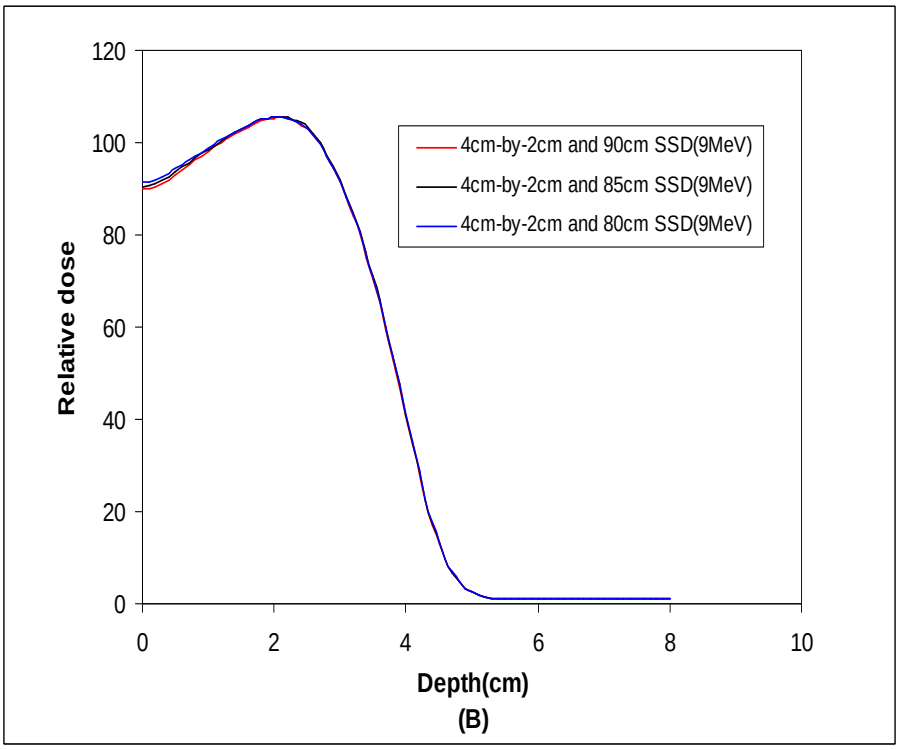

Figure 2.6: The central axis percentage depth dose of the static electron beam measured at different SSDs with 4 cm-by-2 cm trapezoidal aperture for (A) 6 MeV (B)9 MeV.

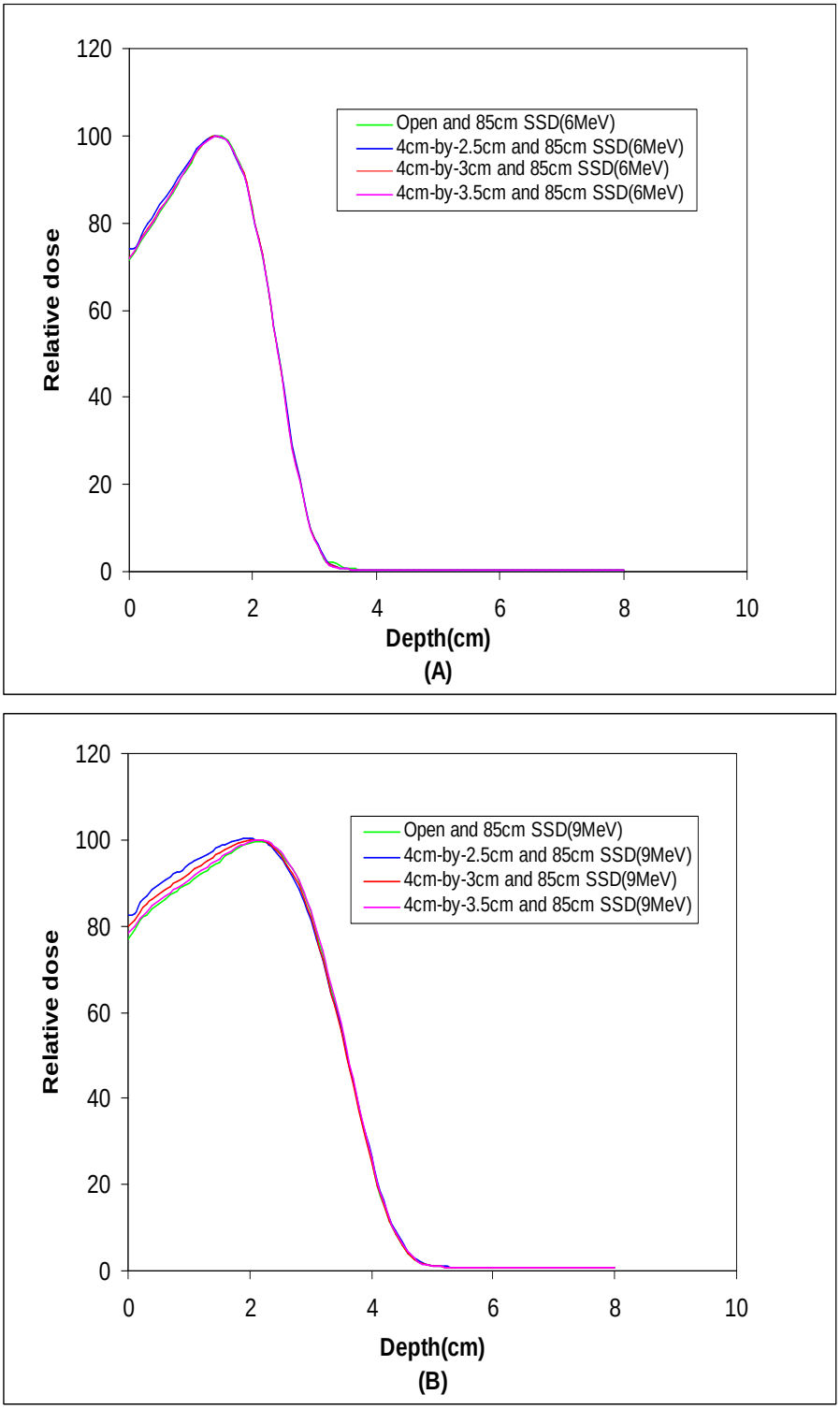

Figure 2.7: Comparison of central axis percentage depth dose of the static electron beam measured at 85 cm SSD with open aperture and different trapezoidal apertures for (A)6 MeV and (B)9 MeV.

build-up region is relatively small, but still can be distinguished for different apertures. It is also noted that the surface dose increases when the aperture width at the field center decreases. The same trend is observed for the dose region between surface and the depth of maximum dose: the narrower the aperture, the higher the relative dose. Despite of these differences, the position of the depth for maximum dose is not shifted when the aperture becomes smaller.

The dose difference in the build-up region of the PDD curve for different apertures is attributed to photon contamination and lower energy scattered electrons. Because the end of the electron arc applicator is so close to the water surface, photon contamination gives a large contribution to the dose in the build-up region. The photons are produced by the electron beam bombarding the shaper plate and other parts of applicator. Because the electron beam is directly incident on the part of shaper plate, which slides into the aperture, this contributes a large portion of total photon contamination. When the aperture is pinched more, it means a larger portion of the shaper plate slides into the aperture. In turn, more photos are produced by electrons hitting a larger area of shaper plate. This is why the dose in build up region is increasing for the smaller apertures and the depth of maximum dose is not significantly shifted.

Furthermore, the photon contamination is much larger for high energy electron than lower energy electron. This leads to the following observation: the dose difference in the build-up region is much larger for 9 MeV than 6 MeV under the same conditions. Similarly, the low-energy electrons scattered from the edge of shaper plate and other components also contribute to this difference. In addition, because the energy of the scattered electrons and photons is very low, they cannot reach the depth beyond the therapeutic range. Therefore, the falling portions of PDD curves are not influenced by changing the aperture.

2.3.2 Inplane and crossplane profiles

Crossplane profiles

The influence of SSDs and trapezoidal apertures on the crossplane and inplane profiles is also an important part of the investigation. When the gantry and collimator are set to be zero degree, the crossplane and inplane direction coincides with the traverse and longitudinal direction of a rectangular or trapezoidal aperture. Without being stated explicitly in the rest of this chapter, the trapezoidal aperture becomes gradually narrower along the direction from superior to inferior direction. Reflected in the figure(eg. Fig. 2.11), it means that the trapezoidal aperture become progressively narrower from the negative side to the positive side of x-axis. Each profile displayed is normalized to the dose at its own origin.

Fig. 2.8 and Fig. 2.9 show three crossplane profiles for an open aperture and three trapezoidal apertures, which were measured at the depth of maximum dose for 80 cm, 85 cm and 90 cm SSD. As expected, the field size increases with the increase of distance from the measurement point to the effective electron source position. It is also noticed that, under the same SSD, the field size for 9MeV electron beam is slightly smaller than that for 6 MeV beam. This is because the angular scattering from the apertures and other applicator components for 9 MeV electron energy is much less than for 6 MeV electron energy.

The influence of different trapezoidal apertures on the crossplane is displayed in Fig. 2.10. It has the same features as observed in Fig. 2.8 and Fig. 2.9, but the origin of profile is shifted laterally for different trapezoidal apertures with respect to the origin of open aperture profile. The narrower the aperture, more the profile origin is shifted. When the shaper plate is inserted into the aperture, more electron scattering from shaper plate “pushes” the origin of profile away from the origin of open aperture profile.

Inplane profiles

To compare the difference of inplane profiles between the open aperture and various trapezoids, Fig. 2.11 displays the profiles measured at the depth of dose

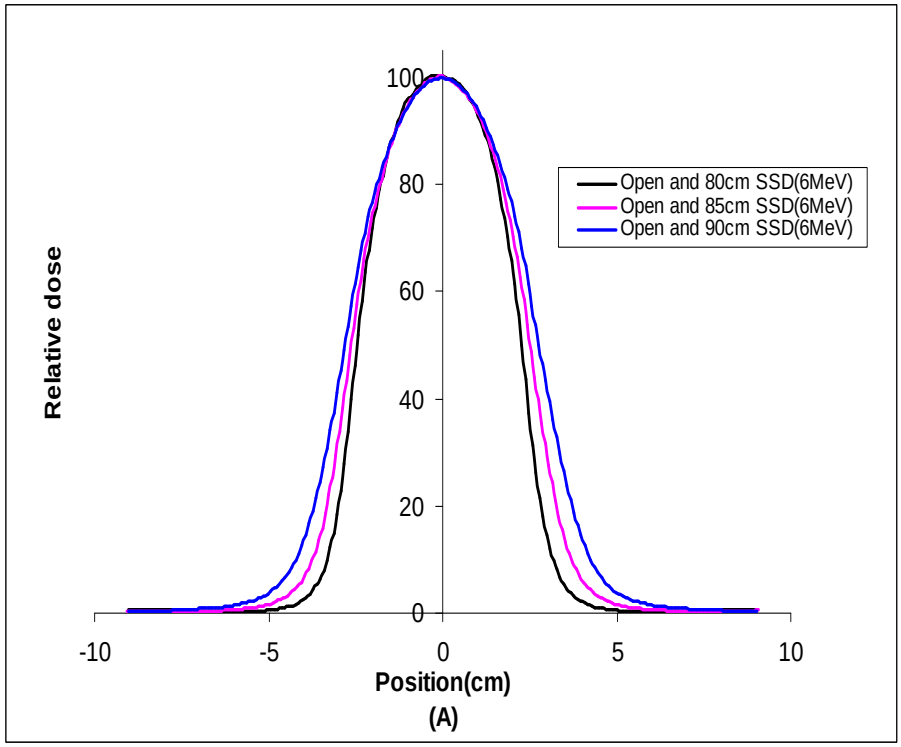

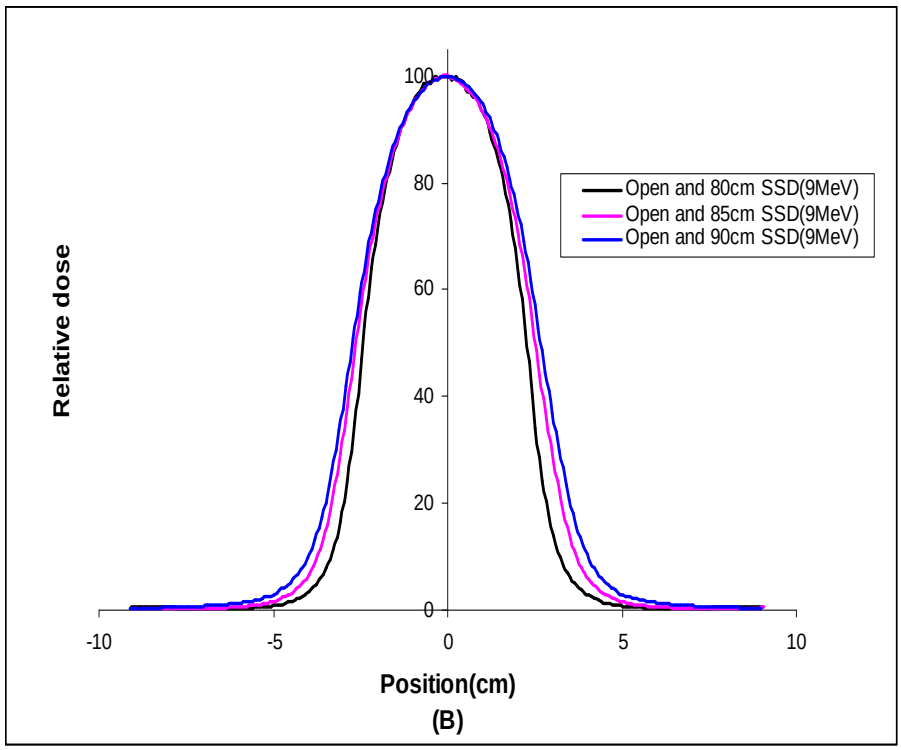

Figure 2.8: The cross-plane profiles of static electron beam measured at the depth of maximum dose and different SSDs with open aperture for (A)6 MeV and (B)9 MeV.

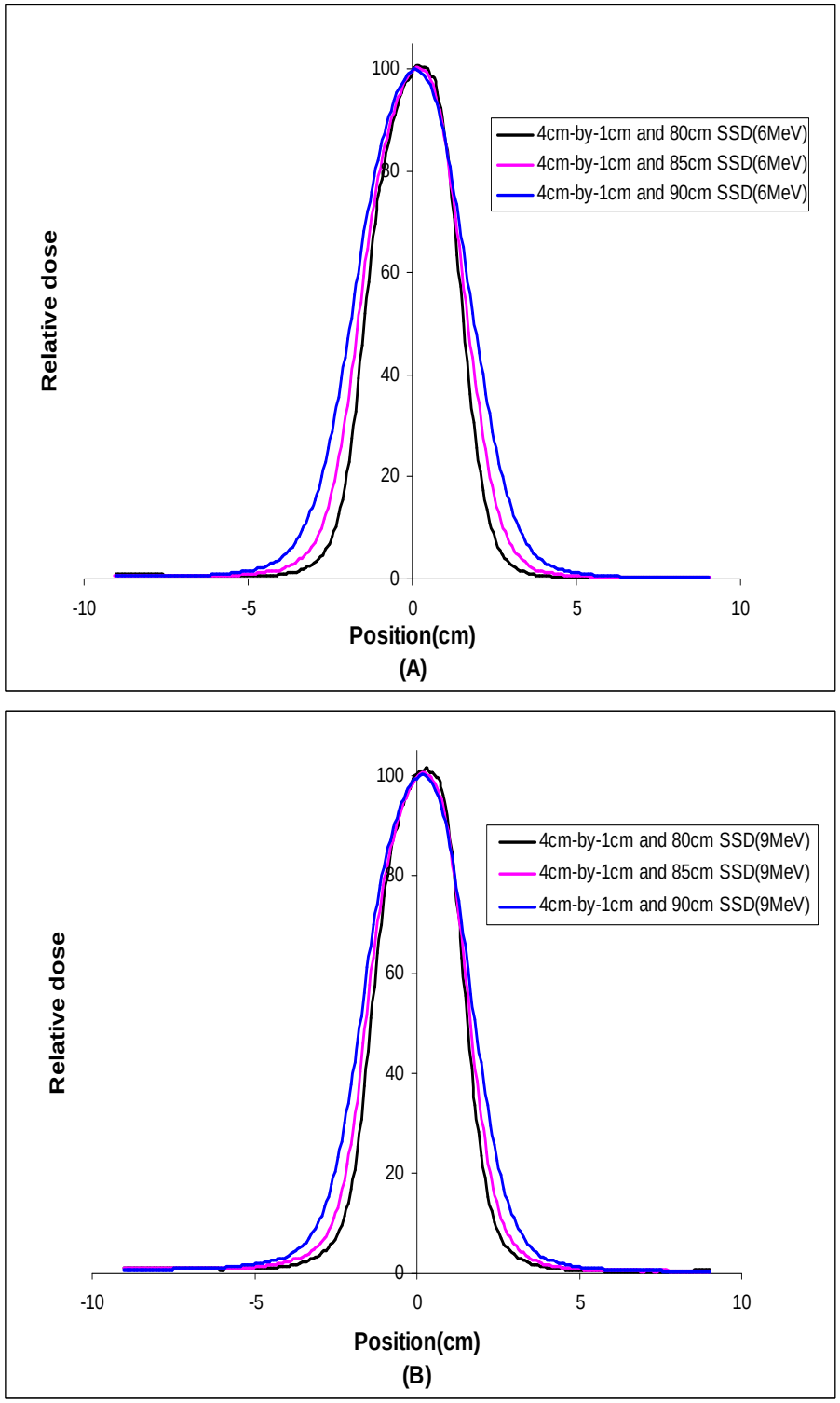

Figure 2.9: The cross-plane profiles of the static electron beam measured at the depth of maximum dose and different SSDs with 4 cm-by-1 cm trapezoidal aperture for (A)6 MeV and (B)9 MeV.

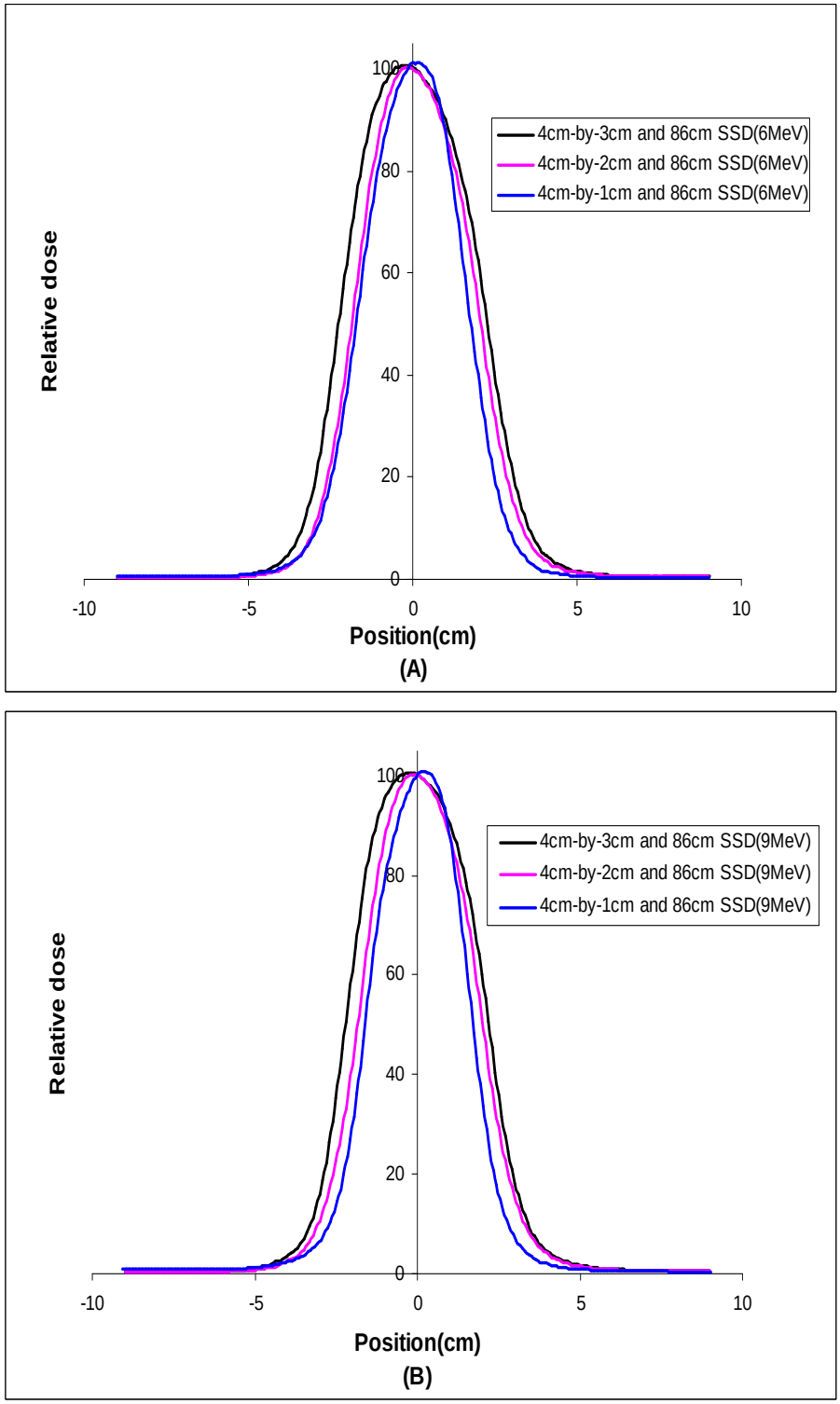

Figure 2.10: The cross-plane profiles of the static electron beams measured at the depth of maximum dose and 86 cm SSD with different trapezoidal apertures for (A)6 MeV and (B)9 MeV.

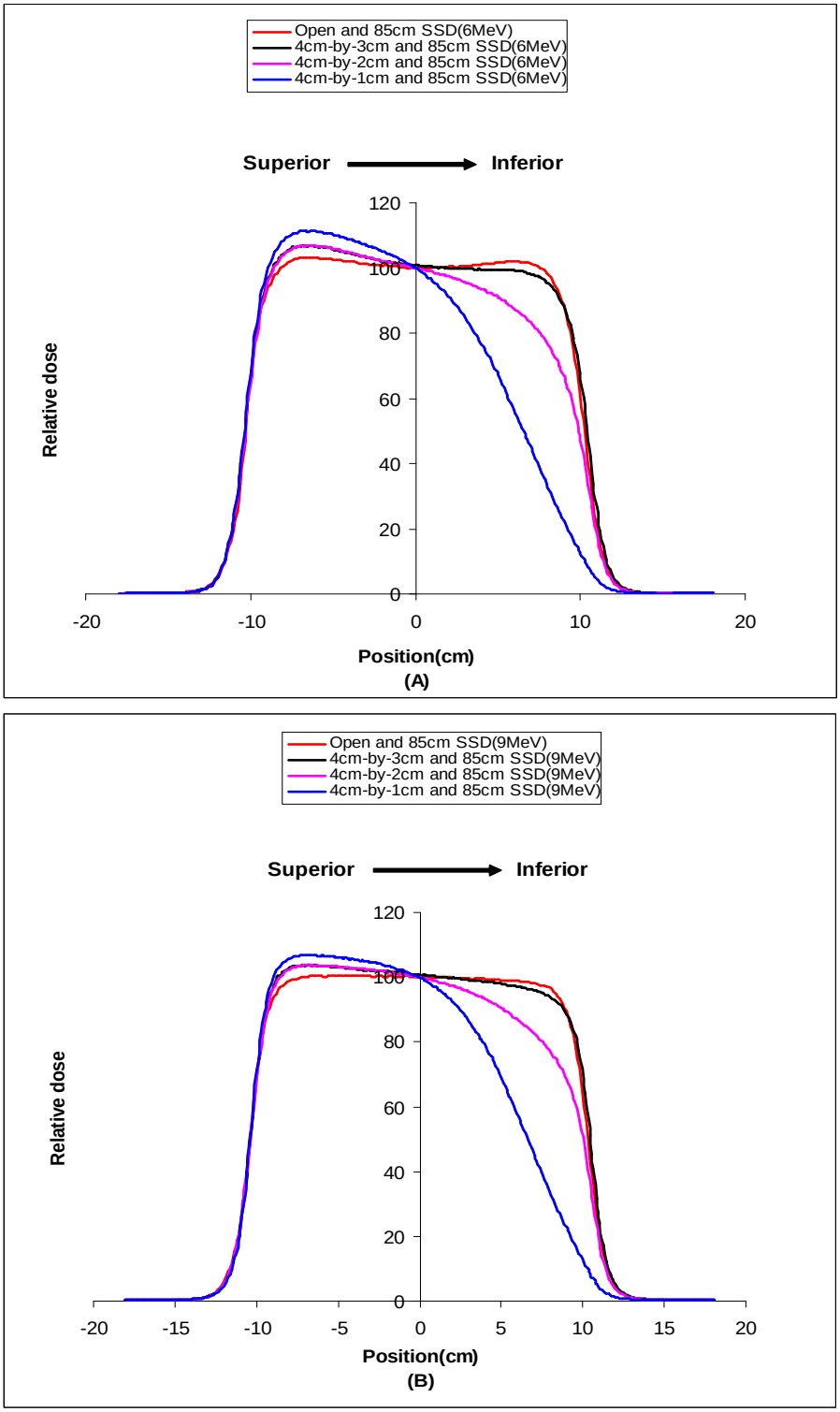

Figure 2.11: Comparison of the inplane profiles measured at the depth of maximum dose and 85 cm SSD with open aperture and different trapezoidal apertures. The trapezoidal apertures becomes progressively narrower from the negative side to the positive side of x-axis.

maximum and 86 cm SSD. There are several interesting features observed from the comparison of inplane profiles.

Firstly, the open aperture can deliver a very uniform dose into the water phantom whose surface is flat. The dose is uniformly distributed across the field. However, it is still noticeable that the profile for an open field has two small shoulders at the end. This may be caused by the scattering of electron from the ends of the apertures.

Secondly, since the trapezoidal aperture varies wider in the superior direction and narrower in the inferior direction, it is found that the dose rate decreases gradually from superior to inferior. The greater the variation of the aperture, the more rapidly the dose rate changes. For example, the dose rate decreases much more for 4 cm-by-1 cm trapezoidal aperture than for the aperture of 4 cm-by-3 cm. When the aperture is narrowed, the fluence of primary and secondary electron is reduced along the trapezoidal aperture. This causes the reduction of dose from superior to inferior. Because the dose rate is normalized to the field centre, the relative dose rate is greater on the superior side of the axis, which corresponds to the wider side of the trapezoidal aperture.

Thirdly, it is found that, although the trapezoidal aperture can vary the dose across the field, there is no single mathematical relation that can be established to describe the dose variation for all trapezoidal apertures. For example, for the 4 cm-by-3.5 cm trapezoidal aperture, the dose decreases nearly linearly, whereas the the dose reduction for 4 cm-by-1 cm drops off quadratically. The central part of the inplane profile was fitted using the second-order polynomial. The results are shown in Fig. 2.12.

Finally, the features displayed by the inplane profiles of trapezoidal apertures are clinically significant. It means one can use the trapezoidal aperture to reduce the dose along the longitudinal direction of aperture. However, one needs to find a method to determine the specific trapezoidal aperture for each individual patient because of the way the dose reduction varies from aperture to aperture.

2.3.3 Equivalence of a trapezoidal aperture and a rectangular aperture

During the investigation, it was found that a trapezoidal aperture has the same crossplane profiles and central axis percentage depth dose as a rectangular aperture under certain conditions. The condition is that the width of the trapezoidal aperture at the aperture center equals the rectangular aperture's width. This rectangular aperture is defined as the equivalent rectangular aperture of a trapezoidal aperture.

Fig. 2.13 and Fig. 2.14 show the typical PDDs and profiles for the trapezoidal apertures and their equivalent rectangular apertures. Two pairs of apertures are presented here: 4 cm-by-3 cm trapezoid versus 3.5 cm rectangle and 4 cm-by-1 cm trapezoid versus 2.5 cm rectangle. The crossplane profiles and PDDs were measured at the 80 cm SSD for the 4 cm-by-3 cm and 3.5 cm cm apertures and at 90 cm SSD for the 4 cm-by-1 cm and 2.5 cm apertures. Because the measured PDD curves for a trapezoidal aperture and its equivalent rectangular aperture overlap each other, for clarity, only part of rectangular PDD curve was drawn in Fig. 2.14. The results clearly show the equivalence of a trapezoidal aperture and a rectangular aperture.

The equivalence of a trapezoidal aperture and a rectangular aperture can be explained using the diagram shown in Fig. 2.15. Although the aperture appears quite different, but the scattering conditions at the central axis of the beam are same, provided that the irradiation conditions are identical. This is because the absence of the electron scattering from the volume in air and medium projected by area C is compensated by the same volume projected by area D below the electron arc applicator. As a result, the electron scattering from and to volume in air and medium near the central axis of the field for the trapezoidal aperture is the same as the rectangular aperture. The equivalence of trapezoidal and rectangular aperture was also used by Hogstrom for developing the electron arc pencil beam algorithm[32].

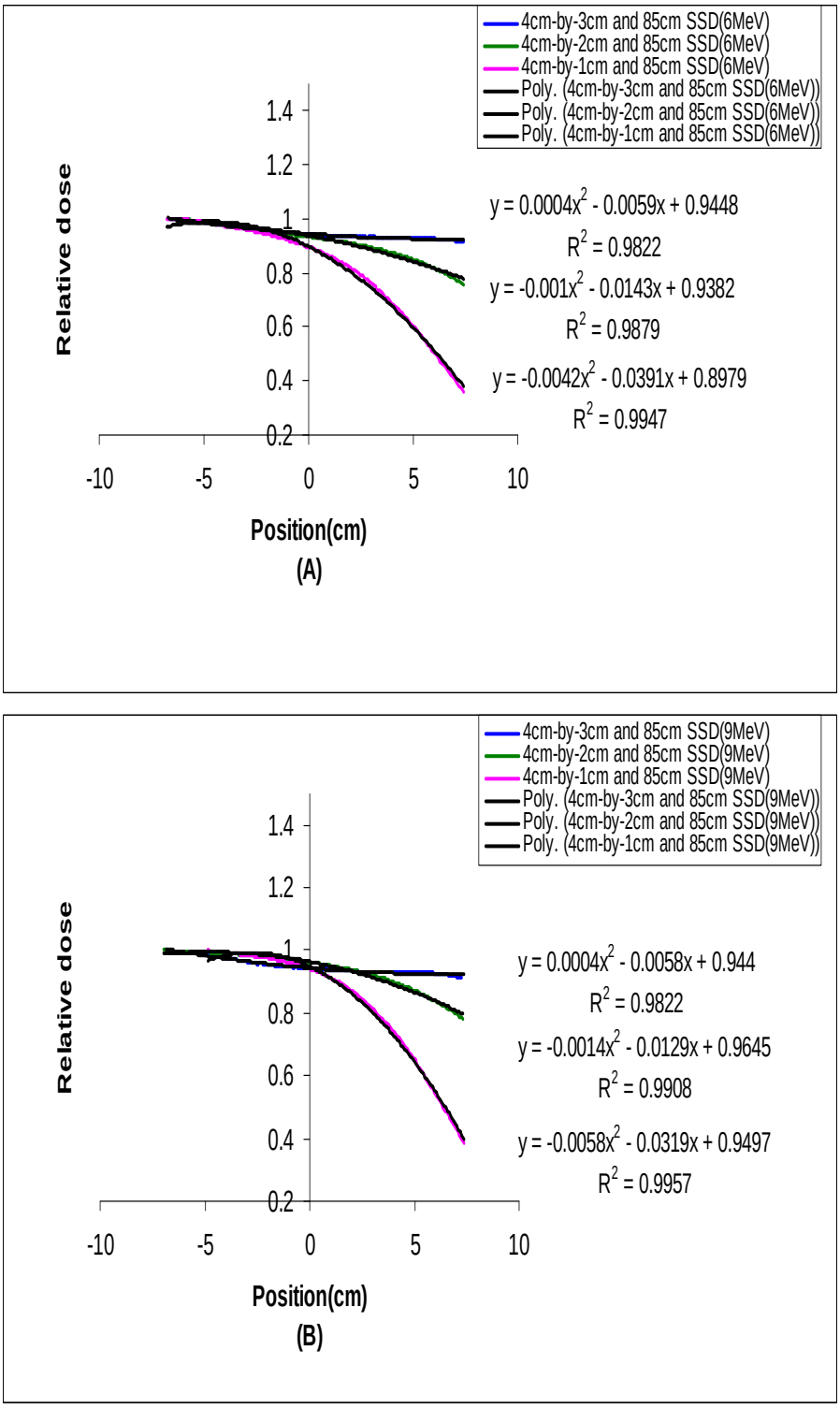

Figure 2.12: The second-order polynomial fitting of the central part of inplane profiles shown in Fig. 2.11 for trapezoidal apertures. The relative dose is the dose normalized to the maximum dose found in the central portion of each profile.

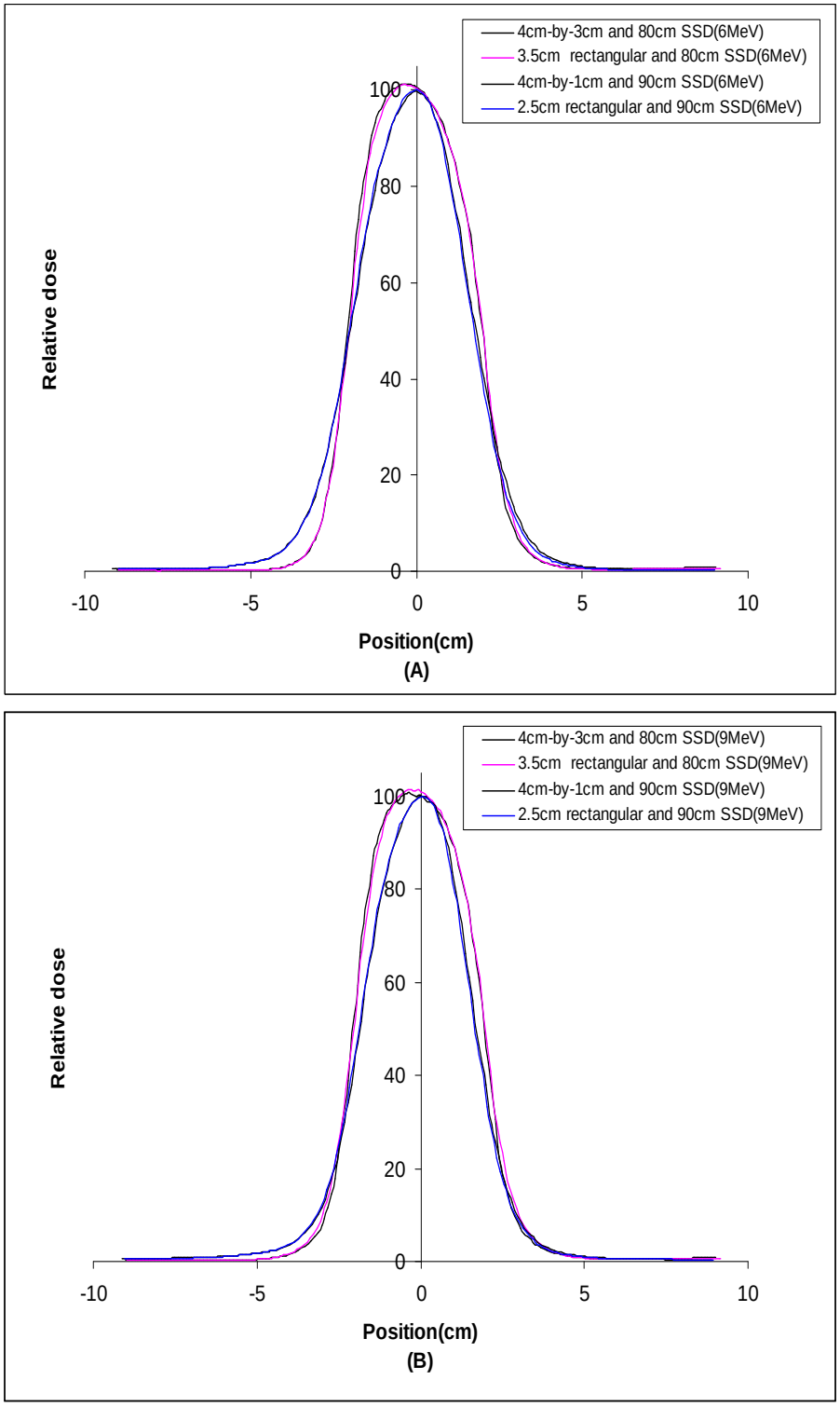

Figure 2.13: Comparison of the cross-plane profiles of the static electron beam measured at the depth of maximum dose with a trapezoidal aperture and its equivalent rectangular aperture for (A)6 MeV and (B)9 MeV.

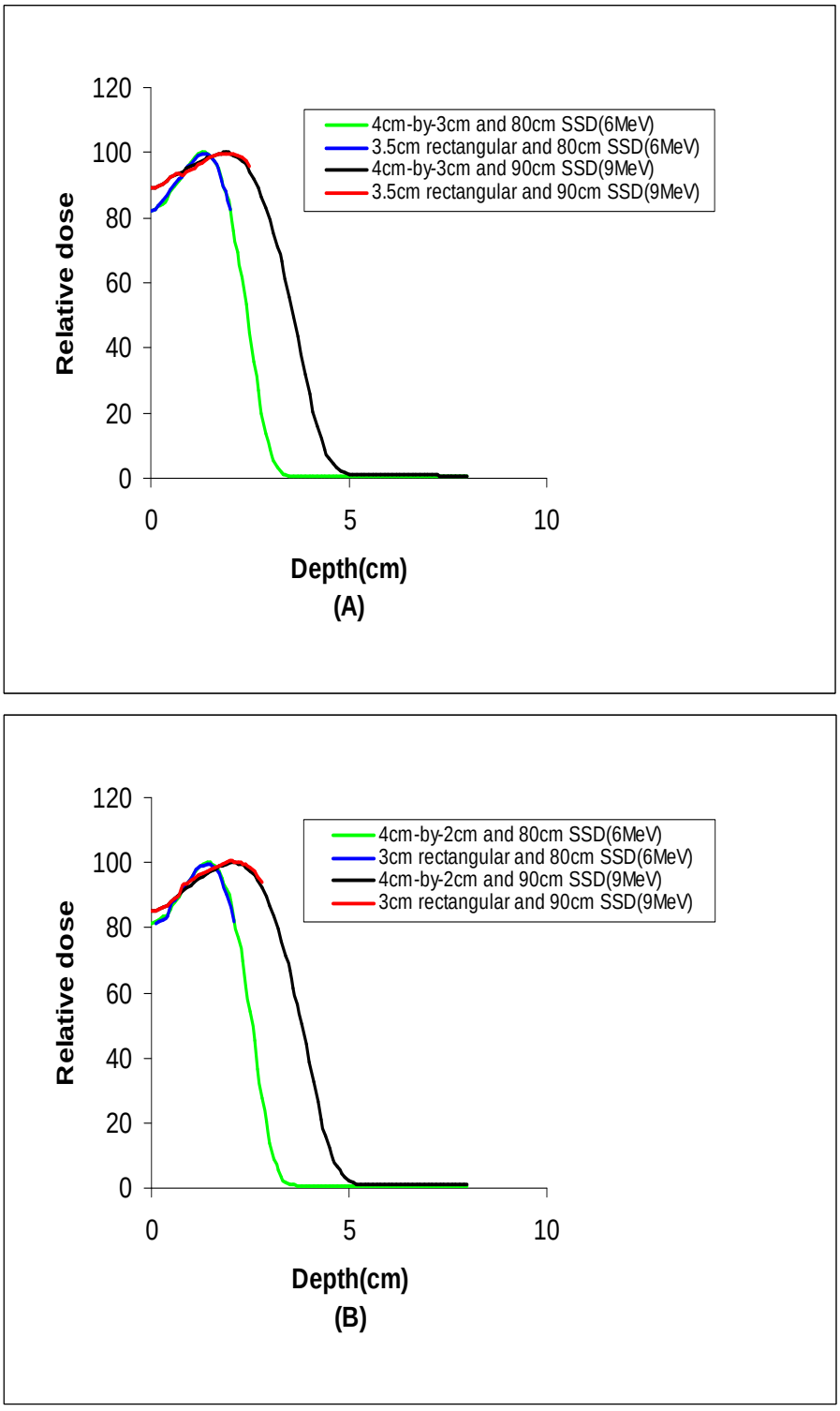

Figure 2.14: Comparison of central axis percentage depth dose of the static electron beam measured with a trapezoidal aperture and its equivalent rectangular aperture for (A)6 MeV and (B)9 MeV.

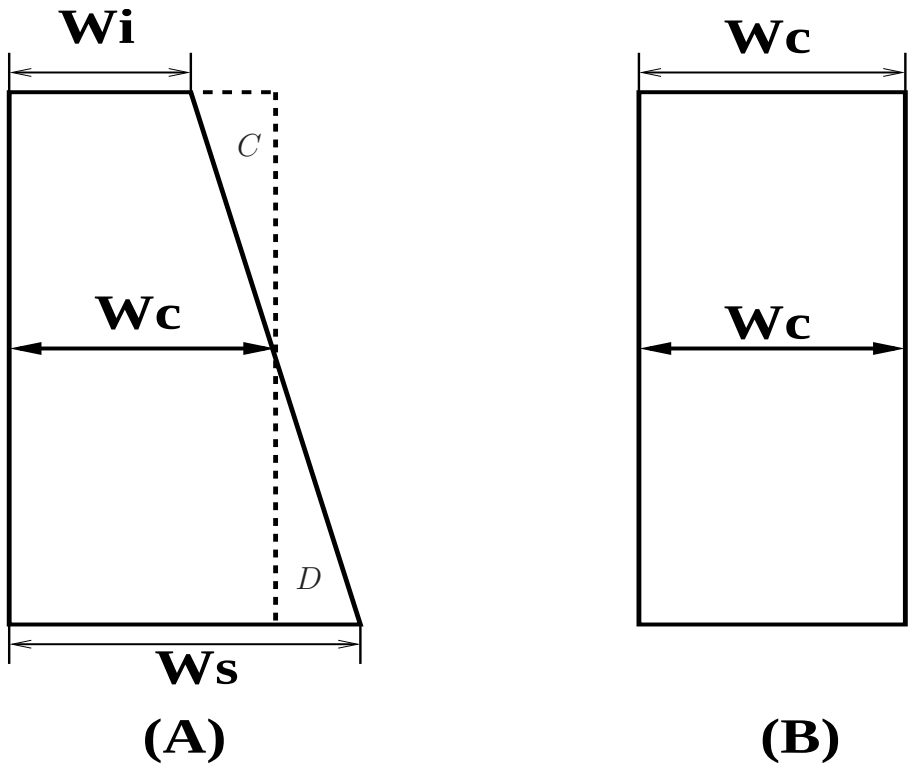

Figure 2.15: (A)A Ws cm-by-Wi cm trapezoidal aperture of electron arc applicator. The width of the aperture at its center is Wc cm. (B)The equivalent Wc cm rectangular aperture of the trapezoidal aperture.

Chapter 3

Clinical implementation of a method for calculating monitor units

3.1 Introduction

To deliver the prescribed dose to a reference point in a patient, the number of monitor units(MU) required for delivering the dose must be known accurately. The monitor unit calculation is an important process in radiation therapy treatment planning[97, 98], in which the prescribed dose is converted to the readings of the monitor chamber on a treatment machine for the individual radiation fields(ports) or beam segments to be used.

The MUs are often determined outside the treatment planning system and based on the dose per MU determined at d_{max} for a specific geometric setup of the patient as well as the dose prescription. However, the dose per MU is difficult to predict due to the variation in electron scattering with a variety of linear accelerators, beam energies, SSDs and beam collimation systems[7, 24, 60]. As a result, the dose per MU of a specific treatment is usually measured individually in order to achieve acceptable accuracy. As suggested by Khan[44], this patient-specific measurement could be applied to electron arc treatment, but it requires a customized cylindrical water or solid phantom to be fabricated for every individual patient[51]. The radius of the phantom needs to be the average radius of patient. Obviously this is impractical in terms of the resources and man-hours.

In 2004, Keith Croft, the chief physicist of radiotherapy department in Palmer-

ston North Hospital, proposed a method for calculating the MUs for the electron arc treatment with an open field. In this chapter, this method is extended to the treatments using different trapezoidal and rectangular fields.

3.2 Materials and methods

3.2.1 Theory

Formalism

For simplicity, it is assumed that the contour of a patient can be approximated closely by a cylinder, as shown in Fig. 3.1(A). A point P lies on a central axis that passes through the isocenter and the middle point of the arc. The central axis depth of this point is d. When the beam rotates through the arc, which is represented by the dashed line in the diagram, the dose at point P is equivalent to the dose accumulated by moving point P along the arc in a stationary beam centered at P. Sandison et al. demonstrated[89]that the electron arc treatment can be delivered by rotating the phantom while keeping the beam at a fixed position.

Fig. 3.1(B) shows the dose profile along the arc in the stationary beam. $K(s)$ is the dose at a point on the arc relative to the maximum dose in the stationary field. The dose at point P can be calculated by first assuming that the central axis of the beam passes through P and then integrating the dose profile along the arc to the left and right up to the limits of the arc. It can be shown that the dose $D^P_{arc}(d)$ at point P per arc is given by[47]:

$$D^p_{arc}(d) = \frac{\dot{D}_0(d_{max})}{2\pi n}\left[\int_{-s}^{+s} K(s)ds\right] \tag{3.1}$$

where $\dot{D}_0(d_{max})$ is the dose rate per minute in the stationary beam at the depth of dose maximum. n is the speed of rotation in the unit of radians/minute. $-s$ and $+s$ are the arc limits, which can also be represented by the angle θ_1 and θ_2, respectively. The term in the bracket is the area under the dose profile along the arc within the arc limits.

Equation(3.1) is a general formula and applied for any point on the arc.

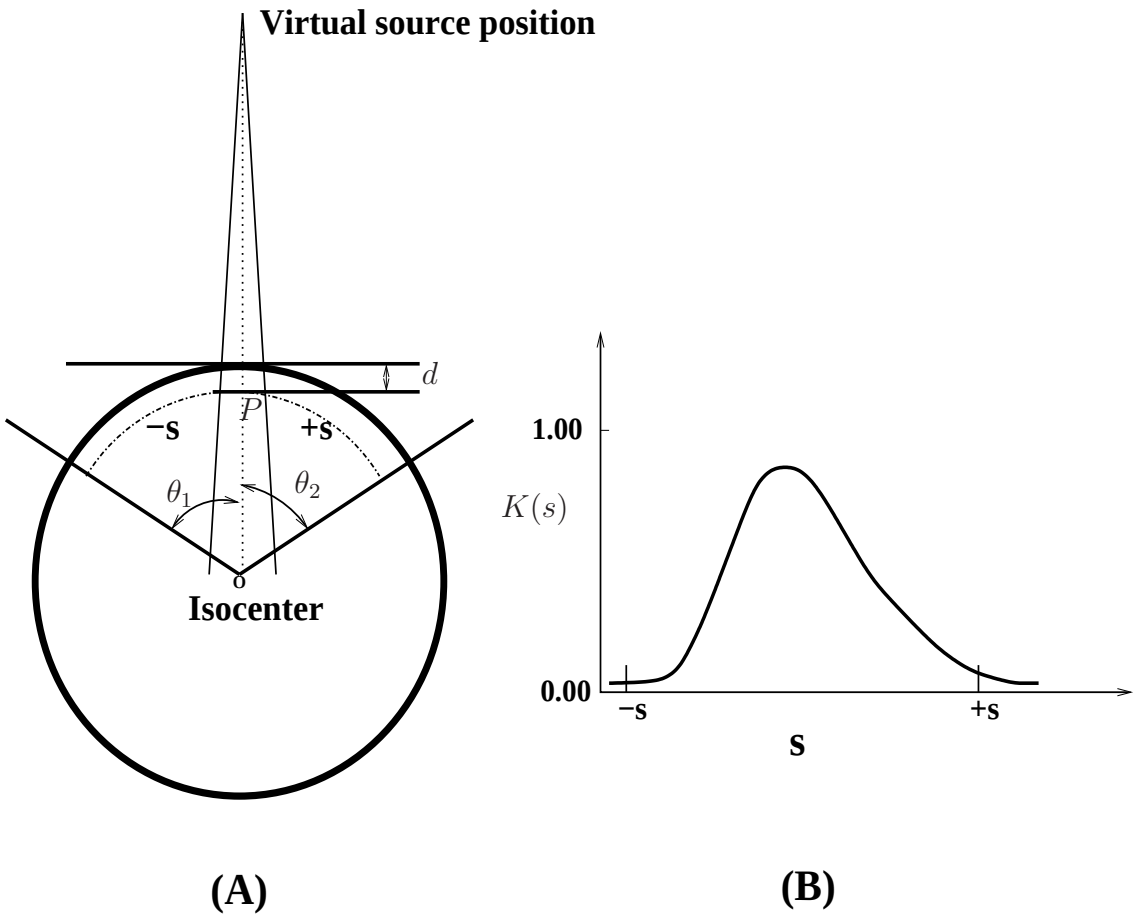

Figure 3.1: Diagram illustrating the electron arc MU calculation procedure:(A)The point of interest, P, forms an arc represented by dashed line when an electron beam rotates around the cylindrical phantom. The arc limits are represented either by $\pm s$ or θ_1 and θ_2. (B) The dose profile along the arc for point P at the depth of d. The profile is normalized to the maximum dose in the static beam.

The dose $D^p_{arc}(d)$ at point P per arc is determined by the dose rate of the static electron beam, the angle of the arc and the area under the profile. It is not dependent on the direction of rotation and the symmetry of the profile. For a modern linear accelerator, the dose rate for electron beam is usually calibrated at d_{max} and expressed as $\dot{D}_0(d_{max}) = n\,\mathrm{Gy/MU}$, where n is a constant. If the point P coincides with the point of the maximum dose, the dose per degree can be derived from Eq.3.1:

$$D_{perdegree}(d_{max}) = \frac{\dot{D}_0(d_{max})}{|\theta_1| + |\theta_2|}\left[\int_{\theta_1}^{\theta_2} K(\theta)d\theta\right] \tag{3.2}$$

where $\dot{D}_0(d_{max})$ is the dose rate calibrated at d_{max} for a static beam in term of Gy per MU. The area under the profile is the sum of the relative dose without unit. Therefore the unit for the quantity $D_{perdegree}(d_{max})$ is Gy/MU/degree.

The dose profile and the dose rate at d_{max} vary with the beam energy, the dimension and the shape of the electron field and SSD. Therefore, the dose per degree is a function of beam energy, SSD and electron field. Once $D_{perdegree}(d_{max})$ is determined, the monitor units, MU^{eArc}, required for delivering the prescribed dose, $D^{eArc}_{pres}(d_{max})$, to d_{max} can be calculated as:

$$MU^{eArc}[\mathrm{MU}] = \frac{D^{eArc}_{pres}(d_{max})}{D_{perdegree}(d_{max})}[\mathrm{MU/degree}] \times \psi[\mathrm{degree}] \tag{3.3}$$

where ψ is the travel angle when the beam rotates through the whole arc. The terms in brackets are the units of the quantities.

Calculation of dose per degree

As seen from Eq.3.2, the dose per degree is related to the dose profile along the arc and the dose rate at d_{max}. The dose profile can be obtained in the following way[16, 49, 51]: first, a matrix of depth dose distribution data for the stationary beam is measured in a series of cylindrical phantoms in a plane containing the central axis of the beam. The radii of the phantoms are chosen carefully to cover a range of typical treatment conditions encountered in electron arc therapy. Then the dose profile along the arc for a point can be derived from the tabulated PDD data through interpolation or extrapolation.

Due to the limited resources in the department, it is recognized that making a series of cylindrical phantoms using perspex or high impact polystyrene slabs is not feasible. In order to calculate the dose per degree, Keith Croft, the chief physicist in the oncology department of Palmerston North Hospital, proposed a concept of equivalent impulse[39].

The concept is illustrated in Fig. 3.2(A). Assuming that the patient curvature is very small in comparison with the width of profile, the profile along the arc can be approximated by the profile measured in a flat water phantom. This condition is satisfied as long as the patient radius R is very large relative to the field width. Then the length of the arc can also be replaced approximately by a straight line with the length of l. The mean percentage dose rate, $\bar{D}_{\%}$, averaged over the arc length l for the traveling beam is defined as:

$$\bar{D}_{\%} = \frac{\left[\int_{-s}^{+s} K(s)ds\right]_{flat}}{l} \tag{3.4}$$

where the subscript indicates that profile integration uses the profile measured in a flat water phantom. l is chosen properly to cover the whole profile considering the width of the profile at d_{max}.

By defining the quantity $\bar{D}_{\%}$, it is equivalent to transforming the original profile into an equivalent square pulse. When beam sweeps through the point P, the equivalent square pulse effectively travels through the whole arc but with a constant mean dose rate. This procedure is schematically represented in Fig. 3.2(B).

In our center, the electron beams from the Siemens Primus were calibrated to deliver 1 Gy at d_{max} for a given 100 MUs under the reference conditions recommended by the international protocol[5]. Therefore, $D_0(d_{max})$ can be expressed as $D_0(d_{max}) = D_0^{flat}(d_{max})/100$, where $D_0^{flat}(d_{max})$ is the dose per 100 MUs at d_{max} in a flat water phantom for the electron arc applicator and a specific SSD. In addition, the arc angle corresponding to the arc length l can be approximated by $\frac{l}{R} \times \frac{180}{\pi}$. Then the dose per MU per degree can be simply calculated as[39]:

$$D_{perdegree}^{flat}(d_{max}) = \frac{D_0^{flat}(d_{max}) \times \bar{D}_{\%} \times l \times 180}{R \times \pi \times 100\% \times 100} \tag{3.5}$$

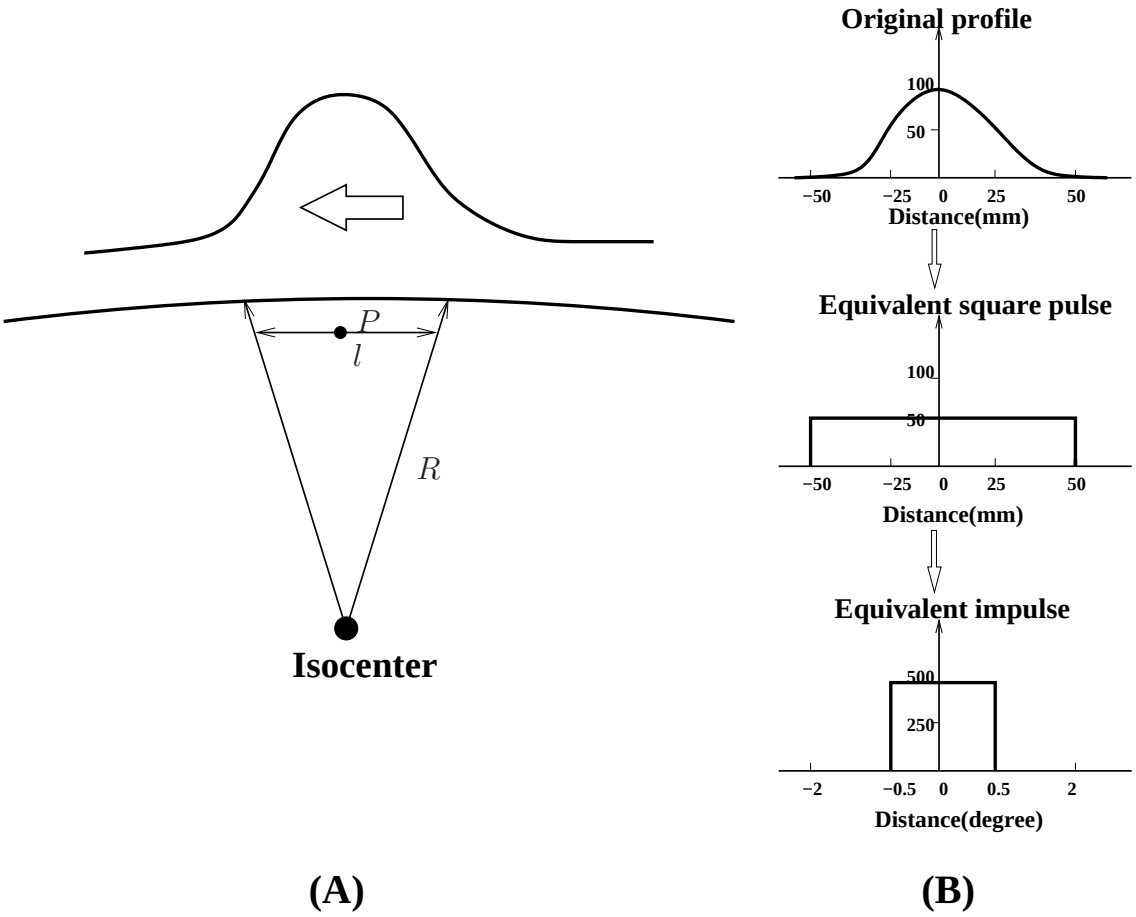

Figure 3.2: Diagram illustrating the concept of equivalent impulse:(A) The profile measured in a flat water phantom travels through a near-flat surface, where R is the radius of patient and l is the length of the straight line approximating the length of the arc.(B)The procedure that transforms an original profile into an equivalent impulse.

Notice that Eq.3.5 is an approximation of Eq.3.2 under the assumption of small patient curvature. It defines a narrow equivalent angular impulse that travels along the arc with an unchanged dose rate in the unit of dose per degree, as shown in Fig. 3.2(B).

3.2.2 Beam data acquisition

To commission the MU calculation algorithm for electron arc treatment, the fundamental dosimetry data for a given beam energy and electron field are:(1)the d_{max}, which is determined from the central axis percentage depth dose;(2) the crossplane profiles at d_{max};(3) the output at d_{max}. These beam data are required for a range of SSDs, which represent the typical treatment conditions.

Measurement of the depth of dose maximum and dose profile

The following electron fields were used for the measurement:(1)rectangular fields: open, 3.5 cm, 3 cm, 2.5 cm and 2 cm, and (2)trapezoidal fields: 4 cm-by-3 cm, 4 cm-by-2 cm, 4 cm-by-1 cm. For each combination of beam energy and electron field, the PDDs and profiles were measured at 80 cm, 82 cm, 84 cm, 85 cm, 86 cm, 88 cm and 90 cm SSD. The profiles and PDDs were measured using the Scanditronix RFA300 scanning water tank and an electron diode in the same way as described in Section 2.2.3. The position of d_{max} was located from measured PDDs for each beam energy and electron field size at different SSDs.

Determination of output factors

The output factor(OF) is defined as the ratio of the absorbed dose in water at d_{max} on the central axis of the beam for the field of interest under the non-reference conditions to the reference field under the reference conditions for the same number of monitor units.

As recommended in the International Atomic Energy Agency Technical Report NO.398 (IAEA TRS-398)[5], the reference conditions used here were: field size of 10 cm $\times$ 10 cm, defined by the standard electron applicator supplied by Siemens at 100 cm SSD. Under these reference conditions, 6 MeV and 9 MeV

electron beams were calibrated with the Roos chamber at d_{max}, 1.3 cm and 2 cm, respectively. The Roos chamber was calibrated against the secondary standard in National Radiation Laboratory (NRL) in New Zealand and used to check the output of machine on the weekly basis.

The output factor (OF) of the electron arc cone was measured at the individual d_{max} for a specific field size and SSD. The OF for an electron field at a certain SSD is determined as[46, 1]:

$$OF(A) = \frac{D_{perMU}(A, SSD, d_{max})}{D_{perMU}(A_0, SSD_0, (d_{max})_0)} \tag{3.6}$$

where A is defined by the electron arc cone and the aperture shaper, whereas A_0 is the reference field size, 10 cm $\times$ 10 cm. SSD_0 is taken as 100 cm. Under these reference conditions, the depth of dose maximum, $(d_{max})_0$, is 1.3 cm for 6MeV and 2 cm for 9MeV. D_{perMU} is the absorbed dose to water per monitor unit at the depth of dose maximum.

The absorbed dose to water is linked to the readings of ionization chamber by following relation[3, 1]:

$$D_{water} = MN_{gas}\left(\frac{\bar{L}}{\rho}\right)_{air}^{water} P_{ion}P_{repl}P_{wall} \tag{3.7}$$

where M is the electrometer reading, N_{gas} is the cavity-gas calibration factor which is a constant, and P_{ion}, P_{repl}, P_{wall} are ion recombination factor, replacement factor, and wall correction factor, respectively. $\left(\frac{\bar{L}}{\rho}\right)_{air}^{water}$ is the Spencer-Attix restricted mass collisional stopping power ratio of water to air at measurement depth.

Substituting Eq.3.7 into Eq.3.6, one gets:

$$OF(A) = \frac{M_{perMU}(A, SSD, d_{max}) \times \left(\frac{\bar{L}}{\rho}\right)_{air}^{water} (A, SSD, d_{max}) \times P_{repl}(d_{max})}{M_{perMU}(A_0, SSD_0, (d_{max})_0) \times \left(\frac{\bar{L}}{\rho}\right)_{air}^{water} (A_0, SSD_0, (d_{max})_0) \times P_{repl}((d_{max})_0)} \tag{3.8}$$

where M_{perMU} is ionization reading per monitor unit.

The equation 3.8 was used to calculate the output factor for each electron arc field from the measurement. The measurements were performed with the Roos chamber for the open field and a small cylindrical chamber, Wellhofer CC13,

for other small fields to avoid the volume-average effect, which occurs when a large chamber is used for small field dosimetry[61]. The chamber readings were recorded using a Scanditronix Dose 1 electrometer[91]. The CC13 ionization chamber is water-proof and fully guarded with the active volume of 0.13 cm^3[90]. The active length of the cavity is 5.8 mm and the inner diameter of the cylinder is 6 mm. The diameter of the inner electrode is 1 mm. The effective point of measurement for CC13 is taken as $0.5r$, where r is the inner radius of chamber.

A small water tank made in-house, which is used for the absolute dosimetry every week, was also used for the measurements. It was made from Perspex with the physical size of 22 cm $\times$ 22 cm $\times$ 25 cm. The water phantom has a thin(1.8 mm) Perspex entrance window and a manual positioner. The water-equivalent thickness of the entrance window was taken into account when the chambers were positioned at each d_{max}. The Roos and CC13 chambers were positioned in the water tank using two specially designed holders with the precision of 0.5 mm.

A parallel beam geometry was used with the gantry and collimator angle of 270^0. The output factors for different SSDs and apertures were measured in one day. The output of the machine was checked using the Roos chamber for both 6 MeV and 9 MeV electron beam at the beginning and end of the measurement. The chamber was preirradiated by 3 Gy to stabilize them before starting measurements. The leakage of the chamber was also checked at the beginning. For each measurement, three readings were taken. The readings were corrected for temperature and pressure. As the measurements were taken over the course of several hours, the water temperature and room pressure were monitored through the course of measurement. The ion recombination and polarity effect, which are applied during the ionization dosimetry, were found to be very small, less than 0.1% and 0.4%, respectively. Previous investigations also showed that the polarization correction factor is independent of field size[105]. For these reasons, the ion chamber readings were not corrected for these factors. Another perturbation factor, P_{repl} is unity for Roos chamber. The variation of P_{repl} with depth for CC13 is approximately constant near the depth of maximum dose[3]. Therefore there is no correction for this factor when output factors were calculated

with Eq.3.8. For the two types of chambers, the measurement uncertainty was found to be less than $\pm 0.2\%$(one standard deviation).

3.2.3 Data analysis and curve fitting

The measured outputs for different electron arc fields were recorded into a Microsoft Excel spreadsheet. Similarly, the profiles can be exported directly into different worksheets of an excel file using the function provided by OmniPro 6 software. Before exportation, the profile was renormalized and smoothed. Then the area under the profile in Eq.3.4 was calculated by numerically integrating the profiles as follows:

$$A_{profile}(d_{max}, SSD, A) = \sum_{i=-s/2}^{i=s/2} f(s_i) \triangle s \tag{3.9}$$

where $A_{profile}(d_{max}, SSD, A)$ stands for the integration of the profile measured at d_{max} for field A at a specific SSD. $-s/2$ and $s/2$ are the scanning limits on either side of origin, respectively. $f(s_i)$ is the percentage dose value on the profile at the point, s_i, of the arc. $\triangle s$ is the interval between two adjacent points and is taken as 1mm.

The numerical integration of profile was done in Excel. Once the output factors and the area under the profile were tabled for each field and SSD, the dose per degree was calculated using Eq.3.5. For the calculation, the arc length l is chosen as 10 cm based on the profiles at 85 cm SSD. Sixteen tables of dose per degree were obtained for the combination of beam energy and field size. As the dose per degree is a function of not only the beam energy and SSD but also the field size, the dose per degree was plotted against field size and SSD for 6 MeV and 9 MeV beam. More than thirty two curves were graphed and some of them are presented in Section 3.3.

The curves were fitted either polynomially or linearly. For the detailed analysis of how the dose per degree varies with SSD and the width of aperture, see Section 3.3. The equations obtained by fitting the experimental data are presented here. The variation of the dose per degree with SSD for open field is

well described by the following second-order polynomial functions:

$$D^{flat}_{perdegree}(6MeV, SSD) = 0.0008SSD^2 - 0.1227SSD + 4.9047 \tag{3.10}$$

$$D^{flat}_{perdegree}(9MeV, SSD) = 0.0007SSD^2 - 0.0991SSD + 3.9116 \tag{3.11}$$

For a given SSD, the dose per degree varies linearly with the aperture width at the center of a trapezoidal or rectangular aperture:

$$D^{flat}_{perdegree}(6MeV, W) = 0.1587 \times W + 0.317 \tag{3.12}$$

$$D^{flat}_{perdegree}(9MeV, W) = 0.1885 \times W + 0.2231 \tag{3.13}$$

where W is the physical width of aperture at its center.

Based on the equations from Eq.3.10 to Eq.3.13, the dose per degree for a rectangular field or a trapezoidal field can be interpolated or extrapolated for a patient or a phantom with an arbitrary radius. Then the MUs required for delivering the prescribed dose D^{eArc}_{pres} in n fractions to d_{max} are:

$$MU^{eArc} = \frac{\frac{D^{eArc}_{pres}}{n}}{D^{flat}_{perdegree} \times C_{curv}} \tag{3.14}$$

where C_{curv} is the correction factor for the curvature.

The curvature correction is a rough attempt to account for the following fact: the beam travel being on a radial, rather than along the linear direction the absolute and relative dosimetry was performed. This is effectively compressing the delivered energy into a smaller volume, thus increasing the dose per degree[39]:

$$C_{curv} = \frac{100 - SSD}{100 - SSD - d_{max}(E)} \tag{3.15}$$

where $d_{max}(E)$ is the depth of maximum dose for open field and beam energy E.

3.2.4 Implementation of a MU calculation program

When the data acquisition and the fitting of dose-per-degree curves were finished, a monitor unit calculation program called "EarcMU" was developed to provide a convenient electron MU calculation platform for the physicists and radiation therapist in electron arc treatment. It was also used for the investigations for this thesis.

The program was written using Python programming language[70]. Python is a free but well-developed, dynamic object-oriented programming language that can be used for many kinds of software development. As shown in Fig. 3.3., the program has the following features: (1)It provides a user-friendly front end window. Two types of data input are required: patient information and treatment parameters. For the patient data, only the treatment radius is mandatory and all others will be given default values if they are left blank. In this case, the maximum and minimum radii equal the treatment radius. If they differ from the treatment radius, the program will calculate the dose at d_{max} for maximum and minimum radii; (2)It is based on the equations Eq.3.10 through Eq.3.15. As seen from above, the amount of measurement for commissioning this program is reasonable; (3)The calculated MUs, the electron dose at treatment, maximum and minimum radii, the patient records as well as the treatment parameters can be exported directly into an Excel file or a portable document file (PDF); (4)The EarcMU program is a platform-independent stand-alone program, which can run on the most popular operating systems, such as Windows XP, Linux and Macintosh.

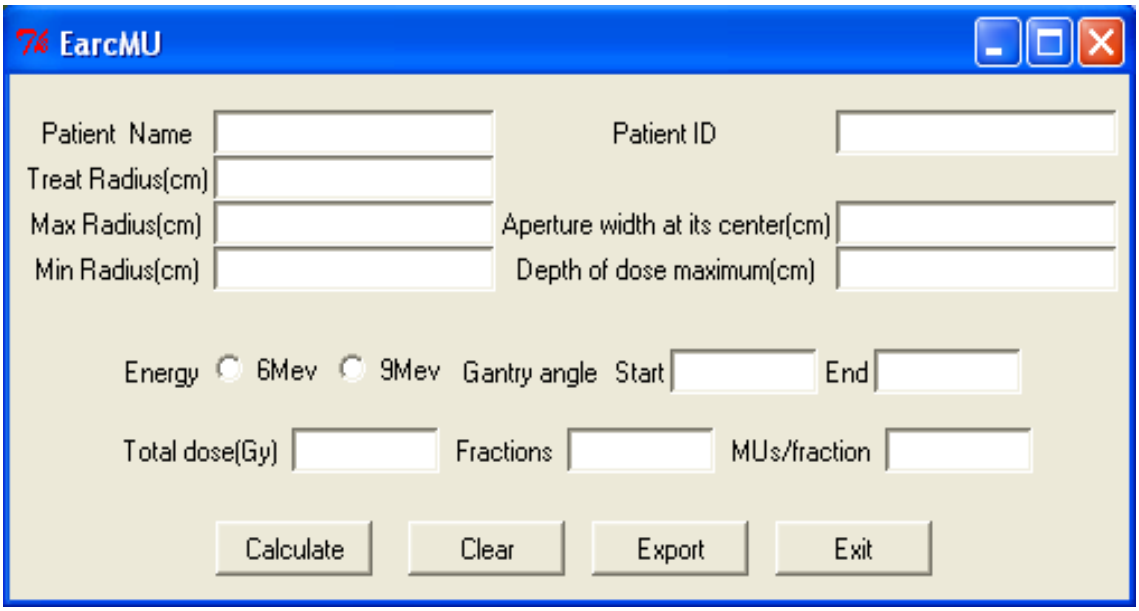

Figure 3.3: The graphic user interface of EarcMU program written in Python programming language.

3.2.5 Verification of EarcMU program

Before the EarcMU program was used clinically for treatment and for other investigations in this thesis, the calculated MUs from the program using the input parameters must be verified to make sure that the accuracy is acceptable. The goal of the EarcMU program verification is to (1) evaluate the accuracy of the MU calculated by the program in clinically relevant situations;(2) validate the determination of the beam parameters used in MU calculation algorithm.

Phantoms

To verify the EarcMU program, as shown in Fig. 3.6 and Fig. 3.7, two cylindrical water phantoms were employed. The big cylindrical phantom was designed to represent the typical treatment conditions encountered in electron arc treatment. The radius of this phantom was chosen to represent the typical radius of a patient chest wall. From the treated patients with breast cancer, it was found the radius of patient chest wall falls between 15 cm and 20 cm. The small cylindrical phantom is used to test the limits of the mathematical model underlying the MU calculation. It is assumed to work well for the patient with large radius and small curvature. Another purpose is to check the validity of curvature correction used in final MU calculation.

The large phantom was made from Poly Methyl Methacrylate(PMMA). Its radius is 16 cm and the thickness of side wall is 0.8 cm. The diameter and thickness of two circular ends are 38 cm and 2.3 cm, respectively. One end is fixed to cylindrical body and the other is a removable lid. The lid is tightly fitted into the cylinder using a nylon screws and a rubber O ring seal. The phantom was first filled with water to ensure there were no air bubbles inside, the lid replaced and screwed down. This ensures that there was no water leakage during the measurement.

The small phantom with radius of 9 cm and length of 23 cm is just a plastic bucket bought from a supermarket. It was also filled with water and sealed with a small plastic lid. The length of phantom is considered to be enough to provide the

longitudinal scattering equilibrium for 6 MeV and 9 MeV electron beam under the measurement conditions.

Dosimeters

The ideal detectors for the measurement of a point dose in electron arc beam have a small sensitive volume, dose rate independence and minimum corrections to the raw readings. Three types of dosimeters were used for the EarcMU verification measurement: a Scanditronix RK thimble ionization chamber(type RK8304 No.1283), metal-oxide-silicon semiconductor field-effect transistor(MOSFET) dosimeters (Thomson Nielson MOSFET 20) and Gafchromic® EBT film. The dimensions of the detectors used are summarized in Table 3.1.

Table 3.1: Geometric features of the employed dosimeters.

Scanditronix	Cavity volume:	Cavity length:	Cavity radius:
RK chamber	0.12cc	10mm	2mm
Thomson Nielson	Sensitive area:		
MOSFET20	$0.04mm^2$		
Gafchromic®film	Sensitive volume thickness:		
EBT QD+	$17\mu m$		

A. RK chamber

The Scanditronix RK chamber is a small cylindrical unsealed air ionization chamber intended for measurements in water or a water equivalent solid phantom. Although the physical size of the chamber is larger than the other dosimeters, it is still considered to be relatively small compared to the field sizes used in measurement. Furthermore, the point-dose measurement does not require very high resolution as was for the measurement of PDD and profiles. The RK chamber was chosen to provide a reference. It was calibrated against the local reference dosimeter: a Farmer electrometer(type 2570/1 SN.1311) plus Wellhofer FC65-G chamber(type NE2570/1 SN. 457), which was calibrated by National Radiation

Laboratory(NRL) in New Zealand following IAEA TRS398 protocol.

The RK chamber was cross calibrated together with Theradose dual channel electrometer, which is shown in Fig. 3.6(A). The bias voltages were -200 V for RK chamber and -250 V for the reference chamber. The calibration followed the standard procedure provided in TRS398. The first step is to get the chamber's calibration factor using the highest electron energy beam(18 MeV) as follows:

$$N^{RK}_{D,W,Q_{cross}} = \frac{M^{ref}_{Q_{cross}}}{M^{RK}_{Q_{cross}}} N^{ref}_{D,W,Q_0} k^{ref}_{Q_{cross},Q_0} \tag{3.16}$$

where $N^{RK}_{D,W,Q_{cross}}$ is the calibration factor of RK chamber in terms of beam quality Q_{cross}(18 MeV). N^{ref}_{D,W,Q_0} is the calibration factors of local reference dosimeter, which was obtained in terms of ^{60}Co. $M^{RK}_{Q_{cross}}$ and $M^{ref}_{Q_{cross}}$ are the charges collected by the RK chamber and reference chamber, respectively. The readings from both chambers were corrected for pressure and temperature, polarization and ion recombination for both chambers. The quality conversion factor for reference chamber, $k^{ref}_{Q_{cross},Q_0}$ was interpolated from the data provided in IAEA TRS398[5].

The second step is to determine the quality conversion factor, $k^{RK}_{Q,Q_{cross}}$, for RK chamber in 6 MeV and 9 MeV electron beams. The $k^{RK}_{Q,Q_{cross}}$ is not tabulated in the protocol for RK chamber. it was experimentally measured using PTW Roos chamber as a reference, whose quality conversion factor $k^{Roos}_{Q,Q_{cross}}$ are tabulated[7, 5]. This method is the same as the Karaj et al. used[36]. Specifically, the 6 MeV and 9 MeV electron beams produced by the Primus accelerator were employed to perform the measurements with both chambers under the reference conditions as listed in Table 3.2. The experimental values of $k^{RK}_{Q,Q_{cross}}$ for RK chamber were obtained by:

$$k^{RK}_{Q,Q_{cross}} = \frac{N^{Roos}_{D,W,Q_{cross}} M^{Roos} k^{Roos}_{Q,Q_{cross}}}{N^{RK}_{D,W,Q_{cross}} M^{RK}} \tag{3.17}$$

where $N^{Roos}_{D,W,Q_{cross}}$ and $N^{RK}_{D,W,Q_{cross}}$ are the cross calibration factors for RK and Roos chamber in 18 MeV electron beam, respectively. M^{Roos} and M^{RK} are Roos and RK chamber readings corrected for temperature and pressure.

Once the RK chamber was calibrated, the factors were verified under the reference conditions. The calibration and verification were performed on two different days. The verification procedure and setup are exactly the same as the

one used for checking the output of machine with the in-house made little water tank and Roos chamber[43]. The Roos chamber was calibrated following TRS398 and used to calibrate electron beams available on the Primus linear accelerator on a weekly basis. The 6 MeV and 9 MeV electron beams were calibrated to deliver 1 cGy/MU at the maximum-dose depths. For the RK and Roos chambers, the dose is calculated as $D_w = M^x\, K^x_{total}$, where the total dosimetric factor is $K_{total} = N^x_{D,\,w,Q_{cross}} k^x_{Q,Q_{cross}}$ and M^x is the chamber readings (nC) corrected for temperature and pressure. Here the superscript x stands for either the Roose chamber or RK chamber. The calibration and verification results are shown in Table 3.2 and 3.3, respectively. The results clearly show that the calibrated RK chamber gives 1 Gy/100MU within 1% under the reference conditions, which validated the calibration factors obtained for RK chamber.

The RK chamber was used to measure the absolute dose at the depth of maximum dose in a rotational electron beam. The dose was determined as the ratio of dose measured under the electron arc treatment conditions to the dose under the reference conditions, which was calculated using Eq.3.8.

Table 3.2: Results of RK chamber cross calibration.

Chamber	Reference	Field
	NE2571 chamber	RK chamber
N^{NE2571}_{D,W,Q_0}(Gy/nom.Gy)	0.986	
Nominal energy(MeV)(Q_{cross})	18	18
R_{50}(g cm^{-2})	7.67	7.67
SSD(cm)	100	100
field size(cm $\times$ cm)	10×10	10×10
z_{ref}(cm)	4.5	4.5
$N^{RK}_{D,W,Q_{cross}}$(Gy/nom.Gy)		0.050134252
$N^{RK}_{D,W,Q_{cross}}$(Gy/nC)		0.0024538779

Table 3.3: RK chamber verification results.

Chamber	RK chamber	
Nominal energy(MeV)	6	9
SSD(cm)	100	100
Field size(cm × cm)	10 × 10	10 × 10
z_{ref}(cm)	1.3	2
$k_{Q,Q_{cross}}$	1.04408	1.03363
K_{total}(Gy/nC)	0.002562	0.002536
MUs	100	100
Averaged Readings(nC)	390.056	395.291
Dose to water $D_W(z_{ref})$(Gy)	0.9993	1.003

B. MOSFET dosimeter

The MOSFET dosimeter offers several advantages, including dose rate independence, permanent storage of dose, immediate retrieval of the measured dose, immediate reuse and its ability to conduct multiple dose measurements. The patient dose verification system model TN502RD manufactured by Thomson & Nielson was used. The TN502RD is a standard, isotropic product with less angular-dependence response[101]. As shown in Fig3.7., the TN502RD dosimeter consist of three parts:(A)a reader with a liquid crystal display;(B)A 9-V bias supply box;(C) the MOSFET detector bonded with an expoxy to the end of a 20 cm-long flexible cable, resulting in a flat surface on one side and a rounded,1-mm-thick epoxy coating on the other.

Four MOSFETS were placed at the point of measurement. They were connected to two bias voltage supply boxes, labeled with letter B and C by manufacturer, respectively. Each box has five channels numbered from 1 to 5, allowing five detectors to plug into the same box. The MOSFET detectors are identified by the combination of box name and channel number. In this case, they are labeled as B4, B5, C2 and C3. Each MOSFET detector is a dual bias, dual MOSFET transistor. Two identical MOSFETS were fabricated on a silicon chip,

each operating at a different positive gage bias. Its structure and how it works are described by Soubra et al.[95]. Basically, before exposure, when a negative voltage is applied, an appreciative amount of current flows between the source and the drain: the threshold voltage is defined as the gate voltage needed to allow a predetermined current to flow from source to drain. Exposing the detector to radiation causes a negative shift of the threshold voltage that is proportional to the dose. This voltage shift is directly read out by the reader.

To measure absolute dose, each MOSFET also needs to be calibrated individually to convert the voltage shift in mV to the absolute dose value in cGy. The calibration factors were determined using the Plastic Water® slabs under the reference conditions(10 cm × 10 cm field size and 100 cm SSD). The Roos chamber was first used to check the outputs at d_{max} for 6 MeV and 9 MeV beams. A MOSFET was then placed at same depth on the central axis of beam and irradiated under the same conditions with fully backscattering. The calibration factor, CF, is calculated as follows:

$$\text{CF} = \frac{\text{MOSFET reading(mV)}}{\text{dose(cGy)}} \tag{3.18}$$

The CFs given in Table 3.4 were used to convert the voltage shift to dose. The effective measurement point of MOSFET detector was taken as the center of its sensitive volume. The bias supply voltage provides two bias settings: low and high sensitivity. The high sensitive setting was used for the measurement and dose reproducibility is within 1.2% for the dose range of around 1 Gy . As the measurement is to be performed on a cylindrical phantom, the angular dependence of MOSFET used was verified to be less than ±1.5% through 120 degrees of rotation.

Table 3.4: MOSFET calibration factors(mV/cGy).

Energy(MeV)	B4	B5	C2	C3
6	2.855	2.91	2.88	2.805
9	2.79	2.86	2.84	2.815

For dose measurement, the MOSFET detectors are plugged into the bias box,

which is connected to the reader through an interface cable. Before irradiation, the zeroing function of the reader was used to get the total threshold voltage. Then the reader is disconnected from the bias box. Four MOSFETS were placed and taped into the measurement point with the flat surface facing the beam. After the irradiation, the reader was reconnected to the bias box and the read function was used to get the the threshold voltage shift in milivolts by depressing the key on the front panel of the reader. For the description of operation procedure in details, the reader is referred to reference[101].

C. EBT Gafchromic® film dosimeter

Gafchromic® film has been used widely not only for the measurement of relative dose distribution, but also suitable for the absolute dosimetry. It gives permanent values of absorbed dose with an acceptable accuracy and precision[20, 103].

Before the film was used for the dose measurement, it was calibrated. Several film pieces from two different sheets were cut to approximately 4 cm $\times$ 4 cm and the orientation on each film was marked. The film pieces were then irradiated on the Siemens machine to the following doses: 5, 10, 15, 20, 40, 60, 80, 100, 120, 140, 160, 180, 200, 220, 240, 260, 280 and 300cGy. The films were placed horizontally inside a solid Plastic Water® slab phantom of 30 cm $\times$ 30 cm size and placed on central axis of 10 cm $\times$ 10 cm field at the depth of maximum dose.

The optical density(OD) of exposed film was read using a spot densitometer(Pehamed Normscan). The densitometer operates at 9.5 V supplied by a power adapter. The repeatability and uncertainty of OD measurement are both less than 2% within the measuring range between 0 and 4.5. The same calibration measurement was repeated on a different day. The average values of OD from films irradiated to the same dose were recorded. The irradiated films were read 24 hours after exposure to allow the color to stabilize[69]. The net OD was calculated by measuring the OD($OD_{measured}$) of the calibration pieces first and extracting the mean background OD value of a unexposed film piece($OD_{background}$). The net OD for each film was expressed as $OD_{net} = OD_{measured} - OD_{background}$. The calibrated Roos chamber was inserted in the phantom at d_{max} to check the linac

output before, after and between film calibration.

The plot of the averaged net OD with respect to the delivered dose is displayed in Fig. 3.4 and Fig. 3.5. The measured OD values are reproducible and well within 2% over the entire delivered dose range. There was no detected change observed in the linac output during the calibration measurement. The fitted curve, represented by the solid line, is composed of two separate fits, the linear one for the dose region around 1 Gy and the third-order polynomial fitting for all data points. A dose uncertainty of 3% was measured for the dose range between 40 cGy and 250 cGy and 4% for the lower dose range less than 40 cGy and above 250 cGy. The linear portion of the calibration curve was used to convert the ODs of film pieces exposed in electron arc beam to the absolute dose. During the measurement,the effective measurement point of film piece was assumed to be at the center of the sensitive layer of film.

Experimental setup and procedure

Although two phantoms and three dosimeters were used in the measurement, the experimental setup and procedure were essentially same. Fig. 3.6 and Fig. 3.7. show the phantom setups and the dosimeters. The following procedure was followed:

1. The cylindrical phantom was placed on the couch. The phantom was then aligned so that its longitudinal axis coincided with the rotational axis of gantry. The center of longitudinal axis of the phantom was set at the isocenter of linac.

2. The dosimeter(RK cylindrical chamber, MOSFETs, or a 4 cm $\times$ 4 cm piece of film)was placed on the phantom surface or the surface of bolus, which was draped on the phantom. The detector was positioned carefully along the longitudinal direction of the field to make sure its sensitive volume received uniform dose. In addition, the effective measurement points of detectors were aligned to be on the central axis of the field with zero gantry and collimator angle using the crosshair of reticule.

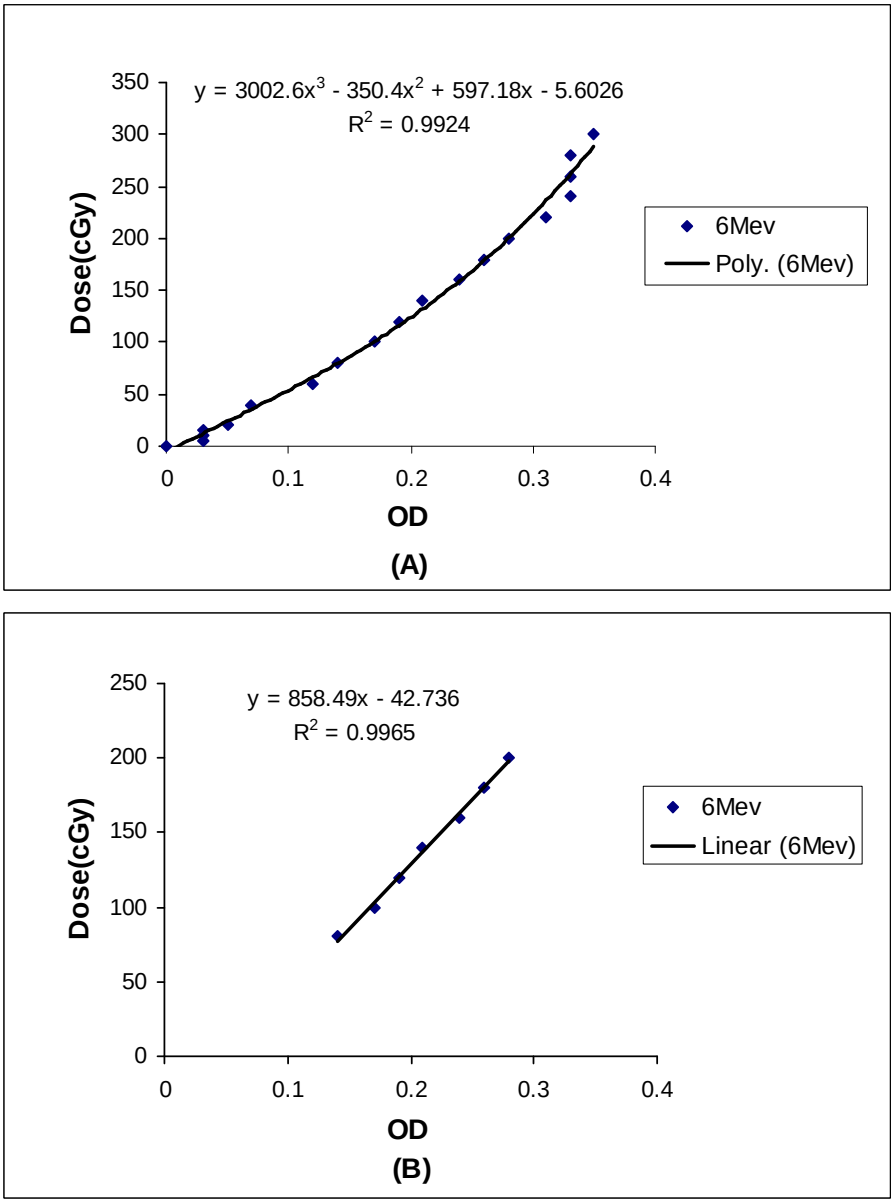

Figure 3.4: (A)EBT Gafchromic film calibration curve for the 6 MeV electron beam obtained with a sport densitometer. (B)The linear portion of the curve between 80 cGy and 200 cGy.

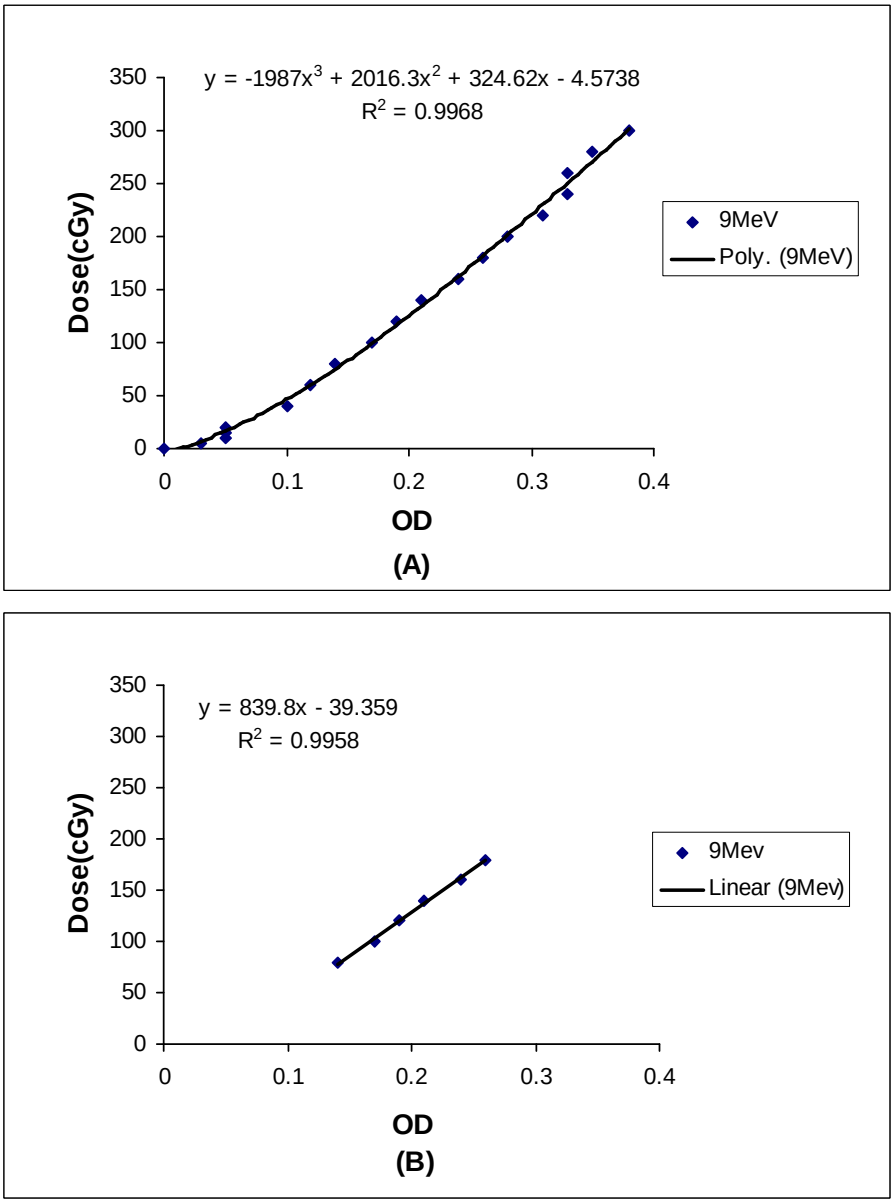

Figure 3.5: (A)EBT Gafchromic film calibration curve for the 9 MeV electron beam obtained with a sport densitometer. (B)The linear portion of the curve between 80 cGy and 200 cGy.

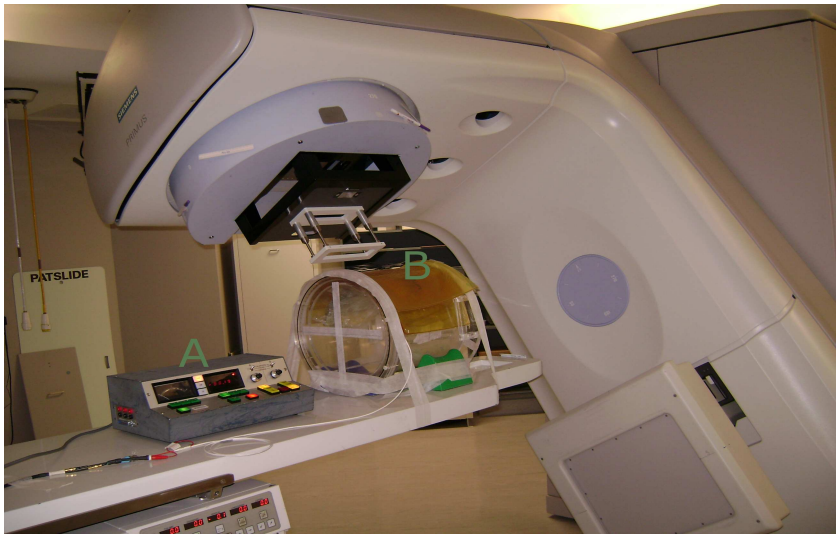

Figure 3.6: The experiment setup for EarcMU program verification using a large radius cylindrical phantom: (A)the Therodose electrometer (B)the large cylindrical water phantom with bolus sheets draped over the RK Chamber. Note that Therodose electrometer was in the control room during the measurement and that this photo of the phantom setup along with dosimeter was taken after finishing measurement.

Figure 3.7: Experiment setup for EarcMU program verification using a small radius cylindrical phantom: (A)the MOSFET reader (B)two bias supply boxes (C)the small cylindrical water phantom with four MOSFET detectors taped on its surface. Note that the MOSFET reader was in the control room during the measurement and that this photo of the phantom setup along with dosimeter was taken after finishing measurement.

3. A number of bolus sheets with different thicknesses were draped over the detectors to provide the depth of measurement. The sheets of bolus were placed carefully, ensuring there was no air gaps between them.

4. The phantom was set to the desired SSD calculated as $100 - r$, where r is the radius of phantom taking into account of the bolus. Then the arcs for both energies were determined. In our case, a 90^0 arc was used for the large radius phantom, whereas 120^0 for the small phantom.

5. The treatment parameters(phantom radius, arc angle and field size) were input into the EarcMU program. The program was used to calculate the MUs required for delivering 1 Gy to the d_{max}. Then the linac was programmed and the electron arc treatment was delivered with the zero collimator angle. The beam was rotated from one half arc angle to the opposite angle going through the zero angle position either in clockwise direction or anti-clockwise direction.

6. Once the setup was finished, the phantom was left in the room for the period long enough to establish temperature equilibrium before the measurement began. Temperature and pressure were checked throughout the measurement. The accelerator was brought to operating equilibrium before measurement by running 500 monitor units. Measurement was repeated three times for ion chamber measurement. The dose measured with MOSFETs was averaged from four dosimeters. The mean OD of each film piece was averaged over four readings of spot densitometer.

3.3 Results and discussion

3.3.1 Measured dose per degree

A. Dose per degree for open field

The dependence of dose per degree on the SSD for the open field is plotted in Fig. 3.8. For both 6 MeV and 9 MeV electron beams, the variation of dose per degree with SSD displays similar trends. It shows a slow increase of dose

per degree with increasing SSD initially and followed by rapidly increasing. The turning point is around 85 cm SSD, which corresponds to the typical chest wall radius of patient(15 cm). For a given arc angle and beam energy, if the curvature of patient is changed either in traverse plane or midsagittal plane, the dose at d_{max} could be changed dramatically. For example, suppose the treatment radius of patient is 15 cm and variation of radius from superior to inferior is 2 cm, the dose non-uniformity is 10.1%.

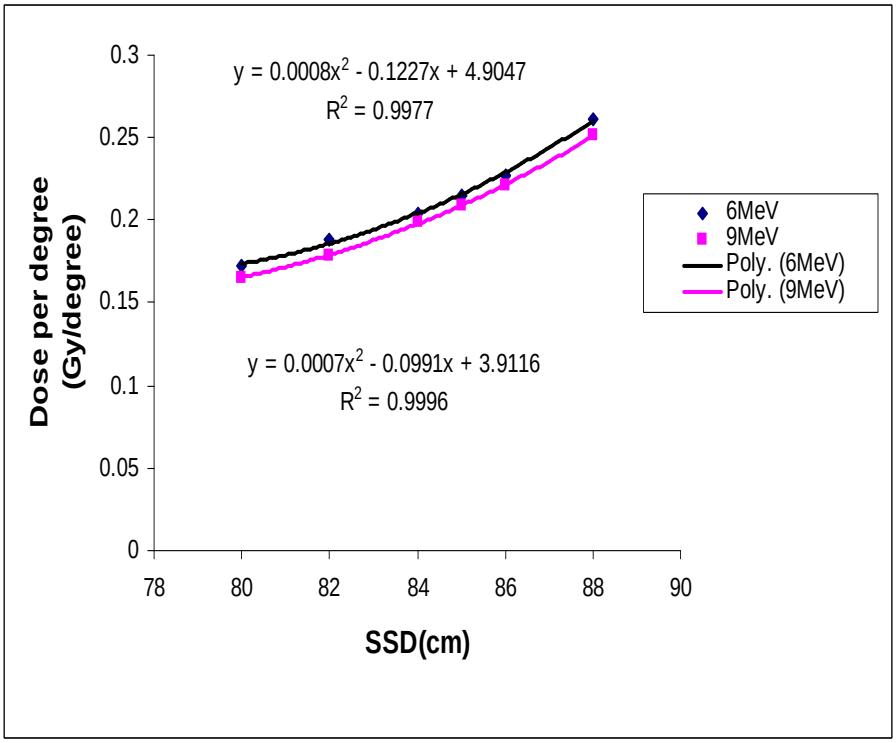

Figure 3.8: The variation of dose per degree with SSD for the open field.

The trend displayed by the dose-per-degree curve is the combination of the dose rate at d_{max} and the area under the profile. The dose rate follows the effective inverse square law, decreasing with the increase of the effective SSD. On the other hand, the profile becomes wider and wider when the SSD is increased. As a result, the area under the profile is increased with SSD. The profile area increase dominates the decrease of dose rate, leading to monotonically increasing of dose per degree with SSD.

For both energies, this increase is well fitted by a second-order polynomial.

It means that, for the treatment with open field, these polynomials can be used to predict the dose per degree for an arbitrary radius in the range between 20 cm and 10 cm, which correspond to the maximum and minimum SSD limits of electron arc machine.

B. Dose per degree for rectangular fields

Variation of dose per degree with SSD

Fig. 3.9 shows the change of dose per degree with SSD for different rectangular apertures. Four rectangular apertures are chosen to represent the typical range of physical dimension that may be encountered in a clinical situation. They all show a similar trend as open field displayed.

For a given SSD and energy, the dose per degree increases with the aperture width. This is because of the field size dependence of output due to the lack of lateral electron equilibrium. It is well-known that the output increase with the field size when the physical dimension of field is less than the practical range of the electron beam. The widest aperture(3.5 cm) is much smaller than the practical range of the 9 MeV electron beam(4.5 cm) and on the order of the 6 MeV practical range(3 cm). This also explains why the dose per degree for 9 MeV is less than that for 6 MeV at a given SSD, which is clearly seen in Fig. 3.8 and by the comparison between Fig. 3.9(A) and Fig. 3.9(B).

Variation of dose per degree with the physical width of applicator aperture

The dose per degree is plotted, in Fig. 3.10 , against the physical width of the rectangular aperture of electron arc applicator. Notice that the dose per degree for the aperture is normalized to that of open field.

There are three points that are worth to be emphasized here: (1)The normalized dose per degree linearly increases with the physical width of rectangular aperture. The curves are fitted very well using a linear fitting with the confidence of 99%;(2)The change of normalized dose per degree with aperture width is also

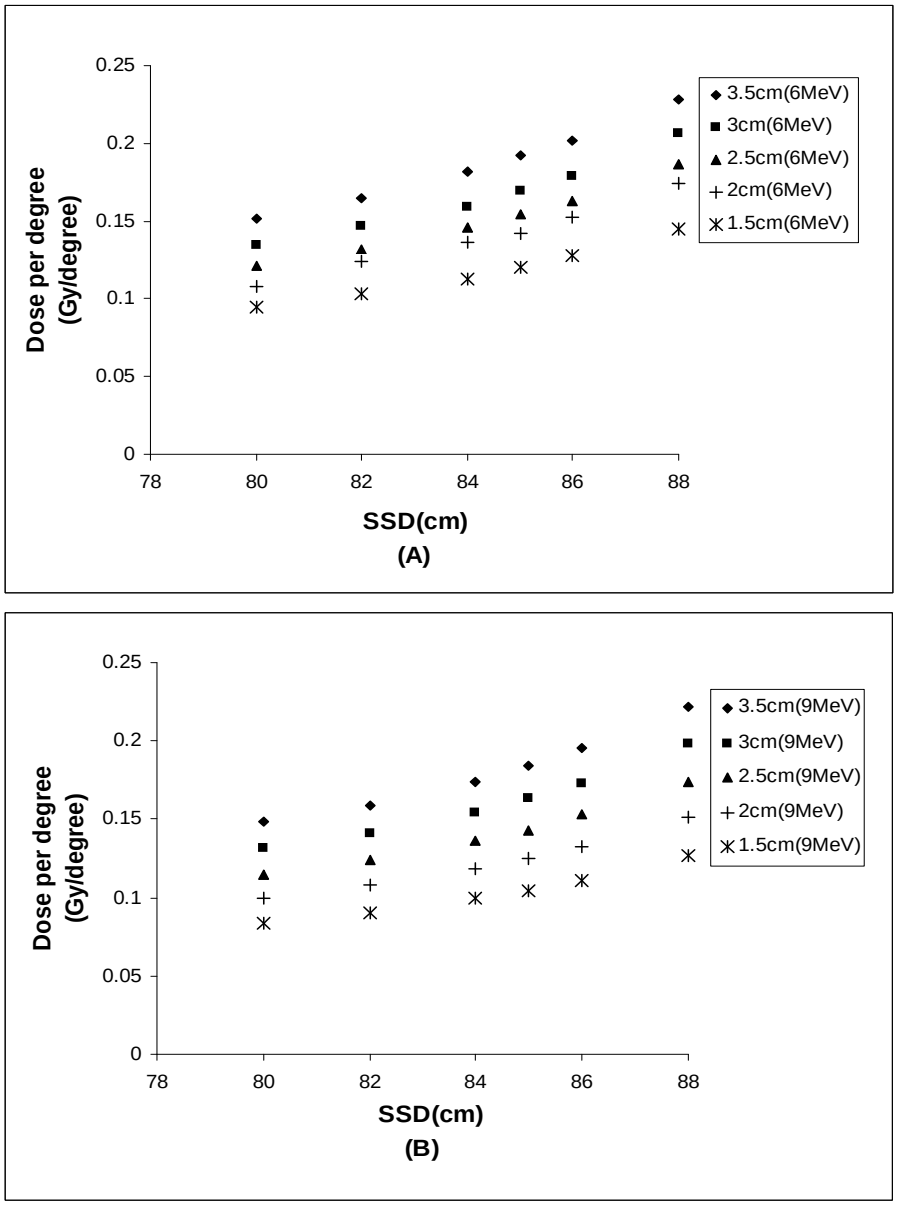

Figure 3.9: The variation of dose per degree with SSD for different rectangular apertures:(A) for 6 MeV electron beam (B) for 9 MeV electron beam.

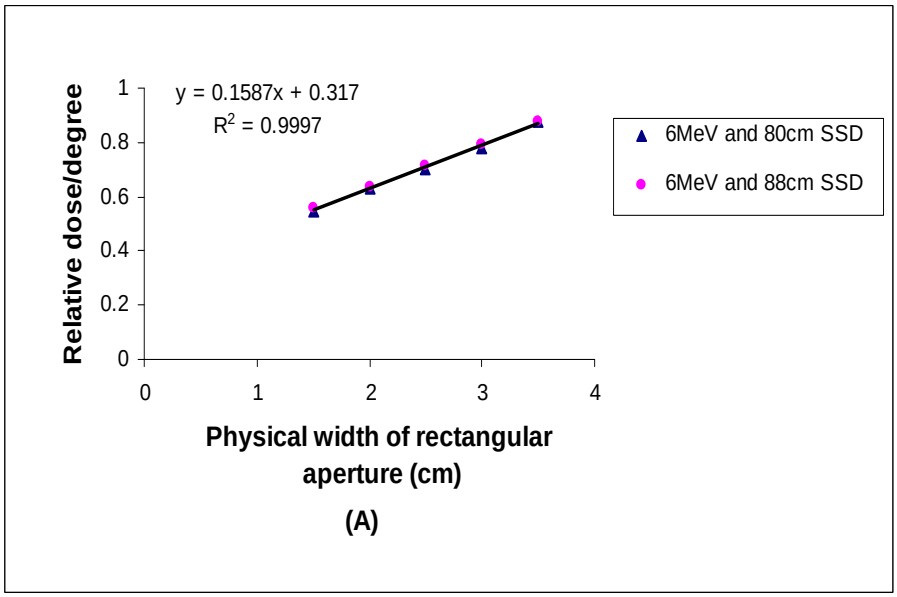

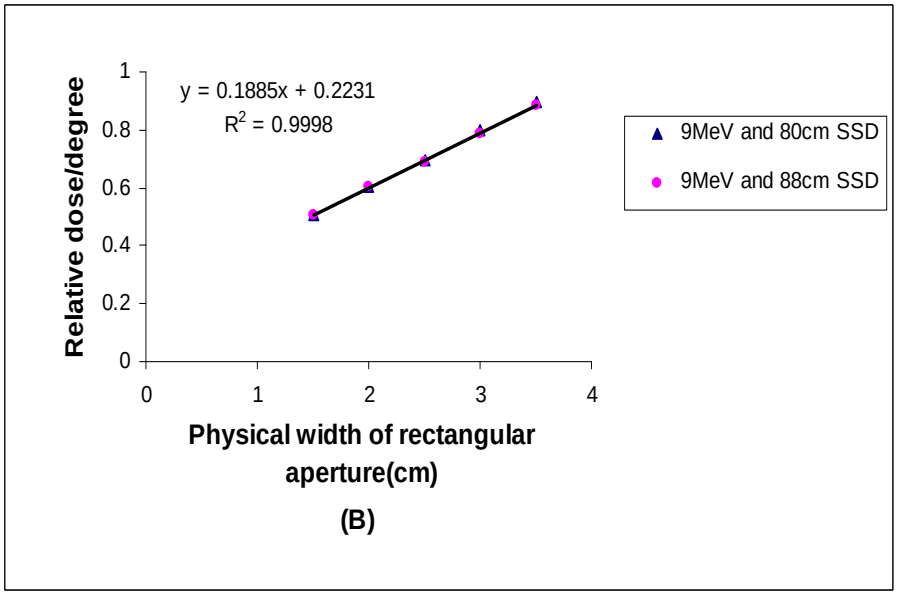

Figure 3.10: The dose per degree versus the physical width of rectangular aperture:(A)for 6 MeV electron beam (B) for 9 MeV electron beam. Note that the dose per degree is expressed as ratio of the rectangular shaped aperture to the open aperture.

independent of SSD. The data for shortest and longest SSD are only drawn in the figures;(3)The dose per degree for any rectangular aperture can be interpolated from the curves shown in Fig. 3.10 and Fig. 3.8 using the fitted polynomials.

C. Dose per degree for trapezoidal fields

Variation of dose per degree with SSD

For the trapezoidal aperture, the dose per degree at the field center on the central axis changes with SSD in the same way as a rectangular field does.

The results are shown in Fig. 3.11(A) and Fig. 3.11(B) for 6 MeV and 9 MeV beams, respectively. The dose-per-degree curves are parallel to each other as seen before. As expected, the dose per degree is larger for the wider aperture than for the narrower aperture. For the same reason as discussed above for the rectangular field, the dose per degree of 6 MeV is also less than that of 9 MeV electron beam.

Comparison between trapezoidal field and rectangular field

To investigate the relationship of dose per degree between rectangular apertures and trapezoidal apertures, the dose-per-degree curves of the trapezoidal apertures are plotted together with those of the rectangular apertures.

The width of trapezoidal aperture at its center is equal to the width of the rectangular aperture. Considering the the range of typical aperture dimensions that may be used in clinical treatment, three pairs of apertures are chosen: 4 cm-by-3 cm trapezoidal versus 3.5 cm rectangular, 4 cm-by-2 cm trapezoidal versus 3 cm rectangular and 4 cm-by-1 cm trapezoidal versus 2.5 cm rectangular.

The results are shown in Fig. 3.12. Taking into account the measurement uncertainties, it is clearly seen that the dose per degree of a trapezoidal aperture is the same as that of a rectangular aperture, whose width equals the width of the trapezoidal aperture at its center. This is because of the equivalence of a trapezoidal aperture and a rectangular aperture, as discussed in Section 2.15 in Chapter 2. The results are clinically significant. It means that the monitor

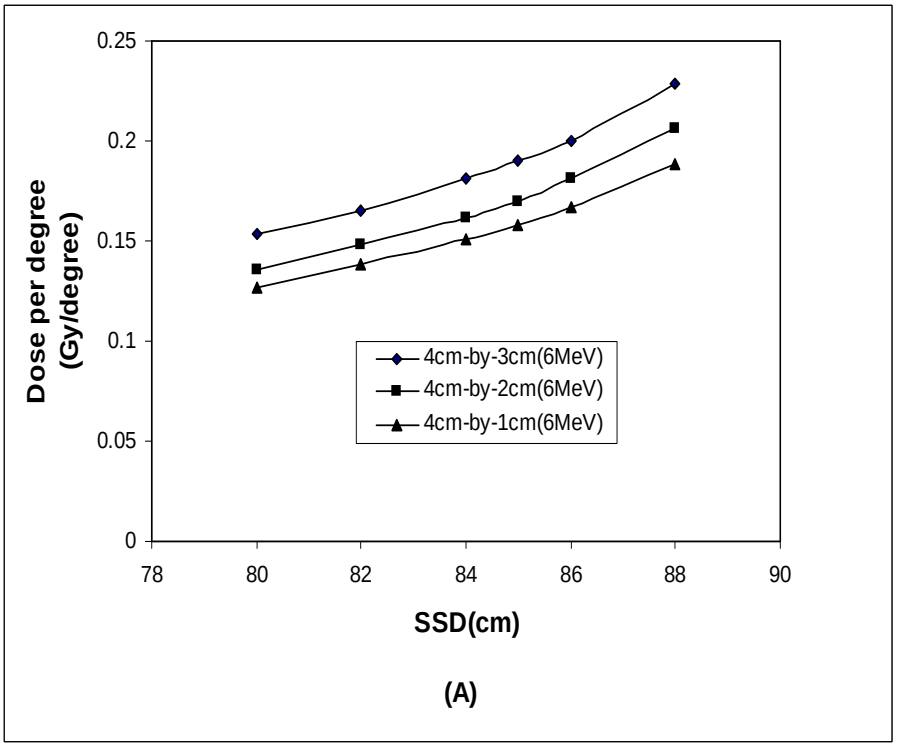

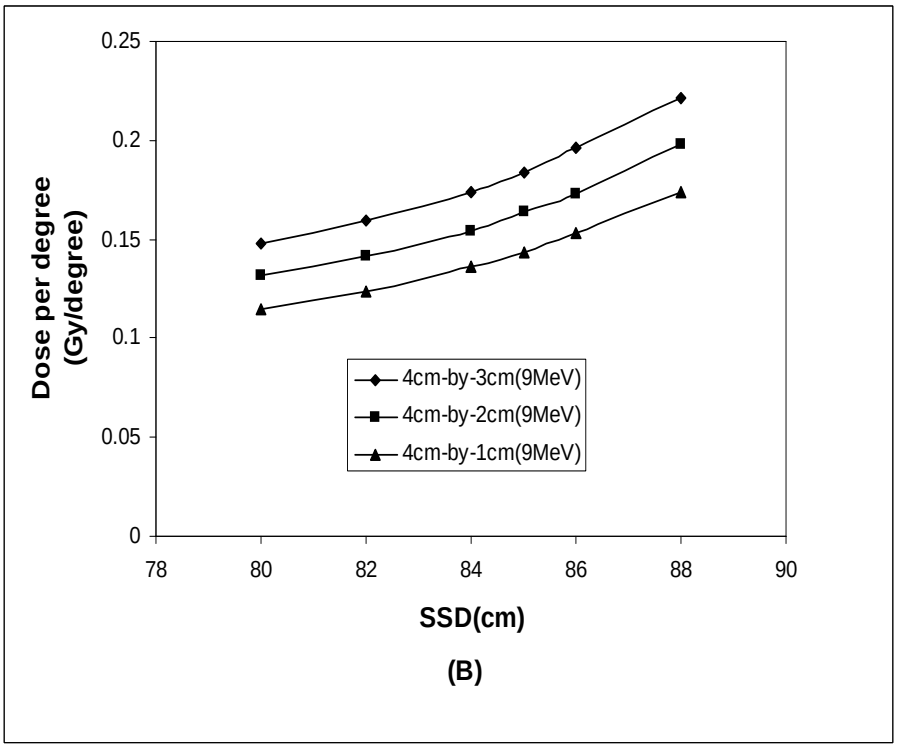

Figure 3.11: (A) The variation of dose per degree with SSD for different trapezoidal apertures and 6 MeV electron beam (B) The variation of dose per degree with SSD for trapezoidal apertures and 9 MeV electron beam.

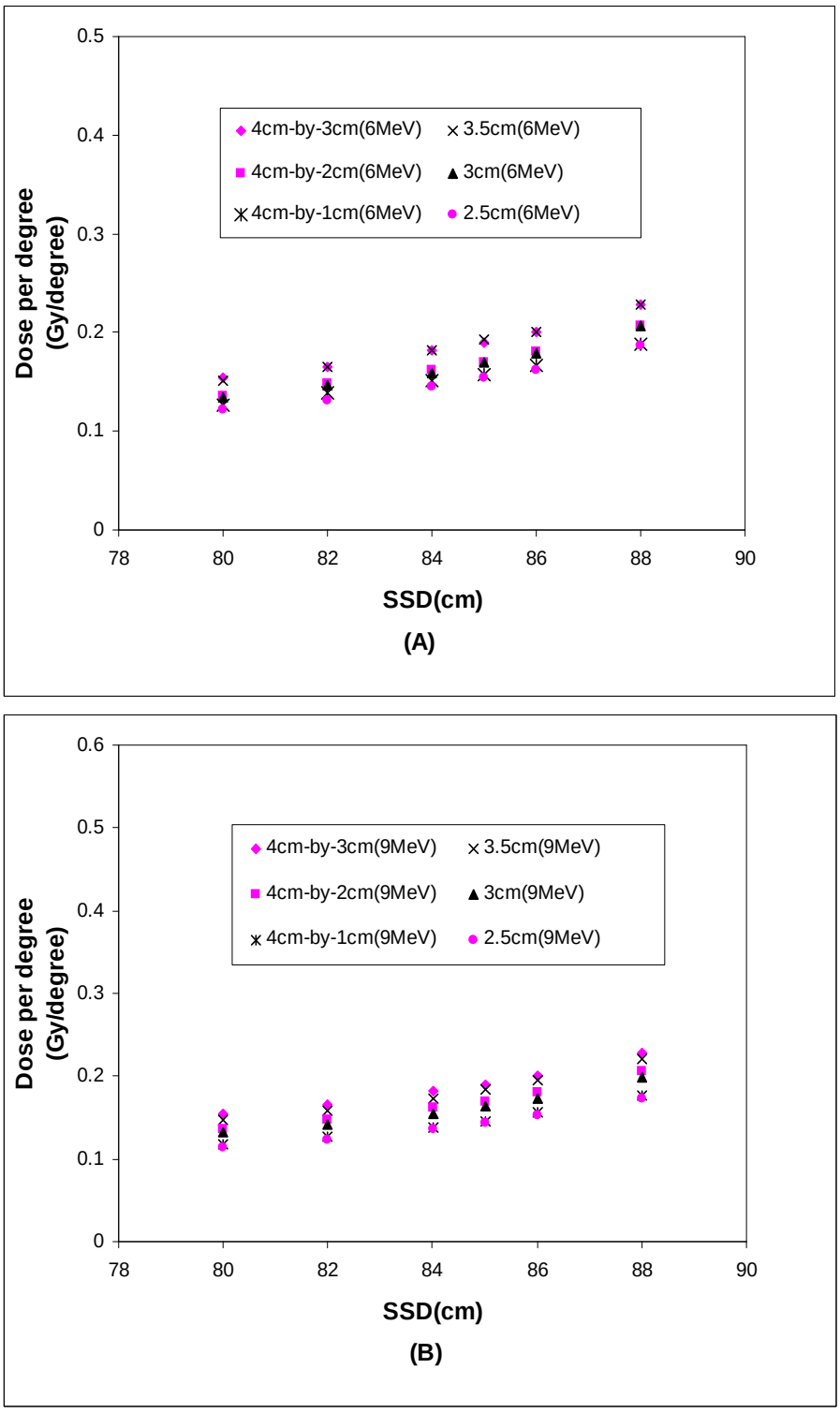

Figure 3.12: Comparison of the dose per degree between a trapezoidal aperture and its equivalent rectangular aperture for (A) 6 MeV electron beam (B) 9 MeV electron beam. The width of trapezoidal aperture at its center equals the width of the rectangular aperture.

units for a trapezoidal aperture can be calculated using its equivalent rectangular aperture.

3.3.2 Comparison between the measured dose and the dose predicted by EarcMU program

A. Results for the large cylindrical phantom

As mentioned in Section 3.2.5, the phantom was designed to represent a typical radius of patient chest wall. The purpose of the experiment using the big cylindrical phantom is to verify how accurately EarcMU program predicts the doses delivered to the d_{max} by comparing them with the measured doses. A series of experiment was performed during the verification measurement.

Open field

The first experiment was done using the electron arc cone with the open aperture. The treatment radius was chosen as 18.5 cm for both the 6 MeV and 9 MeV electron beams. The gantry was rotated from -45^0 to 45^0 in clockwise or anti-clockwise direction. The planned dose to be delivered to the depth of maximum dose was set as 100 cGy. Once these treatment conditions were determined, EarcMU program calculates the MUs required to deliver 100 cGy dose to d_{max}. In this case, the number of MUs required are 445 aand 423, respectively, for 6 MeV and 9 MeV. The results measured with MOSFET and RK chamber are shown in Table 3.5 and Table 3.6, respectively.

The doses measured with RK chamber and MOSFET agree very well with the doses predicted by EarcMU program. The difference between the measured dose and the planned dose is less than 1.3% for 6 MeV electron beam and less than 1% for 9 MeV electron beam. The difference between measured and predicted doses for 6 MeV is slightly higher than the difference for 9 MeV. It may be due to the fact that the 6 MeV electron beam is much more scattered by the electron arc applicator than the 9 MeV electron beam. The difference measured with RK chamber is 1.25%, whereas the difference measured with MOSFET is 1.15%.

Table 3.5: Comparison between the dose predicted by EarcMU program and the dose measured with MOSFET.

Beam Energy(MeV)	6	9
Field size(cm × cm)	open	open
SSD(cm)	81.5	81.5
d_{max}(cm)	1.5	2.5
Arc angle(degree)	90	90
MUs required	445	423
Dose planed(cGy)	100	100
Dose measured(cGy)	101.156	100.046
Difference(%)	1.14	0.046

Table 3.6: Comparison between the dose predicted by EarcMU program and the dose measured with RK chamber.

Beam Energy(MeV)	6	9
Field size(cm × cm)	open	open
SSD(cm)	81.5	81.5
d_{max}(cm)	1.5	2.5
Arc angle(degree)	90	90
MUs required	445	423
Dose planed(cGy)	100	100
Dose measured(cGy)	101.25	100.98
Difference(%)	1.25	0.98

Rectangular apertures versus trapezoidal apertures

The second experiment was performed by shaping the aperture of the electron arc applicator into different rectangular and trapezoidal shapes. The aim of this experiment was to verify that(1)the equivalence of a trapezoidal aperture and a rectangular aperture;(2)if the polynomials fitting the curves shown in Fig. 3.10 can be used to accurately calculate the MUs for rectangular and trapezoidal apertures to deliver the desired dose to d_{max};(3)how precisely the EarcMU program can calculate the MUs for both rectangular and trapezoidal fields.

Except for the shape and size of the trapezoidal aperture, the rest of treatment parameters are the same as those used for open field. The measurement was done first for a trapezoidal aperture then for its equivalent rectangular aperture. Two pairs of apertures were used: 4 cm-by-3 cm trapezoidal versus 3.5 cm rectangular, 4 cm-by-2 cm trapezoidal versus 3 cm rectangular. The width of the rectangular aperture along with other beam parameters are input into the EarcMU program. The program calculated the number of MUs required for both rectangular and trapezoidal apertures. Each pair of apertures use the same MUs.

A comparison of the doses measured with RK chamber and the doses predicted by EarcMU program is shown in Table 3.7 and Table 3.8 for the trapezoidal apertures and their equivalent rectangular apertures. For the rectangular apertures, the actual delivered doses differed from the planned doses, on average, only by 1.02%. The largest difference was 2% for 3 cm rectangular aperture and 9 MeV electron beam, while the smallest was 0.23 % for the 3.5 cm and 6 MeV electron beam. It also can be seen that the difference tends to be larger and larger when the width of the rectangular aperture becomes narrower and narrower. For example, for the 6 MeV beam, the difference increases from 0.23% for 3.5 cm rectangular aperture to 0.98% for the 3 cm rectangular aperture. Similarly, the difference for 9 MeV beam is changed from 0.66% for the 3.5 cm rectangular aperture to 2% for 3 cm rectangular aperture. Therefore, care must be taken when the width of aperture chosen for treating patient is less than 3 cm, although it is very rare in a clinical situation.

Table 3.7: Comparison between the dose measured with RK chamber and the dose predicted by EarcMU program for trapezoidal and rectangular apertures and 6 MeV beam.

Aperture shape	rectangular	4cm-by-3cm	rectangular	4cm-by-2cm
Aperture width(cm) at center	3.5	3.5	3	3
SSD(cm)	81.5	81.5	81.5	81.5
d_{max}(cm)	1.5	1.5	1.5	1.5
Arc angle(degree)	90	90	90	90
MUs required	521	521	573	573
Dose planed(cGy)	100	100	100	100
Dose measured(cGy)	99.77	100.36	99.12	99.08
Difference(%)	0.23	0.36	0.98	0.92

Table 3.8: Comparison between the dose measured with RK chamber and the dose predicted by EarcMU program for trapezoidal and rectangular apertures and 9 MeV beam.

Aperture shape	rectangular	4cm-by-3cm	rectangular	4cm-by-2cm
Aperture width at center(cm)	3.5	3.5	3	3
SSD(cm)	81.5	81.5	81.5	81.5
d_{max}(cm)	2.5	2.5	2.5	2.5
Arc angle(degree)	90	90	90	90
MUs required	463	463	519	519
Dose planed(cGy)	100	100	100	100
Dose measured(cGy)	100.66	100.989	98	97.9
Difference(%)	0.66	0.989	2	2.1

For the trapezoidal apertures, the number of MUs required for delivering 100 cGy of dose to d_{max} were calculated using the aperture width at its center. Similar to the rectangular apertures, for all trapezoidal cases, the uncertainty of the EarcMU program predicted dose is within 1% of the planned dose.

The equivalence of a trapezoidal aperture and a rectangular aperture was verified once again. By comparing the doses measured for trapezoidal apertures and for their equivalent rectangular apertures, it is not difficult to find that the dose delivered by using the trapezoidal aperture is the same as one delivered using its equivalent rectangular aperture. The agreement between two the types of apertures is excellent and within 0.5%.

B. Results for the small cylindrical phantom

Electron arc therapy is used in our center to treat chest wall after mastectomy. The radius of a patient chest wall is usually more than 11 cm. The experiment with the small cylindrical phantom was designed to test the limits of the MU calculation algorithm. The calculation of dose per degree using the static beam profiles measured on the flat water surface was performed by assuming that the curvature of patient or phantom is very small compared with the width of the profiles. Therefore the purpose of measurements using the small cylindrical phantom was to test if the EarcMU program works in an extreme situation in which the radius of chest wall or phantom is very small.

In these measurements, the treatment radius was chosen as 10.3 cm for the 6 MeV electron beam and 11 cm for the 9 MeV electron beam. The open field was used as its profile is the widest one we can get. The arc angle of 120^0 was used for both energies. The doses that were planned to be delivered to the depth of maximum dose are the same as ones used in previous experiments. The calculated MUs were 345 for the 6 MeV electron beam and 321 for the 9 MeV electron beam.

Table 3.9 and Table 3.10 show the results measured with MOSFET and Gafchromic® film, respectively. The averaged difference between the planned dose and predicted dose is 2.07% and the standard deviation is 0.8%. Taking into ac-

Table 3.9: Comparison between the dose predicted by EarcMU program and the measured dose with MOSFET.

Beam Energy(MeV)	6	9
Field size	open	open
SSD(cm)	89.7	89
d_{max}(cm)	1.3	2
Arc angle(degree)	120	120
MUs required	345	321
Dose planed(cGy)	100	100
Dose measured(cGy)	102.3	99.11
Difference(%)	2.3	0.89

Table 3.10: Comparison between the dose predicted by EarcMU program and the measured dose with Gafchromic® film.

Beam Energy(MeV)	6	9
Field size	open	open
SSD(cm)	89.7	89
d_{max}(cm)	1.3	2
Arc angle(degree)	120	120
MUs required	345	321
Dose planed(cGy)	100	100
Dose measured(cGy)	97.5	97.4
Difference(%)	2.5	2.6

count the typical uncertainties associated with the dosimeters, the measured doses agree well with the planned doses. The accuracy of MOSFET and Gafchromic® film is the order of 3%[101, 103]. The largest difference between the measured dose and the predicted dose occurs at 2.3% for MOSFET detector and 2.6% for Gafchromic® dosimeter. They are in the same order of dosimeter's uncertainty limit. Under the same conditions, the dose measured with Gafchromic® film is slightly less than the dose measured with MOSFET detector. It is because the sensitivity of Gafchromic® film depends on the dose range. At low dose range(less than 5 Gy), it underestimates the dose[69].

C. Comparison with other investigator's results

Calculation of monitor units is an important procedure in electron arc treatment. Recently, two other methods were developed to predict the output for electron arc therapy. One was developed by Duchesne et al.[21] and based on a large amount of measured data. Basically, five cylindrical phantoms were fabricated with different radii ranging from 5.1 cm to 15.2 cm. The outputs and PDDs of electron arc beams were measured using these cylindrical phantoms. Then an analytical mathematical model of the output as a function of radius and depth was obtained by fitting the measured data. Verification of this model showed the agreement between the predicted dose and the measured dose is within 3%. In 2006, Hogstrom et al.[17] developed a physics-model based algorithm for electron arc therapy. The algorithm is based on the electron pencil beam redefinition algorithm. It can accurately calculate the output for electron arc treatment. Their results indicated that the calculated outputs agree with the output measured in a cylindrical water phantom within 2%.

Our method is a measurement-based method and belongs to the same group as one developed by Duchesne. The accuracy of MU calculation based on dose per degree is comparable to these two methods. Overall, it can predict the output in all combinations within 3%. In a clinical-related geometry, it can calculate output for electron arc treatment with the uncertainty of less than 2.1%.

Chapter 4

Determination of the trapezoidal aperture for electron arc treatment

4.1 Introduction

When the post-mastectomy chest walls of the patients are treated using the electron arc with an open field, the dose delivered to the reference point in the central plane of electron field can be determined accurately using the method developed in Chapter 3. However, the dose in the plane superior or inferior to the central plane varies significantly due to the variation of the curvature of patient contours. The degree of dose variation depends on the specific contour of the individual patient. From the treated patients in our centre, as shown in section 1.2.2 , the averaged dose variation was found to be 10%.

The simple technique to improve the uniformity of dose distribution across the treatment area along the direction from superior to inferior is to shape the rectangular aperture of an open field into a trapezoidal aperture. This method was first demonstrated by Blackburn[12] in 1981. Later, the University of Utah Medical Center clinically applied this technique in the electron arc treatment of patients[66].

Before using a trapezoidal aperture to treat patients clinically, the key issue that needs to be resolved is how to customize the trapezoidal shape for an individual patient based on the contour information. To determine the trapezoidal aperture for electron arc treatment, Leavitt et al.[59]derived an empirical mathematical formula, which relates the dose at a point in the central plane to the

dose at any point with a certain distance outside the central plane. The dose at any point in a plane other than the central plane is also expressed as a function of the light field width and the distance between the central plane and this plane. These two functions were obtained by fitting the measured data. The width of the shaped aperture for a given distance above or below the central plane is determined by equating the dose at a point in central plane and the dose in the distant plane. Recently, another empirical method was developed based on the angle-β concept by Pla et al.[79] for determining the secondary collimator shape for pseudo electron arc therapy.

In this chapter, a simple method is developed to determine the trapezoidal aperture for the patient to be treated with electron arc therapy. The method is based on the quantity, dose per degree, defined and measured in Chapter 3.

4.2 Materials and methods

4.2.1 Theory

Separation of the variation of dose-per-degree with SSD and aperture width

The dose per degree is a function of several beam parameters. For a given electron beam energy, it varies with the SSD and the width of the aperture of the electron arc applicator. The quantity, $D_{perdegree}$, can be mathematically expressed as:

$$D_{perdegree} = D_{perdegree}(SSD, W) \tag{4.1}$$

where W is the aperture width of rectangular field.

If the SSD and aperture width has a very small change, δSSD and δW, around a certain value SSD_0 and W_0, the change of dose per degree is:

$$\delta D_{perdegree} = \frac{\partial D_{perdegree}}{\partial SSD}|_{SSD=SSD_0}\,\delta SSD + \frac{\partial D_{perdegree}}{\partial W}|_{W=W_0}\,\delta W \tag{4.2}$$

where $\delta SSD = SSD - SSD_0$ and $\delta W = W - W_0$.

From Eq.4.2, the following equation can be derived:

$$(\delta D_{perdegree})^2 = (\frac{\partial D_{perdegree}}{\partial SSD}|_{SSD=SSD_0}\,\delta SSD + \frac{\partial D_{perdegree}}{\partial W}|_{W=W_0}\,\delta W)^2 \tag{4.3}$$

where $\delta SSD = SSD - SSD_0$ and $\delta W = W - W_0$.

By simplifying Eq.4.3, one obtains:

$$\delta D_{perdegree}(SSD, W) \approx \delta D_{perdegree}(SSD)\delta D_{perdegree}(W) \tag{4.4}$$

where $\delta D_{perdegree}(SSD) = \sqrt{2}(\frac{\partial D_{perdegree}}{\partial SSD}|_{SSD=SSD_0}\,\delta SSD)^{1/2}$. The terms containing $(\delta SSD)^2$ and $(\delta W)^2$ are neglected. $\delta D_{perdegree}(W) = (\frac{\partial D_{perdegree}}{\partial W}|_{W=W_0}\,\delta W)^{1/2}$.

From the medical physics point of view, Eq.4.4 means that the variation of dose per degree with SSD and the aperture width can be separated, provided the change of SSD and aperture width is very small. This was the underlying assumption when Leavitt and Blackburn determined the trapezoidal aperture for electron arc treatment. They assumed that the dose at point in the patient or phantom in electron arc irradiation independently varies with SSD and the aperture width[12, 59].

Determination of the trapezoidal aperture of electron arc applicator

To simplify the analysis, the variation of the patient contour of the chest wall from superior to inferior is approximated by a conical phantom. For a conical phantom that best fits the chest wall of an individual patient, as shown in Fig.4.1, the radius linearly decreases in the longitudinal direction. The superior-to-inferior direction is assumed to be from the upper side with the larger radius to the lower side with the smaller radius. The treated radius is denoted by R_c. The superior and inferior radii in treated area are R_s and R_i, respectively.

When the phantom is treated with the rectangular aperture of the open field, the dose at same depth in the phantom increases from superior to inferior. This is because the dose per degree increase with the increase of SSD, corresponding to the decrease of radius. In Fig. 4.2, the polynomial function fitting the variation of dose per degree with SSD for the open aperture and its derivative are plotted. Even when the radius of the phantom or patient contour is changed linearly, the dose per degree varies in a nonlinear way. As shown in Fig. 4.2(b), the increase of dose per degree with the decrease of radius becomes greater when the radius is decreased.

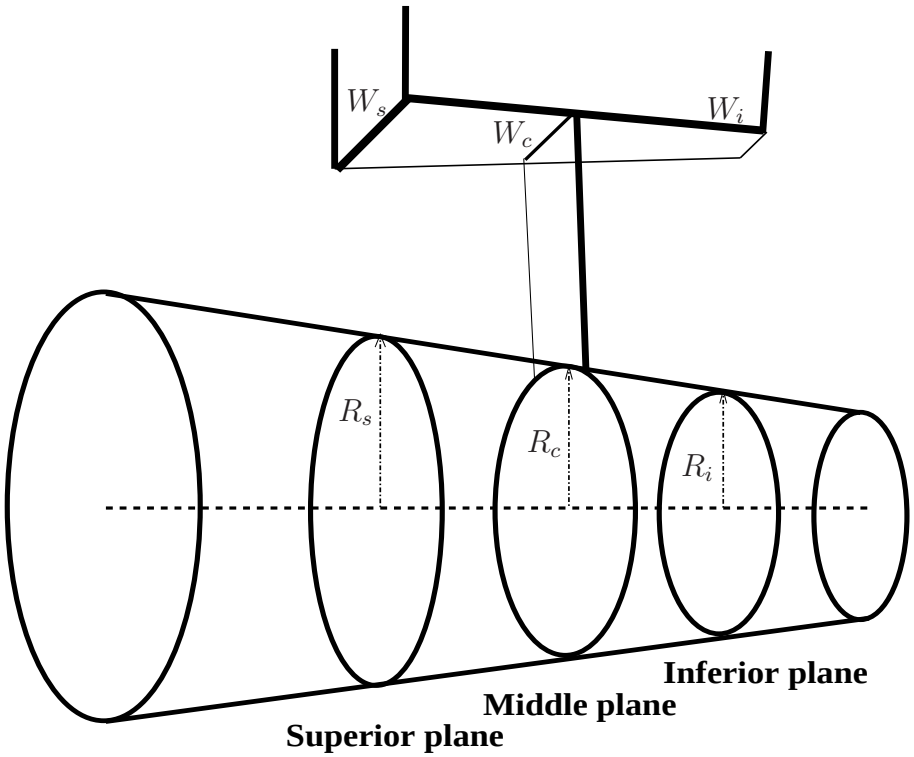

Figure 4.1: The diagram illustrating the determination of the trapezoidal aperture of electron arc applicator using a conical phantom. The treated radius is R_c. The maximum and minimum radii in treated area are R_s and R_i. The aperture width at center, long and short side of trapezoidal aperture are denoted by W_c, W_s and W_i, respectively.

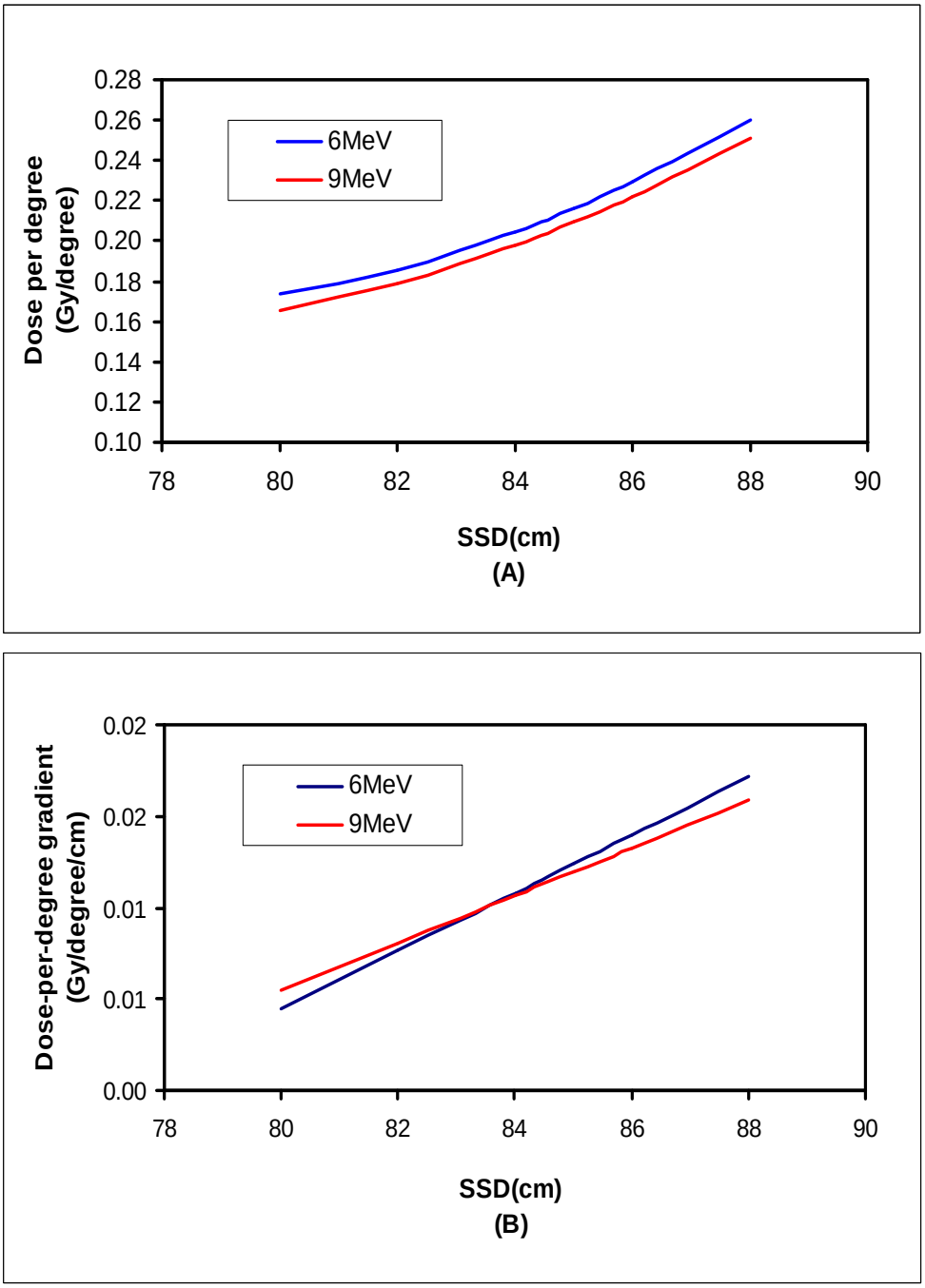

Figure 4.2: (A)The plot of polynomial function 4.8 and 4.9 that fit the variation of dose per degree with SSD for open field. (B)The plot of first derivative of polynomial function 4.8 and 4.9.

The dose per degree in the superior and inferior plane at same depth is denoted as $D_{perdegree}(R_s)$ and $D_{perdegree}(R_i)$. Then the increase of dose per degree in the inferior plane relative to the dose per degree in middle plane can be expressed as:

$$\Delta D_{perdegree}(R_c, R_i) = \frac{D_{perdegree}(R_i) - D_{perdegree}(R_c)}{D_{perdegree}(R_c)} \tag{4.5}$$

where $\Delta D_{perdegree}(R_c, R_i)$ is the relative change of dose per degree normalized to the dose per degree at middle plane at same depth. A similar expression can also be defined for the superior plane.

On the other hand, as discussed in Chapter 3, the dose per degree decreases linearly with the aperture width of rectangular field. To counteract the increase of dose per degree due to the decrease of radius, the aperture has to be wider in the superior plane and narrower in the inferior plane. The dose per degree corresponding to the aperture width at the center, long and short edges of the trapezoidal aperture, as shown in Fig. 4.1, are represented by $D_{perdegree}(W_c)$, $D_{perdegree}(W_s)$ and $D_{perdegree}(W_i)$, respectively. Similarly, the relative change of dose per degree at inferior plane due to the aperture width is:

$$\Delta D_{perdegree}(W_c, W_i) = \frac{D_{perdegree}(W_i) - D_{perdegree}(W_c)}{D_{perdegree}(W_c)} \tag{4.6}$$

where $\Delta D_{perdegree}(W_c, W_i)$ is the relative change of dose per degree normalized to the dose per degree corresponding the aperture width at the center.

As the variation of dose per degree caused by the change of radius and aperture width can be treated independently under the the approximation of a small variation, the physical width of the aperture corresponding to the inferior plane is determined using the following equation:

$$\Delta D_{perdegree}(R_c, R_i) = -\Delta D_{perdegree}(W_c, W_i) \tag{4.7}$$

In Eq.4.7, $\Delta D_{perdegree}(R_c, R_i)$ and $\Delta D_{perdegree}(W_c, W_i)$, are calculated separately using the following equations:

$$D^{flat}_{perdegree}(6MeV, SSD) = 0.0008SSD^2 - 0.1227SSD + 4.9047 \tag{4.8}$$

$$D^{flat}_{perdegree}(9MeV, SSD) = 0.0007SSD^2 - 0.0991SSD + 3.9116 \tag{4.9}$$

$$D^{flat}_{perdegree}(6MeV, W) = 0.1587 \times W + 0.317 \tag{4.10}$$

$$D^{flat}_{perdegree}(9MeV, W) = 0.1885 \times W + 0.2231 \tag{4.11}$$

where these equations were obtained by fitting the experimental data as discussed in Section 3.2.3.

Using Eq.4.6-Eq.4.11, the trapezoidal aperture W_s-by-W_i, as shown in Fig. 4.1, are obtained. W_s and W_i are the aperture widths corresponding to the superior and inferior planes, respectively. As the maximum aperture width of the electron arc applicator is 4 cm and physical length is 17.2 cm, the physical aperture of the electron arc applicator can only be shaped as a 4 cm-by-N cm trapezoidal aperture. The short edge of this trapezoidal aperture is calculated by scaling the trapezoidal aperture W_s-by-W_i into 4 cm-by-N cm while keeping the slopes of two trapezoidal apertures same. Specifically, N is determined in the following way:

$$\tan(\theta) = \frac{W_s - W_i}{17.2} \tag{4.12}$$

$$N = 4cm - 17.2\text{cm} * tan(\theta) \tag{4.13}$$

The factors influencing the trapezoidal aperture of electron arc applicator

From the analysis above, it can be seen that the trapezoidal aperture required for improving the dose distribution from superior to inferior direction is determined by several parameters.

The first factor is the treatment radius in the middle plane. If the treatment radius lies in a range of radii in which the gradient of dose per degree is very large, the open aperture is pinched much more to compensate for the increase of dose per degree due to the change of radius. For example, the short side length of the trapezoidal aperture N, defined by Eq.4.13, is much shorter for a treatment radius of 11 cm than that for treatment radius of 16 cm, provided the difference between the superior SSD and the inferior SSD is the same. This is because, as seen from Fig. 4.2(B), the gradient at the radius of 11 cm is larger than the gradient at the radius of 16 cm.

The change of radius from the superior and inferior plane to the middle plane is the second parameter affecting the trapezoidal aperture. For a given treatment radius, the variation of dose per degree is large if the difference between superior and inferior radius is very large. Correspondingly, a small trapezoidal aperture is required to correct the large change of dose per degree. Finally, the trapezoidal aperture is also energy dependent. This is obvious because the equations used to calculate the trapezoidal aperture is energy dependent, as seen from Fig. 4.2.

4.2.2 Implementation of an aperture calculation program

Following the method described in Section 4.2.1, the trapezoidal aperture can be calculated manually. However, for a large number of patients, the manual calculation procedure is time-consuming, error-prone and cumbersome. The easy way to void these disadvantages is to encapsulate the mathematical procedure into a computer program. A computer program written in Python and named "EarcAperture"was developed for calculating the trapezoidal aperture for the patient in electron arc treatment. It is a very simple program and Fig.4.3 shows its graphic user interface.

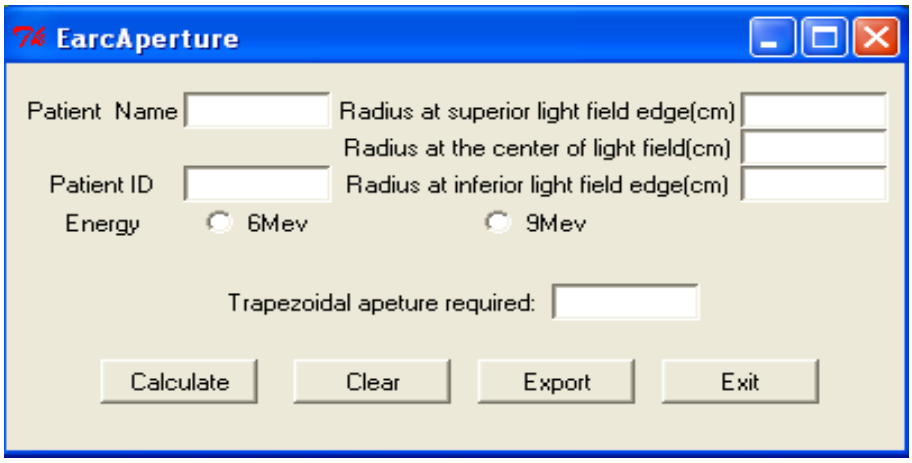

Figure 4.3: The user graphic interface of EarcAperture program written in the Python programming language.

The input of demographic patient information, such as patient ID and patient name, is optional. To get the required trapezoidal aperture for a specific electron arc treatment, the patient contour information the program requires is

the superior radius(R_s), the radius at field center(R_c) and the inferior radius(R_i). The superior radius and inferior radius are defined as the radii at superior and inferior edge of light field on the phantom surface or patient skin. Similarly, the radius at field center is measured at the light field center on the phantom surface or patient skin. The EarcAperture program also provides the function of exporting the calculated trapezoidal aperture with treatment parameters into an Excel or a PDF file for further analysis or as a record. The EarcAperture program is used for the rest of this investigation.

4.2.3 Verification of EarcAperture program

Verification of the EarcAperture program is essentially to verify the method used for determining the trapezoidal aperture of electron arc applicator. Firstly, it is to check if the trapezoidal aperture calculated by this method can improve the uniformity of dose distribution along the direction from superior to inferior. Secondly, if it works, to what extent the dose distribution is to be flattened. The verification was done by comparing the dose distributions delivered with the open aperture and trapezoidal apertures, which were measured on the conical phantoms using film dosimetry.

Conical phantoms

Several conical phantoms were made for the verification experiments. The phantoms have different lengths and are long enough to provide the electron equilibrium of lateral scattering in the longitudinal direction. Tapering conical phantoms with different angles were used to simulate the range of patient geometries encountered in clinical situation.

The phantom was made from expanded polystyrene instead of Perspex or high impact polystyrene. The choice of phantom materials was based on the following reasons:(1)The phantom made from polystyrene is only used to provide the framework of the conical shape. Before any measurement, 5cm bolus is draped over the phantom following the conical curvature. The practical range is 3 cm for 6 MeV and 4.5 cm for 9 MeV. The polystyrene phantoms covered with the

bolus provide enough backscattering for both energies;(2)Due to the limitation of resources, the high impact polystyrene is not always available to the department. If a series of phantoms were made from Perspex or high impact transparent polystyrene, the cost of materials and labor is much higher. On the other hand, the expanded polystyrene is much cheaper and easily machined.

EDR2 film dosimeter

In order to verify the EarcAperture program, the relative dose distributions for open and trapezoidal apertures needed to be measured under the same irradiation conditions. Electron arc is a time-dependent dose delivery technique. It requires an integrating dosimeter to quantify the delivered dose. The dosimeter should also have high spatial resolution. Film dosimetry is an ideal option. It is widely used to obtain the relative dose distribution of clinical electron beam in a solid phantom[73, 104].

Kodak EDR2 film was used for the verification measurement. Before the film is used for measurement, the film was calibrated to get the sensitometric curves for 6 MeV and 9 MeV electron beam. The calibration procedure follows the guidelines recommended by AAPM[73]. The perpendicular beam geometry was used for the calibration. The linac was first calibrated to make sure that the delivered dose was known accurately. The films, wrapped in ready pack, were all irradiated in a Plastic Water®in one session with the Siemens Primus linear accelerator using a 10 cm × 10 cm electron cone. A SSD of 100 cm to the top of the Plastic Water® phantom was used. The films were placed at the depth of maximum dose and perpendicular to the central axis of the beam. A thickness of 10 cm Plastic Water® slabs were placed below the film for all irradiations. The films were exposed with the following doses to develop the characteristic curves for EDR2 film: 0, 10 ,20, 40, 60, 80, 100, 125, 150, 180, 200, 230, 250, 280, 300, 325, 350, 370 and 400 cGy. The 0 cGy film corresponds to a film that was developed without being irradiated to determine the base plus fog optical levels.

The films were developed in one session in a Kodak X-Omat processor four hours after irradiation. Before the films were developed, several wasted film were

fed into the processor to warm up and stabilize the processor conditions. The stability of processor operation condition is ensured by daily, weekly and monthly quality assurance (QA). Then the films were digitized into bitmap(BMP) images using a Vidar film digitizer (VXR-16). The images were analyzed using an in-house program called IMRT Checker. The IMRT Checker is a high quality and complicated computer program, which was designed and programmed by the chief physicist Keith Croft. The IMRT Checker program has been using for the patient-specific verification for IMRT treatment of head and neck in our department. For the description of its function and how to use it in detail, see Appendix A.

For each film image, the average of pixels in a small area at the radiation field center was measured using the IMRT Checker program. The pixel value of the developed and non-irradiated film was subtracted from the mean pixel value of each irradiated film. The calibration curves are plotted in Fig. 4.4. It is found that, for both energies, the film response is quite linear up to 4 Gy. In electron arc verification measurement, the calibration curves are used to convert the pixel value of the film into dose.

After the calibration of the film, the accuracy of the film dosimetry was checked by comparing the dose profiles measured with EDR2 film and an electron diode. A typical result is shown in Fig. 4.5. The crossplane profiles were measured at the depth of maximum dose and 85 cm SSD using the open aperture. The Scantronix RFA300 water tank was used for the measurement with the electron diode while Plastic Water® used for the film measurements. The signal from electron diode is considered to be proportional to the dose without any other corrections. Then the profile was obtained by normalizing to the maximum dose. For the film measurement, the IMRT Checker was used to first get the OD profile from the exposed and developed film. Then the calibration curves were used to get the dose profile which is renormalized to the maximum dose. For both energies, it can be seen that the profile measured with EDR2 film agrees very well with the one measured using the electron diode.

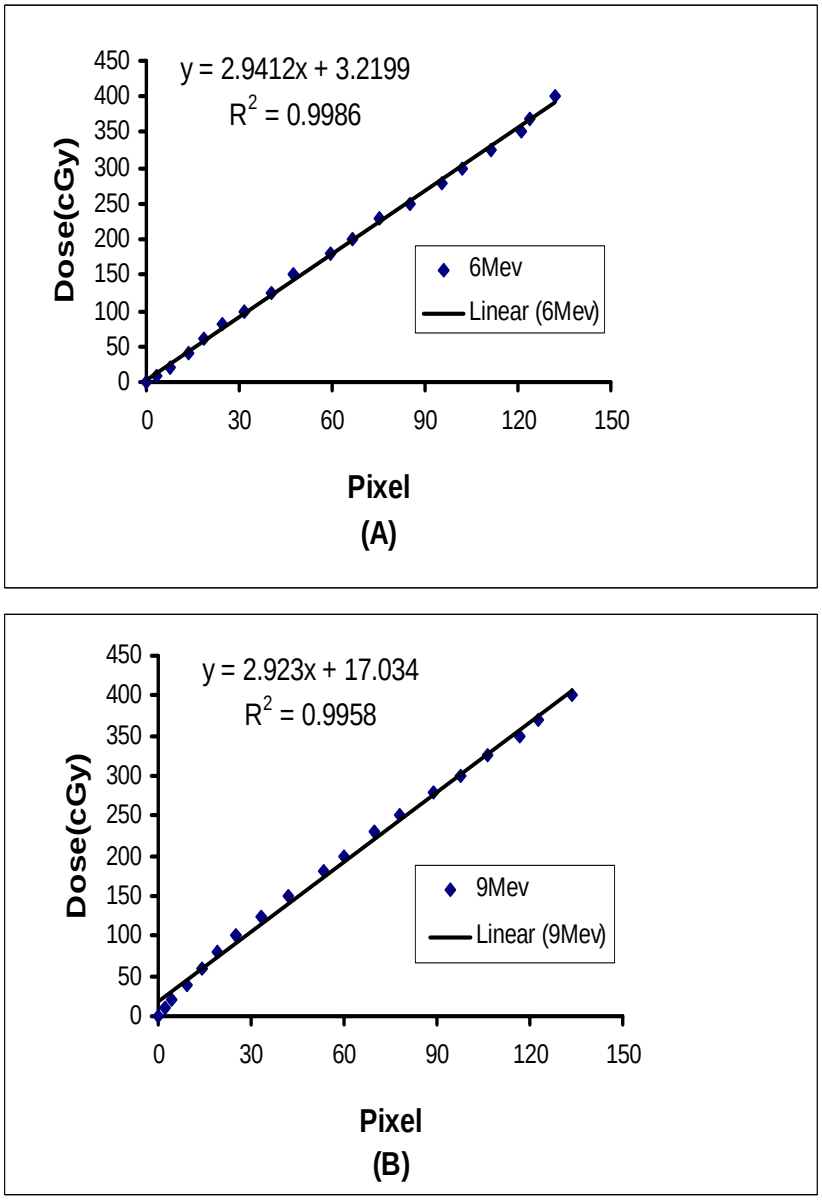

Figure 4.4: The EDR2 film calibration curves obtained with Vidar film digitizer and IMRT Checker program for (A)6 MeV and (B)9 MeV.

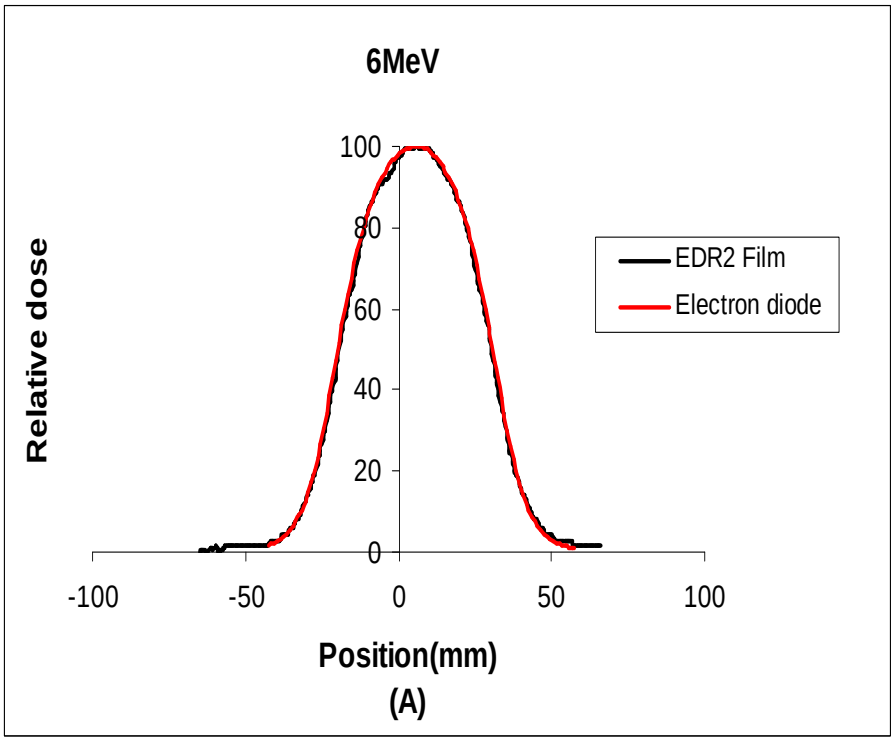

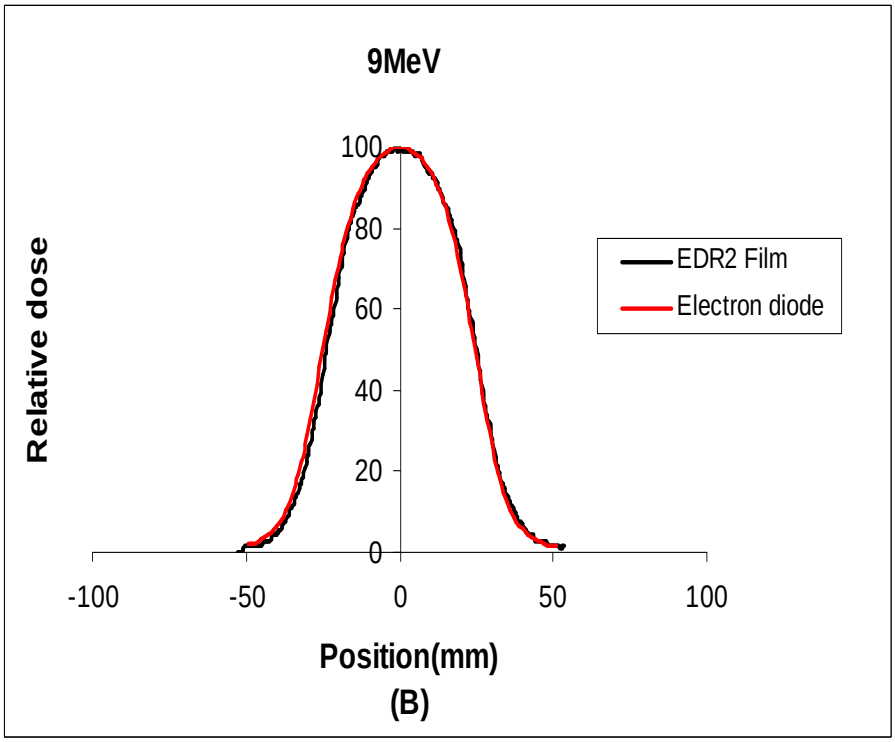

Figure 4.5: The comparison of the crossplane dose profiles measured with the EDR2 film and an electron diode for (A)6 MeV and (B)9 MeV. The profiles were measured at the depth of maximum and 85 cm SSD using open aperture. The Scantronix RFA300 water tank and Plastic Water® were used for electron diode and EDR2 film measurement, respectively.

Experimental setup and procedure

The setup of the conical phantom was similar to the cylindrical phantom setup procedure as described in Section 3.2.5. Briefly, the phantom was first placed on the couch. The tapered phantom surface lay along the inplane direction with the radius decreasing from superior to inferior. The central axis of conical phantom was aligned with the rotation axis of gantry.

Then the bolus sheets with the thickness of 5 cm were draped around the phantom. Extreme care was taken here to make sure the bolus exactly followed the curvature of the phantom surface by taping the edge of the bolus on the phantom.

The film used for the measurement was placed on the top of 5 cm bolus. The center of the film was aligned with the center of light field using the cross hairs with the gantry and collimator at zero degrees. The film was placed with its longer dimension across the phantom in the crossplane direction and its shorter dimension along the surface from superior to inferior in the inplane direction.

The film was pricked at one corner with a small pin to allow any trapped air to escape. The punctured small hole also serves as a marker for the superior position. The desired depth of measurement was provided by draping the bolus sheets over the film. The bolus sheets were also laid over each other carefully so that there was no air gap between the bolus sheet. The procedure was the same for the open and trapezoidal apertures.

Processing and analyzing of film

The films were taken from the same batch as ones used for the calibration. One unexposed film was separated from the rest for the zero dose base value. Film measurements were finished in one session. After 6 hours, the films were developed, scanned into the computer and saved as BMP images in the same way as described above.

The film images were analyzed with Keith's IMRT Checker program as mentioned earlier. Once the image is opened with the program, the inplane profile

along the direction from superior to inferior can be easily obtained using the function provided by the program. This original profile represents a relative dose distribution in terms of pixel values. The pixel values at each point on the profile can be exported into an Excel file. The pixel value at one point is subtracted from the mean pixel value of a developed but non-irradiated film to get net pixel values for that point. These net pixel values are converted to the dose using the calibration curves shown in Fig. 4.4. Thus the original profile is converted into a dose profile.

Taking into account the small fluctuation of film sensitivity and film processing conditions, the inplane profiles along different straight lines were found to be essentially same for all exposed films. This is as expected because the whole film was irradiated following the arc length at the same depth. These straight lines are drawn across the whole arc along the direction from superior to inferior.

As an example, Fig. 4.6(A) shows an image of a scanned film image, which was opened with the IMRT Checker program. The side marked with BD and AC is the superior and inferior side of the film, respectively. The arc is the wide strip of black area, which starts from one side of film and ends with another side. Two straight lines AB and CD were drawn on the image along the direction from superior to inferior. The original profiles along these two lines are shown in Fig. 4.6(B). It can be seen that two profiles agree with each other very well.

4.3 Results and discussion

4.3.1 Test cases

Five test cases were designed to simulate a range of treatment geometries that may be encountered in clinical situations. For each case, the treatment parameters for each case are listed in Table 4.1.

From the patients treated in department, it was found that the range of treatment radius approximately falls between 15 cm and 17 cm. The variation of radius along superior-to-inferior direction is quite different from patient to patient. Typically, the difference between maximum and minimum radii ranges

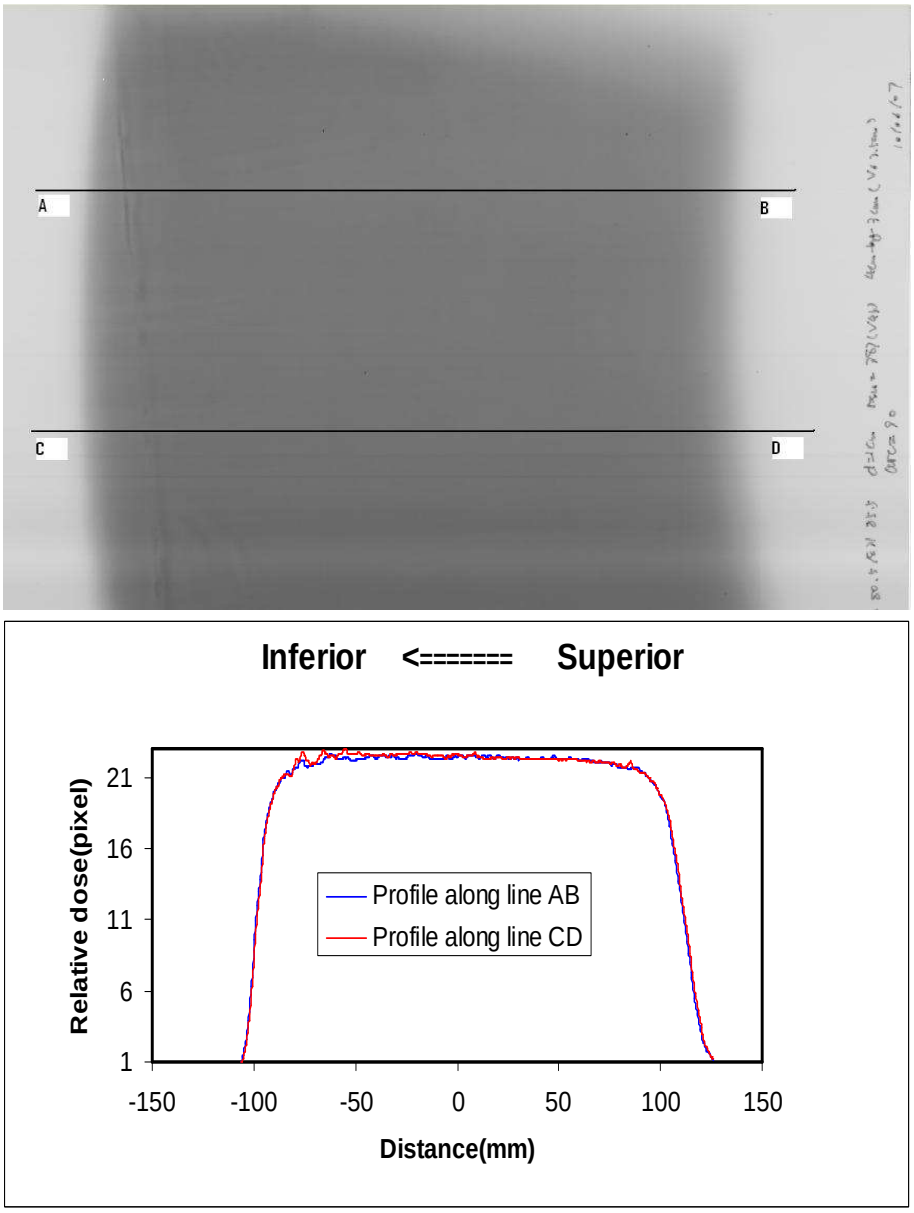

Figure 4.6: The upper graph shows an image of a scanned film, which was exposed at 1cm depth using 9 MeV electron beam with 4 cm-by-3 cm trapezoidal aperture. The arc angle is 90^0. The lower graph displays the inplane profiles obtained along the line AB and CD drawn on the film image.

Table 4.1: List of test cases.

	Case 1	Case 2	Case 3	Case 4	Case 5
Superior radius(cm)	16	17.5	19.5	16.5	14.5
Radius at field center(cm)	15	15	17	14	12
Inferior radius(cm)	14	13	14.5	11.5	9.5
Arc angle(degree)	90	90	90	120	120
Depth(cm)(6MeV)	1.5	1.5	1	1.5	1
Depth(cm)(9MeV)	2.5	2.5	1	1.5	1

Table 4.2: EarcAperture program calculated apertures for test cases.

	6MeV	9MeV
Case 1	4cm-by-3.5cm	4cm-by-3.6cm
Case 2	4cm-by-2.8cm	4cm-by-3cm
Case 3	4cm-by-2.9cm	4cm-by-3cm
Case 4	4cm-by-2.6cm	4cm-by-2.8cm
Case 5	4cm-by-2.5cm	4cm-by-2.6cm

from 2 to 5 cm. Case 1 was used to simulate the patient who has the typical chest wall radius of 15 cm. The chest wall contour of the patient has a small variation of 2 cm. Case 2 served for the similar purpose, but the difference between superior and inferior radii of chest wall is enlarged to be 4.5 cm. Case 3 had treatment geometry similar to Case 1 and Case 2, but treatment radius is 17 cm. Although it is very rare to treat the patient with the small chest wall radius less than 15 cm, Case 4 and Case 5 are used to test if the method used for determining the trapezoidal apertures works in this extreme situation. The patient radii in these two cases are set as 14 cm and 12 cm, respectively.

For a given energy, each test case uses the same number of monitor units for open aperture and trapezoidal aperture. The number of monitor units is chosen arbitrarily, but the dose delivered to the film is ensured to be within the linear range of the film-response curve, between 45 cGy and 110 cGy. The traveling angle is chosen so that the electron arc treatment can cover the length of the film. Once the treatment parameters for each case are input into EarcAperture program, the program will give the apertures required for that specific electron arc treatment. The calculated apertures are listed in Table 4.2.

It was noted that the larger the difference between the superior and inferior radius, the smaller the trapezoidal aperture required. This agrees with the conclusion from the analysis of the factors influencing the aperture. For the same conditions, the apertures required for 9 MeV are wider than those for 6 MeV. This can be explained by Fig. 4.2. For the same treatment conditions, the change of dose per degree of 9 MeV across the chest wall from superior to inferior direction is always smaller than that of 6 MeV, thus requiring a wider trapezoidal aperture.

4.3.2 Comparison of the dose distributions delivered with open and trapezoidal aperture

The inplane profiles from superior to inferior for the open and trapezoidal apertures of the five test cases are shown in Fig. 4.7-Fig. 4.11. By comparing the profiles of the open aperture and the trapezoidal aperture for each test case, the following qualitative features are observed:

1. When the phantom was treated with an open aperture, the dose distribution was not uniform along the direction from superior to inferior. The dose gradually increased towards the inferior side. The way the dose increases and the difference between the superior and inferior dose varied from one case to another, depending on the specific treatment geometry. This is because the increase of dose per degree with radius, as seen from Fig. 4.11, strongly depends on a specific treatment radius and the difference between superior and inferior radius.

2. After the open aperture of the electron arc applicator was shaped into a trapezoidal aperture, which was determined using the method described in Section 4.2.1, electron arc treatment delivered a uniform dose following the slope of the conical phantom surface, regardless of the radius variation from superior to inferior.

What we are really interested is here to an extent the trapezoidal aperture can flatten the dose distribution delivered with an open aperture. In order to do a quantitative comparison, the flatness index(FI) of a profile is used. It is defined as:

$$FI = \frac{D_{max} - D_{min}}{D_{max} + D_{min}} \times 100 \tag{4.14}$$

where D_{max} and D_{min} are the maximum and minimum dose values inside 80% of full width at half maximum(FWHM) of the profile.

The calculated flatness indices of the profiles for open apertures and trapezoidal apertures are listed in Table 4.3. From Table 4.3, it can be seen that the flatness indices of the open aperture profiles are more than 2.28%, whereas those of the trapezoidal apertures are less than 1.4%. The largest and smallest flatness indices are 11.79% for an open aperture and 0.18% for a trapezoidal aperture, respectively. In most cases, the flatness index of a profile was reduced to less than 1 by using a trapezoidal aperture. For example, for Case 5 and the 9 MeV electron beam, the flatness index decrease by 95% from 11.79% to 0.58%. Overall, the mean flatness index is 8% for open aperture and 0.58% for trapezoidal aperture. This indicates that the trapezoidal aperture determined

using the method described in this chapter can greatly improve the uniformity of dose distribution along the direction from superior to inferior.

Table 4.3: The flatness indices of the profiles for the open aperture and trapezoidal apertures.

	6MeV		9MeV	
	Open field	Trapezoidal aperture	Open field	Trapezoidal aperture
Case 1	2.28%	0.62%	3.56%	0.59%
Case 2	4.91%	1.17%	9.97%	0.39%
Case 3	10.17%	0.21%	10.61%	0.23%
Case 4	5.9%	0.18%	10.36%	1.39%
Case 5	10.71%	0.73%	11.79%	0.58%

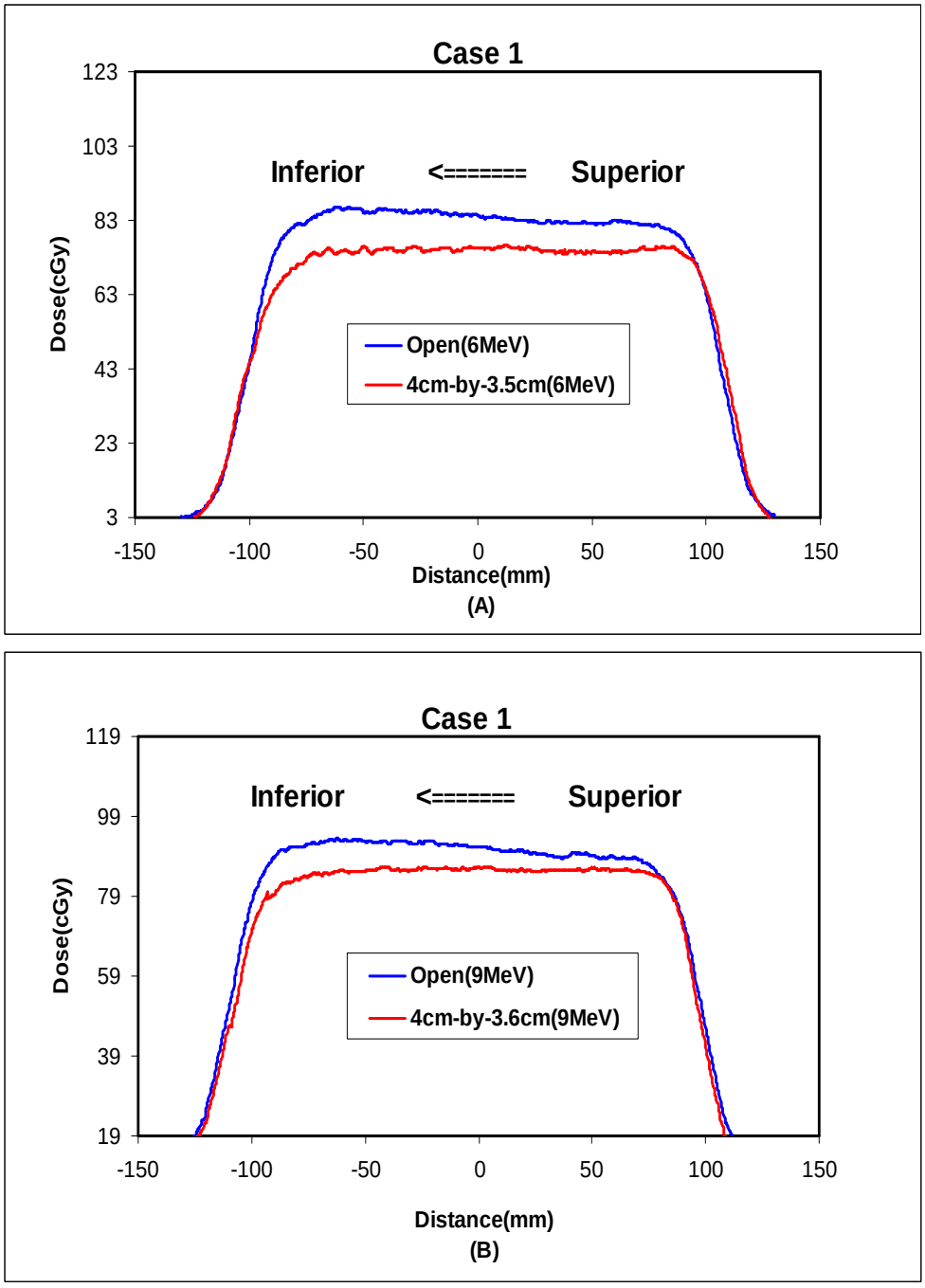

Figure 4.7: The inplane profiles of the open and trapezoidal apertures for superior radius(16 cm), central radius(15 cm) and inferior radius(14 cm). The profiles were measured at 1.5 cm depth for (A) 6 MeV and at 2.5 cm depth for (B)9 MeV. The traveling arc is 90^0 for both energies. The arrows indicate the direction from superior to inferior.

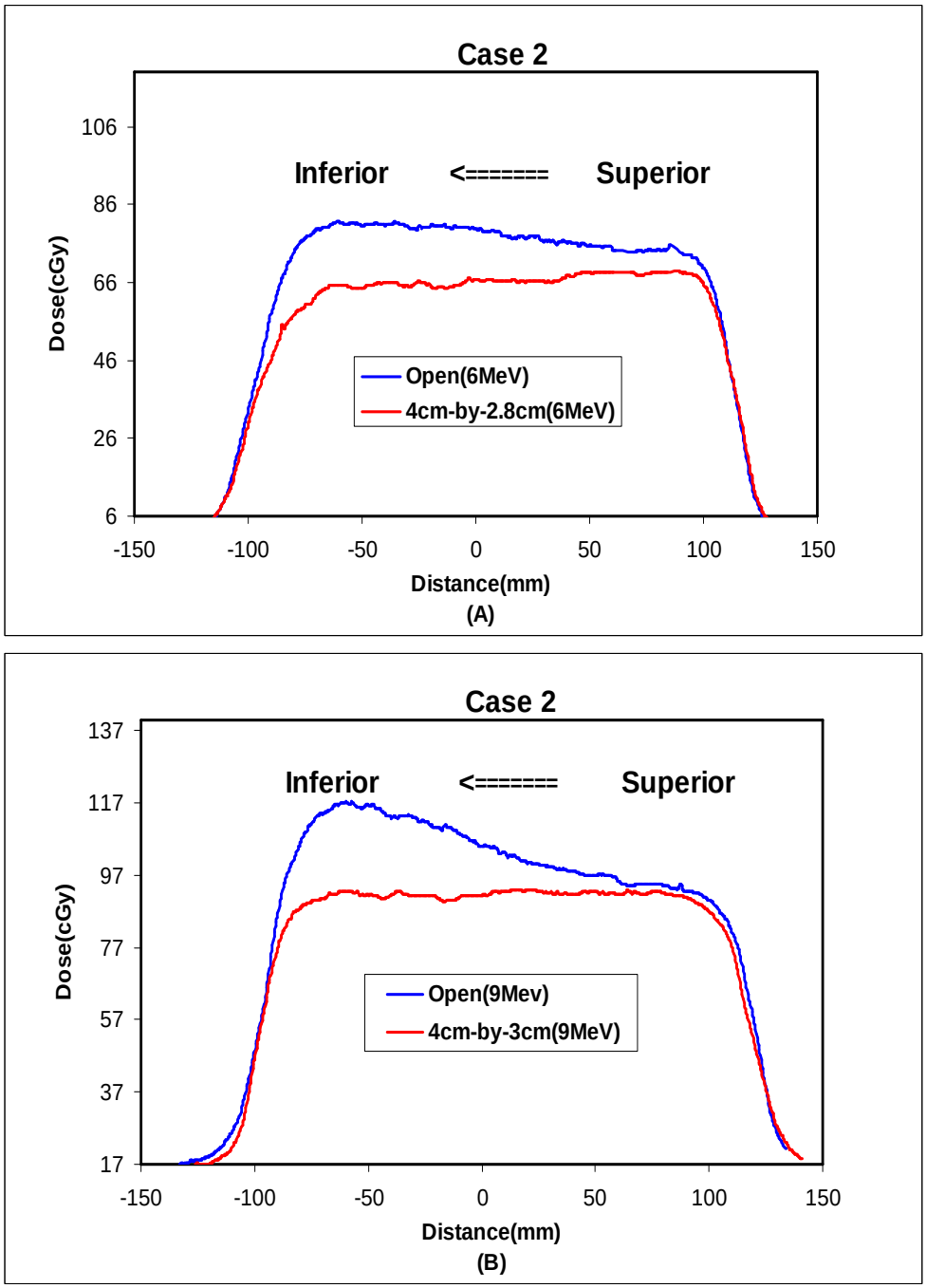

Figure 4.8: The inplane profiles of the open and trapezoidal apertures for superior radius(17.5 cm), central radius(15 cm) and inferior radius(13 cm). The profiles were measured at 1.5 cm depth for (A) 6 MeV and at 2.5 cm depth for (B)9 MeV. The traveling arc is 90^0 for both energies. The arrows indicate the direction from superior to inferior.

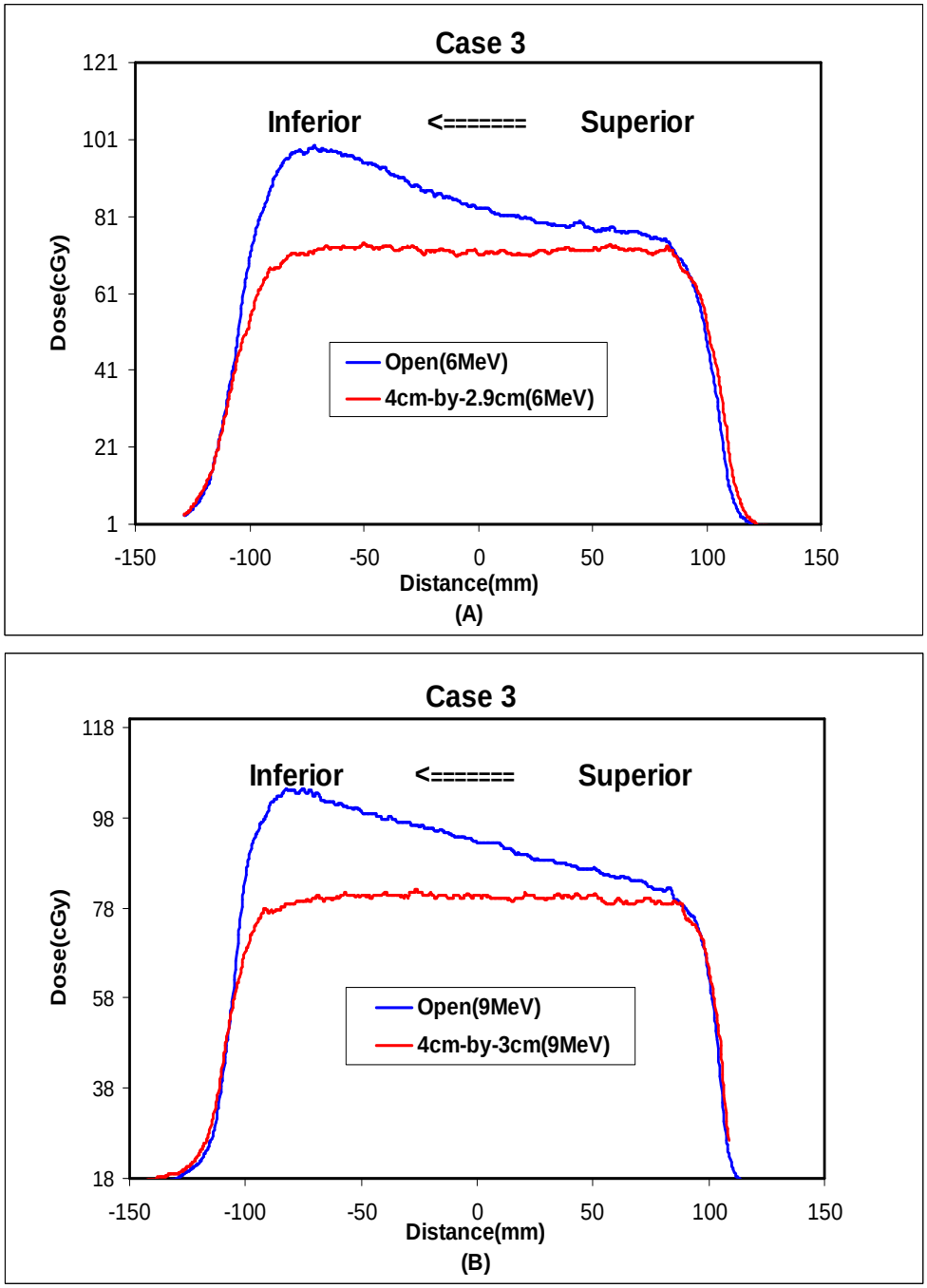

Figure 4.9: The inplane profiles of the open and trapezoidal apertures for superior radius(19.5 cm), central radius(17 cm) and inferior radius(14.5 cm). The profiles were measured at 1 cm depth for both (A) 6 MeV and (B)9 MeV. The traveling arc is 90^0 for both energies. The arrows indicate the direction from superior to inferior.

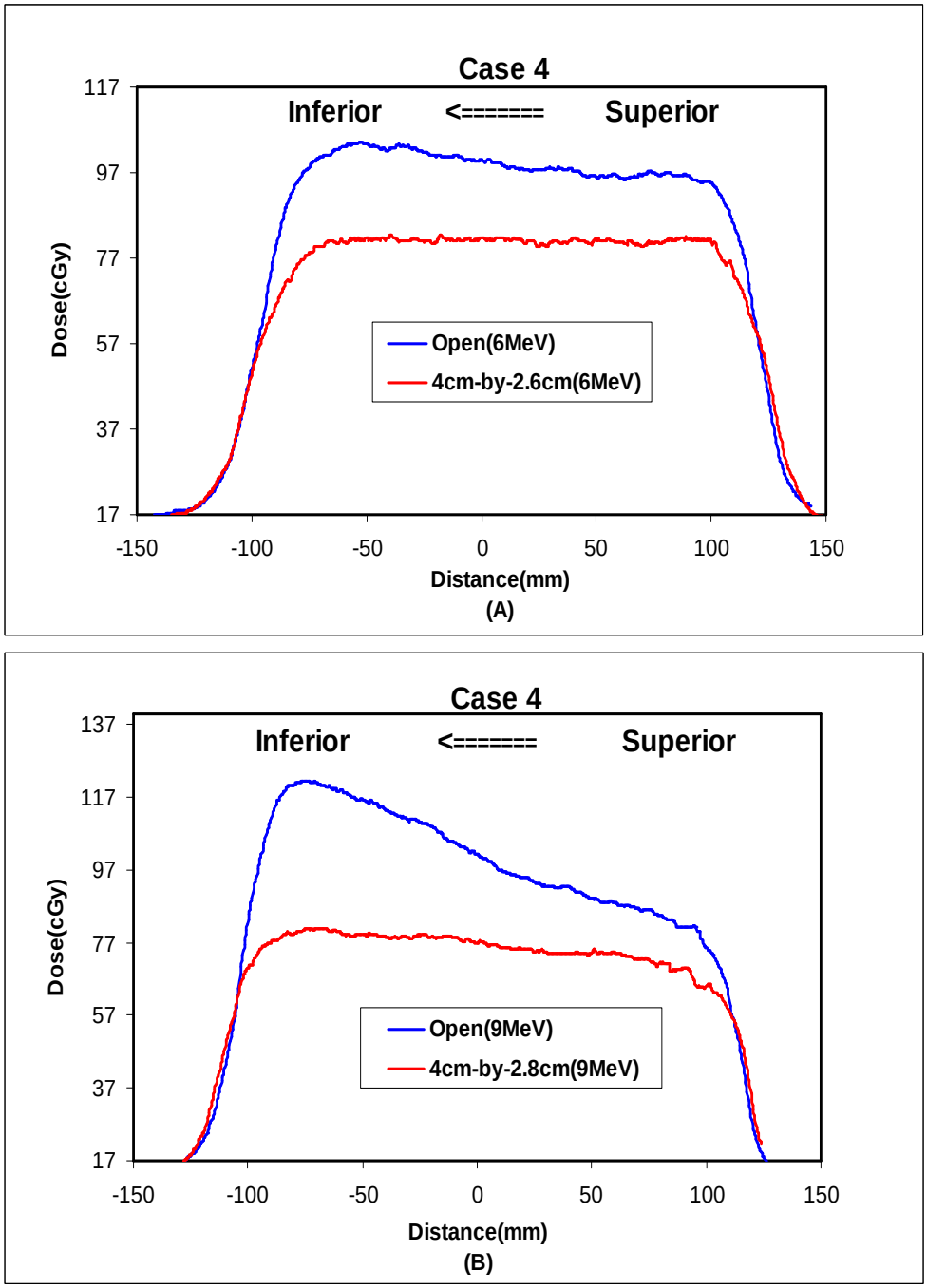

Figure 4.10: The inplane profiles of the open and trapezoidal apertures for superior radius(16.5 cm), central radius(14 cm) and inferior radius(11.5 cm). The profiles were measured at 1.5 cm depth for both (A) 6 MeV and (B)9 MeV. The traveling arc is 120^0 for both energies. The arrows indicate the direction from superior to inferior.

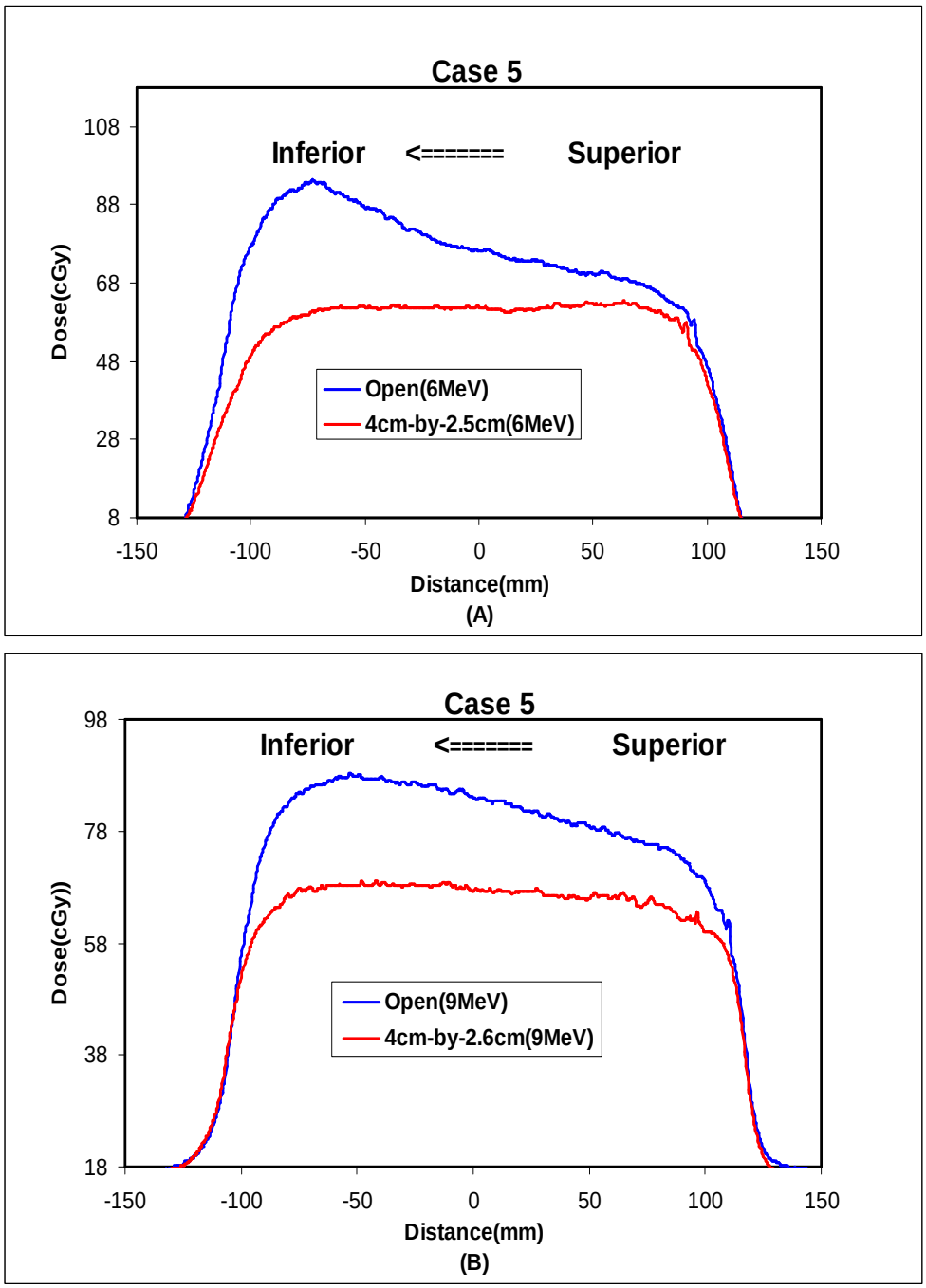

Figure 4.11: The inplane profiles of the open and trapezoidal apertures for superior radius(14.5 cm), central radius(12 cm) and inferior radius(9.5 cm). The profiles were measured at 1 cm depth for both (A) 6 MeV and (B)9 MeV. The traveling arc is 120^0 for both energies. The arrows indicate the direction from superior to inferior.

Chapter 5

Conclusions and future work

As a preclinical investigation, the work done in the thesis provides a basic framework for clinically delivering the electron arc treatment with a trapezoidal aperture. It also showed that treating a patient with a trapezoidal aperture is an effective and simple way to improve the uniformity of dose distribution from superior to inferior. The main results are summarized as follows:

1. The characteristics of the static electron beam, which is collimated by electron arc applicator with the trapezoidal apertures, show the following features: the central axis percentage depth dose is not affected by the change of SSD or the aperture width. A trapezoidal aperture and its equivalent rectangular aperture have the same crossplane profiles and PDDs under the same conditions. The clinical significance of these features lies in that they provide information for oncologist and radiation therapist to do planning for electron arc treatment with a trapezoidal aperture, eg. the choice of energy and treatment depth for an individual patient.

2. The EarcMU program developed in Chapter 2 provides a convenient platform to calculate the number of MUs to deliver the prescribed dose to the reference point in the central plane of treatment volume. The algorithm used in the program was based on the crossplane profiles and PDDs of the static electron beam, which was measured at depth of dose maximum using a flat water phantom. The verification of the EarcMU program showed that uncertainty of monitor unit calculation is less than 2.1%. This is good enough for clinical use.

3. To reduce the non-uniformity of dose distribution due to the variation of patient contour from superior to inferior, the method proposed in Chapter 4 can be used to customize the trapezoidal aperture for the patient in electron arc treatment. The method was verified using the conical phantoms under the various clinically related geometries. The results showed that the uniformity of dose distribution from superior to inferior has been greatly improved with a trapezoidal aperture. Overall, the mean flatness index of dose distribution from superior to inferior drops dramatically from 8% for the open aperture to 0.58% for the trapezoidal apertures.

Based on the work of the thesis, there are several interesting topics that are worth to be further explored. Two of them are listed here:

1. Instead of using a trapezoidal aperture, the better option is to use an aperture determined exactly following the variation of radius of chest wall from superior to inferior. This aperture is supposed to be an irregular polygonal shape. In principle, the shape of this aperture can be determined using the method developed in Chapter 4. This needs a further investigation.

2. Based on the CT images of a patient, a cone could be found that best fits the chest wall contour. This work could be done by extracting the contour information from the digital image communication in medicine(DICOM) file of a patient. Then a conical shape can be obtained using least-square fitting algorithm.

Bibliography

[1] *A protocol for the determination of absorbed dose from high-energy photon and electron beams, AAPM TG-21*, *Med. Phys.*, **10**, 741, 1983.

[2] *Code of safe practice for the use of irradiation apparatus in medical therapy(NRLC12), National radiation laboratory(NRL)*, Ministry of Health in New Zealand, 1992.

[3] *Absorbed dose determination in external beam radiotherapy: an international code of practice for dosimetry based on standards of absorbed dose to water*, Technical report, Technical report series No.277, International atomic energy agency(IAEA), Vienna, 1997.

[4] *The use of plane parallel ionization chambers in high energy electron and photon beams: An international code of practice for dosimetry*, Technical report, Technical report series No.381, International atomic energy agency(IAEA), Vienna, 1997.

[5] *Absorbed dose determination in external beam radiotherapy: an international code of practice for dosimetry based on standards of absorbed dose to water,Technical report series No.389*, Technical report, Technical report series No.389, International atomic energy agency(IAEA),Vienna, 2000.

[6] P. R. Almond, F. H. Attix, S. Goetsch, L. J. Humphries, H. Kubo, R. Nath and D.W.O. Roger, *The calibration and use of plane-parallel ionization chambers for dosimetry of electron beams: An extension of the 1983 AAPM protocol, Report of AAPM Radiation Therapy Committee Task39*, *Med. Phys.*, **21**, 1251, 1994.

[7] P. R. Almond, P. J. Biggs, B. M. Coursey and et.al., *A protocol for the determination of absorbed dose from high-energy photon and electron beams*, *Med. Phys.*, **26**, 1847, 1999.

[8] C. D. Angelis, A. Mattacchioni, S. Onori, D. Aragno, U.D. Paula and V. Panichelli, *Electron arc therapy treatment planning verification with alanine-EPR dosimetry*, *Applied Radiation and isotopes.*, **52**, 1203, 2000.

[9] J. A. Antolak, E. Khatib and J. W. Scrimger, *Verification of a two-dimentional pencil beam arc electron dose calculation algorithm*, *Med. Phys.*, **20**, 1735, 1993.

[10] J. Becker and G. Weitzel, *Neue formen der Bewegungstrahlung beim 15 Mev-betatron der Siemens-Reinger-Werke.*, *Strahlentherapie*, **101**, 180, 1956.

[11] G. R. Benedetti, H. Dobry and L. Taumann, *Computer programe for determination of isodose curves for electron energies from 5 to 42Mev*, *Electromdica*, **39**, 57, 1971.

[12] B. E. Blackburn, *A practical system for electron Arc therapy*, in *Proceeding of the symposium on electron dosimetry and arc therapy*, 249, Madison, USA, September 1981, American institute of physics.

[13] R. A. Boyd, K. R. Hogstrom and G. Starkschall, *Effect of electron pencil-beam redefinition algorithm dose calculation in the presence of heterogeneities.*, *Med. Phys.*, **28**, 2096, 2001.

[14] A. L. Boyer and G. D. Fullerton, *An electron beam pseudoarc technique*, in *Proceeding of the symposium on electron dosimetry and arc therapy*, 249, Madison, USA, September 1981, American institute of physics.

[15] A. L. Boyer, G. D. Fullerton and J.G. Mira, *An electron beam pseudoarc technique for irradiation of large areas of chest wall and other curved surfaces*, *Int. J. Radiation Oncology Biol. Phys.*, **8**, 1969, 1974.

[16] P. C. Chi, K. R. Hogstrom, G. Starkschall, J. A. Antolak and R. A. Boyd, *Modelling skin collimation using the electron pencil beam redefiniation algorithm*, *Med. Phys.*, **32**, 3409, 2005.

[17] P.M. Chi, K.R Hogstrom, R.A Starkschall, G.and Boyd, S.L. Tucker and J.A. Antolak, *Application of the electron pencil beam redefinition algorithm to electron arc therapy*, *Med.phys.*, **33**, 2369, 2006.

[18] B. Cho, S. Kang and H. Park, *Application of Monte Carlo planning system for electron arc therapy*, Private communication, 2006.

[19] Keith Croft and Tim O'Brien, *Physics IMRT Quality assurance procedure*, Oncology department document, technical document at Palmerston North Hospital, 2005.

[20] S. Devic, J. Seuntjens, W. Abdel-Rahman, M. Evans, M. Olivares and E. B. Podgorsak, *Accurate skin dose measurement using radiochromic film in clinical applications*, *Med. Phys.*, **33**, 1116, 2006.

[21] D. Duchesne, M. Mondat and W. Wierzbicki, *Analytical model for electron arc beam output determination using an Elekta SL-25 linear accelerator*, *Med. Phys.*, **33**, 2665, 2006.

[22] D. Duchesne, M. Mondat and W. Wierzbicki, *Electron arc therapy with an Elekta SL-25 10Mev beam using a dedicated short applicator*, *Med. Phys.*, **33**, 2096, 2006.

[23] J. V. Dyk, R. B. Barnett, J. E. Gygler and P. C. Shragge, *Commissionning and quality assurance of treatment planning computers*, *Int. J. Radiation Oncology Biol. Phys.*, **26**, 261, 1993.

[24] M. A. Ebert and P. W. Hoban, *A monte carlo investigation of electron-beam applicator scatter*, *Med. Phys.*, **22**, 1431, 1995.

[25] B. Fisher, C. Redmond and E. Fisher, *The contribution of recent NSABP clinical trials of primary breast cancer therapy to an understanding of biology: an overview of findings*, *Cancer*, **46**, 1009, 1980.

[26] New Zealand Breast Cancer Foundation, *New Zealand breast cancer facts [online]*, Available from: Website: http://www.nzbcf.org.nz [accessed in 08/2007].

[27] B. Fowble, J. Glick and R. Goodman, *Radiotherapy for the prevention of local-regional recurrence in high risk patients postmastectomy receiving adjuvant chemotherapy*, *Int. J. Radiat. Oncol. Biol. Phys.*, **15**, 627, 1988.

[28] D. K. Gaffney, C.M. Lee and D.D. Leavitt, *Electron arc irradiation of the postmastectomy chest wall in locally recurrent and metastatic breast cancer*, *American Journal of Clinical Oncology*, **26**, 241, 2003.

[29] T. Hehr, W. Budach and M. Bamberg, *Postmastectomy electron-beam rotation irradiation in locally advanced breast cancer*, *Strahlentherapie und Onkologie*, **178**, 624, 2004.

[30] K. R. Hogstom and P. R. Almond, *Review of electron beam therapy physics*, *Phys. Med. Biol.*, **51**, R455, 2006.

[31] K. Hogstrom, R., R. Boyd, A., J. Antolak and A., *Dosimetry of a prototype retractable eMLC for fixed-beam electron therapy*, *Med. Phys.*, **31**, 443, 2004.

[32] K.R. Hogstrom, R.G. Kurup, A.S. Shiu and G. Starkschall, *A two-dimentional pencil-beam algorithm for calculation of arc electron dose distributions*, *Phys. Med. Biol.*, **34**, 315, 1989.

[33] K.R. Hogstrom, M.D Mills and P.R. Almond, *Electron beam dose calculations*, *Phys. Med. Biol.*, **26**, 445, 1981.

[34] ICRU62, *Prescribing, recording, and reporting photon beam therapy(supplement to ICRU report 50*, *The Journal of ICRU*, **1**, 1999.

[35] ICRU74, *Prescribing, recording, and reporting electron beam therapy*, *The Journal of ICRU*, **4(1)**, 2004.

[36] E. Karaj, S. Righi and F. D. Martino, *Absolute dose measurements by means of a small cylindrical ionization chamber for very high dose per pulse energy electron beams*, *Med. Phys.*, **34**, 952, 2007.

[37] K. R. Kase and B. E. Bjarngard, *Bremsstrahlung dose to patients in rotational electron therapy*, *Radiology*, **133**, 531, 1979.

[38] Croft Keith, *Contour considerations when planning an electron arc*, Oncology department document, technical document at Palmerston North Hospital, 2004.

[39] Croft Keith, *Determination of MUs for arc electron treatment*, Oncology department document, technical document at Palmerston North Hospital, 2004.

[40] Croft Keith, *Electron arc commissioning and verification*, Oncology department document, technical document at Palmerston North Hospital, 2004.

[41] Croft Keith, *Electron arc protocol*, Oncology department document, technical document at Palmerston North Hospital, 2004.

[42] Croft Keith, *Manufacture of electron arc tertiary shield*, Oncology department document, technical document at Palmerston North Hospital, 2004.

[43] Croft Keith, *Linac beam calibration QA*, Oncology department document, technical document at Palmerston North Hospital, 2005.

[44] F. M. Khan, *Calibration and treatment planning of electron beam arc therapy*, in *Proceeding of the symposium on electron dosimetry and arc therapy*, 249, Madison, USA, September 1981, American institute of physics.

[45] F. M. Khan, F. C. Deibel and A. S. Meigooni, *Obliquity correction for electron beams*, *Med.Phys.*, **12**, 749, 1985.

[46] F. M. Khan, K. P. Doppke, K. R. Hogstrom, R. Nath, S. C. Prasad, J. A. Purdy, M. Rozenfeld and B. L. Werner, *Clinical electron dosimetry: Report of AAPM radiation therapy committee Task group 25*, *Med. Phys.*, **10**, 741, 1983.

[47] F. M. Khan, G. D. Fullerton, J. M. Lee, V. C. Moore and S. H. s Levitt, *Physical aspects of electron-beam arc therapy*, *Radiology*, **124**, 497, 1977.

[48] F.M. Khan, *The physics of radiotherapy*, Lippincott Williams & Wilktins, 2003.

[49] E.E Khatib, J. Antolak and J. Scrimger, *Radiation dose distributions for electron arc therapy using electron of 6-20 Mev*, *Phys. Med. Biol.*, **37**, 1375, 1992.

[50] S. C. Klevenhagen, *Physics and dosimetry of therapy electron beams*, Medical Physics, Madison,WI, 1993.

[51] R.G. Kurup, K.R. Hogstrom, V.A. Otte, S. Tung and A.S. Chiu, *Dosimetric evaluation of a two-demensional, arc electron, pencil-beam algorithm in water and PMMA*, *Phys. Med. Biol.*, **37**, 127, 1992.

[52] K. S. Lam, W. C. Lam, M. J. O'neill and E. Zinreich, *Electron arc therapy: Beam data requirements and treatment planning*, *Clinical Radiology*, **38**, 379, 1987.

[53] D. D. Leavitt, *Electron arc therapy planning, dosimetric measurements, optimization and graphic display*, in *Proceeding of the symposium on electron dosimetry and arc therapy*, 249, Madison, USA, September 1981, American institute of physics.

[54] D. D. Leavitt, L. Earley and J. R. Stewart, *Design and production of customized field shaping devices for electron arc therapy*, *Med. Dosim.*, **15**, 25, 1990.

[55] D. D. Leavitt, D. K. Gaffney, G. A. Watson and R. Levine, *Monte-carlo dose calculation of multi-energy dynamic electron arc therapy using a standard photon multileaf collimator*, *Int. J. Radiat. Oncol. Biol. Phys.*, **57**, S210, 2003.

[56] D. D. Leavitt, D. K. Gaffney, G. A. Watson and R. Levine, *Monte Carlo dose calculation of multiple-energy dynamic electron arc therapy using a standard photon multileaf collimator*, *Int. J. Radiation Oncology Biol. Phys.*, **57**, S210, 2003.

[57] D. D. Leavitt, J. R. Steward, J. H. Moeller and L. Earley, *Optimization of electron arc therapy dose by multi-vane collimator control*, *Int. J. Radiat. Oncol. Bio. Phys.*, **16**, 489, 1989.

[58] D. D. Leavitt, J. R. Steward, J. H. Moeller, W. H. Lee and G. A. Takach, *Electron arc therapy: Design, implementation and evaluation of a dynamical multi-vane collimator system*, *Int. J. Radiat. Oncol. Bio. Phys.*, **17**, 1089, 1989.

[59] D.D. Leavitt, M.P. Peacock, F.A. Gibbbs and J.R. Stewart, *Electron arc therapy: physical measurment and treatment planning techniques*, *Int. J. Radiation Oncology Biol. Phys.*, **11**, 987, 1985.

[60] M. C. Lee, S. B. Jiang and C. M. Ma, *Monte Carlo and experimental investigation of multileaf collimated electron beams for modulated electron radiation therapy*, *Med. Phys.*, **27**, 2708, 2000.

[61] D. A. Low, P. Parikh, J. F. Dempsey, S. Wahab and S. Huq, *Ionization chamber volume averaging effect in dynamic intensity modulated radiation therapy beams*, *Med. Phys.*, **30**, 1706, 2003.

[62] C-M. Ma, T. Pawlicki, M. C. Lee, S. B. Jiang, J. Deng, B. Yi, E Mok and A.L Boyer, *Energy- and intensity-modulated electron beams for radiotherapy*, *Phys. Med. Biol.*, **45**, 2293, 2000.

[63] M. Ma, C. adn Ding, J. S. Li, M. C. Lee and J. Deng, *A comparative dosimetric study on tangential photon beams, intensity-modulated radiation(IMRT) and modulated electron radiotherapy(MERT) for breast cancer treatment*, *Phys. Med. Biol.*, **48**, 909, 2003.

[64] E. Mah, J. Antolak, J. W. Scrimger and J. J. Battista, *Experimental evaluation of a 2D and 3D electron pencil beam algorithm*, *Phys. Med. Biol.*, **34**, 1179, 1989.

[65] L. O. Mattsson, K. A. Johansson and H. Svensson, *Acta Radiol.Oncol.*, **20**, 385, 1981.

[66] L. K. Mcneely, G. M. Jacobson, D. D. Leavitt and J. R. Stewart, *Electron arc therapy: chest wall irradiation of brest cancer patients*, *Int. J. Radiat. Oncol. Bio. Phys.*, **14**, 1287, 1988.

[67] L. K. Mcneely, D. D. Leavitt, M. J. Egger and J.R. Stewart, *Dose-volume histogram analysis of lung radiation from chest wall treatment: comparison of elelctron arc and tangential photon beam techniques*, *Int. J. Radiat. Oncol. Biol. Phys.*, **21**, 515, 1991.

[68] J. Milan and R. E. Bentley, *The storage and manipulation of radiation dose data ina small digital computer*, *British Journal of Radiology*, **47**, 115, 1974.

[69] A. Niroomand-Rad, B. M. Blackwell, K. P. Gall, J. M. Galvin, W. L. McLaughlin, A. S. Meigooni, R. Nath, J. E. Rodger and C.G. Soares, *Radiochromic film dosimetry: Recommendations of AAPM radiation therapy committee Task Group 55*, *Med. Phys.*, **25**, 2093, 1998.

[70] Python organization, *Python programming language guideline [Online]*, Available from: www.python.org [accessed in 08/2007].

[71] P. M. Ostwald, *Variation in calculated effective source-surface distances with depth*, *Phys. Med. Biol.*, **41**, 2067, 1996.

[72] P. M. Ostwald and T. Kron, *Surface dose measurements for highly oblique electron beams*, *Med.Phys.*, **23**, 1413, 1996.

[73] S. Pai, I. J. Das, K. L. Lam, T. J. Losasso, A. J. Olch and D. Wilcox E. E. Palta, J. R. Ritt, *TG-69: Radiographic film for megavoltage beam dosimetry*, *Med. Phys.*, **34**, 2007, 2007.

[74] B. Paliwal, *Proceedings of the symposium on electron dosimetry and arc therapy*, American Institute of Physics, 1981.

[75] L. M. Peacock, *Electron arc therapy planning, dosimetric measurements, optimization and graphic display*, in *Proceeding of the symposium on electron dosimetry and arc therapy*, 249, Madison, USA, September 1981, American institute of physics.

[76] L. M. Peacock, D. D. Leavitt, F. A. Gibbs and J. R. Stewart, *Electron arc therapy: clinical experience with chest wall irradiation*, *Int. J. Radiation Oncology Biol. Phys.*, **10**, 2149, 1984.

[77] M. Pla, C. Pla and E. B. Podgorsak, *The influence of beam parameters on percentage depth dose in electron arc therapy*, *Med. Phys.*, **15**, 49, 1988.

[78] M. Pla, E. B. Podgorsak, E. B. Podgorsak, C. Pla, C. R. Freeman and J. Souhami, L. Guerra, *Physcial aspects of the angle-β concept in electron arc therapy*, *Int. J. Radiation Oncology Biol. Phys.*, **20**, 1331, 1991.

[79] M. Pla, E.B. Podgorsak, C. Plat and C. R. Freeman, *Determination of secondary collimator shape in electron arc therapy*, *Phys. Med. Biol.*, **38**, 999, 1993.

[80] M. Pla, E. B. Poggorsak and C. Pla, *Electron dose rate and photon contamination in electron arc theapy*, *Med. Phys.*, **16**, 692, 1989.

[81] M. O. Pla, E. B. Podgorsak and C. Pla, *Electron arc dose distribution as a function of beam energy*, *Med. Phys.*, **24**, 127, 1997.

[82] J. Rassow, *On the telecentric small-angle pendulum therapy with high electron energies.*, *Electromedica(Siemens)*, **40**, 1, 1972.

[83] G. Rikner, *Semiconductor detector theory*, *Med. Phys.*, **13**, 608, 1986.

[84] G. Rikner and E. Grusell, *General specifications for silicon semiconductors for use in radiation dosimetry*, *Phys. Med. Biol.*, **32**, 1109, 1987.

[85] D. M. Roback, F. M. Khan, J. P. Gibbons and A. Sethi, *Effective SSD for electron beams as a function of energy and beam collimation*, *Med.Phys.*, **22**, 2093, 1995.

[86] D. R. Ruegsegger, S. D. Lerude and D. Lyle, *Electron beam arc therapy using a high energy betatron.*, *Radiology*, **133**, 483, 1979.

[87] D. R. Ruegsegger and D. Lyle, *Electron arc therapy using a high energy betatron*, in *Proceeding of the symposium on electron dosimetry and arc therapy*, 249, Madison, USA, September 1981, American institute of physics.

[88] R. M. Runkel and S. H. Cho, *Evaluation of a commercial three dimensional electron pencil beam algorithm*, *Med. Phys.*, **24**, 91, 1996.

[89] G. A. Sandison, E. Papies, C. Bloch and J. Morphis, *Phantom assessment of lung dose from proton arc therapy*, *Int. J. Radiation Oncology Biol. Phys.*, **38**, 891, 1997.

[90] Scanditronix Wellhofer, *CC13 ionization chamber user's guide*, 2001.

[91] Scanditronix Wellhoffer, *Dose 1 therapy dosimeter users guide*, 2001.

[92] A. S. Shiu and K. R. Hogstrom, *Pencil-beam redefinition algorithm for electron dose distribution*, *Med. Phys.*, **18**, 7, 1991.

[93] Siemens, *Primus linear accelerator specification(online)*, Available from: http://www.sofimednl.org.mx/Archivos/PRIMUSSPEC.pdf [accessed in 08/2007].

[94] M. R. Sontag, *Performance and beam characteristics of the Siemens Primus linear accerator*, *Med.Phys.*, **26**, 734, 1999.

[95] M. Soubra and J. Cygler, *Evaluation of a dual bias dual metal oxide-silicon semiconductor field effect transistor detector as radiation dosimeter*, *Med. Phys.*, **21**, 567, 1994.

[96] R. Stanton and D. Stinson, *Applied physics for radiation oncology*, Medical physics publishing, 1996.

[97] G. Starkschall, R. E. Steadham and N. H. Wells, *On the need for monitor unit calculations as part of a beam commissioning methodology for a radiation treatment planning system*, *Journal of applied clinical medical physics*, **1**, 86, 2000.

[98] John Sutcliffe, Tim O'Brien and Keith Croft, *An empirical model for megavoltage x-ray output factors*, *Phys. Med. Biol.*, **45**, 897, 2000.

[99] N. Tapley, *Clincal application of electron beam*, John Wiley and Sons, New York, 1976.

[100] B. Thomadsen, *Tertiary collimation of moving electron beams*, in *Proceeding of the symposium on electron dosimetry and arc therapy*, 249, Madison, USA, September 1981, American institute of physics.

[101] Thomson & Nielson, Ottawa,Canada, *MOSFET 20 and TABULA^{TM} dose report software operator's manuals*, 2005.

[102] M. Tobler and D. D. Leavitt, *Dosimetry and treatment planning of complex electron arc therapy*, *Med. Dosim.*, **20**, 229, 1995.

[103] J. S. Tsai, M. J. Rivard, M. J. Engler, J. E. Mignano and D. E. Wazer, *Determination of the 4mm Gamma knife helmet relative output factor using a variety of detectors*, *Med. Phys.*, **30**, 986, 2003.

[104] L. J. Van Battum and H. Huizenga, *Film dosimetry of clinical electron beams*, *Int. J. Radiation Oncology Biol. Phys.*, **18**, 69, 1990.

[105] J. A. Williams and S. K. Agarwal, *Energy-dependence polarity correction factors for four commercial ionization chambers used in electron dosimetry*, *Med. Phys.*, **24**, 785, 1997.

[106] C. U. Yee, E. S. Katharina and B. Christine, *The influence of patient geometry on selection of chest wall irradiation techniques in post-mastectomy breast cancer patients*, *Radiotherapy and Oncology*, **57**, 69, 2000.

Appendix A

IMRT Checker: a powerful tool for film dosimetry

IMRT quality assurance requires point dose and film measurement in a phantom. A patient plan is generated on the planning system that is then put onto the IMRTPhantom, doses are calculated and compared to measurements using the film and chamber taken later on the linac.

To analyze the film, an in-house program named "IMRT Checker" was designed and developed by Keith Croft, the chief physicist of department. Fig A.1. shows its graphic user interface. The programs main window is arranged as a series of Tabs. The program has been written to compare two images, these images could be two films, or a Film and a QA file from XiO. It provide a variety of powerful tools to analyze the film. How to use the IMRT Checker is briefly described here with the emphasis on the function of profile analysis. For the description of other functions in details, readers are referred to the reference[19].

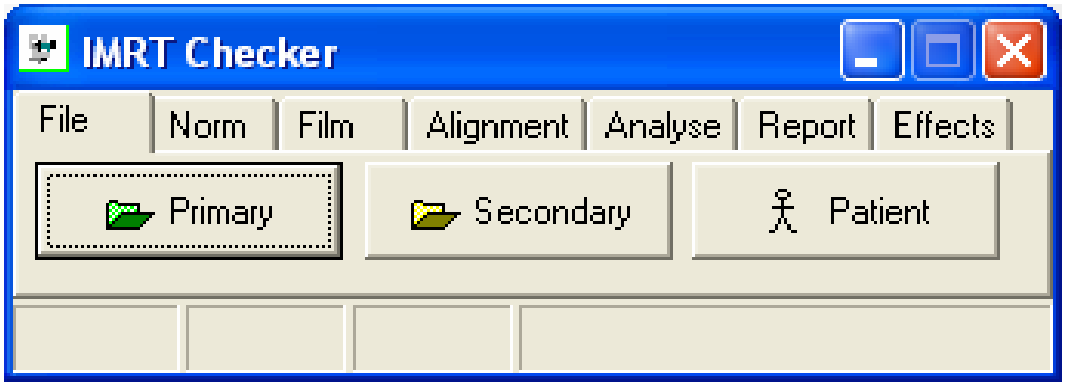

Figure A.1: The main user interface of IMRT checker

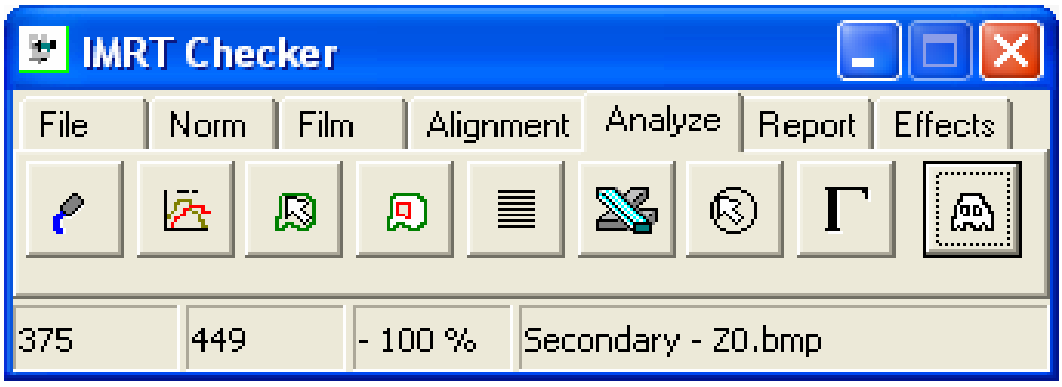

Figure A.2: The functions provided by Analyze Tab for film dosimetry.

File Tab

Primary and Secondary buttons do much the same thing - they pop a window open asking for you to select the file you want to open. This will be either the bitmap (*.bmp) from the film or the text (*.txt) file of the XiO dose plane.

Analyze Tab

Once the Analyze Tab is clicked, there are several buttons appearing, as shown in Fig.A.2. Starting from the left the buttons are 1. Probe spot measurements. 2. Profile charting 3. Isodose on image 4. Isodose on separate chart 5. Multi-profile tool (MLC) 6. Excel Charting tool 7. Spot measurement tool 8. Gamma function test. 9. Ghost - this allows some tools to be applied to both windows simultaneously. Only button 2 and 6 are introduced as follows:

Profile Chart

Move the mouse over the image, and press the left mouse button down mark the start of the profile - drag the mouse with button down to where you want the profile to end. This will generate a chart with the profile drawn, the x-axis will be in mm, starting at zero at the point you first started the profile. This procedure is illustrated in Fig.A.3. If the Ghost button is down, then on the “other” image a ghost mouse, will travel around based on the assigned centre of the image, and when a profile on one chart is selected, then the corresponding profile will be

performed on the "other" image as well. Without Ghost selected - then only the selected profile will be generated.

When the Chart window is activated, then it will plot onto the images concerned a line showing where the profile was taken, clicking on the chart will leave up to two marks on the chart so that measurements can be performed. These are shown as little circles on the line itself. (Also on the image below you can see the ghost mouse that mimics the motion of the standard mouse over the image.) The status bar at the bottom of the chart window displays information about where the cursors are, and separation of them. Once you put to fixed cursors on the image, a third click will remove them.

This chart can be examined in detail by using the left mouse button to drag a box over the section of profile your interested in to zoom in on that section of the chart (dragging from left to bottom right will zoom in, dragging in the opposite direction will restore the chart to normal). Dragging with the right mouse button drags the chart around within the current scaling assigned to the chart window.

Right clicking, without moving the mouse twice, will make a popup menu appear - from this menu you can export the data to a comma separated file (import as Excel .CSV file), or copy the chart to the clipboard to paste into a document, along with a few other options.

Clicking on a profile in the chart will cause the profile to be plotted in a thick line, showing that that line is then selected. You can also select the profile by using the up and down mouse buttons to move from one profile to another. If no profile is selected, then this will also select one of them. Once selected a profile can be copied and pasted using Control+C and Control+V from one chart into another. If you wish to have the profile repeated, then the right mouse menu option repeat will make the profile be recaptured. Pressing delete with a selected profile will delete it. Pressing the left and right cursor keys will move the profile to the left or right by 1mm (shift+arrow key will move the profile by 10mm)

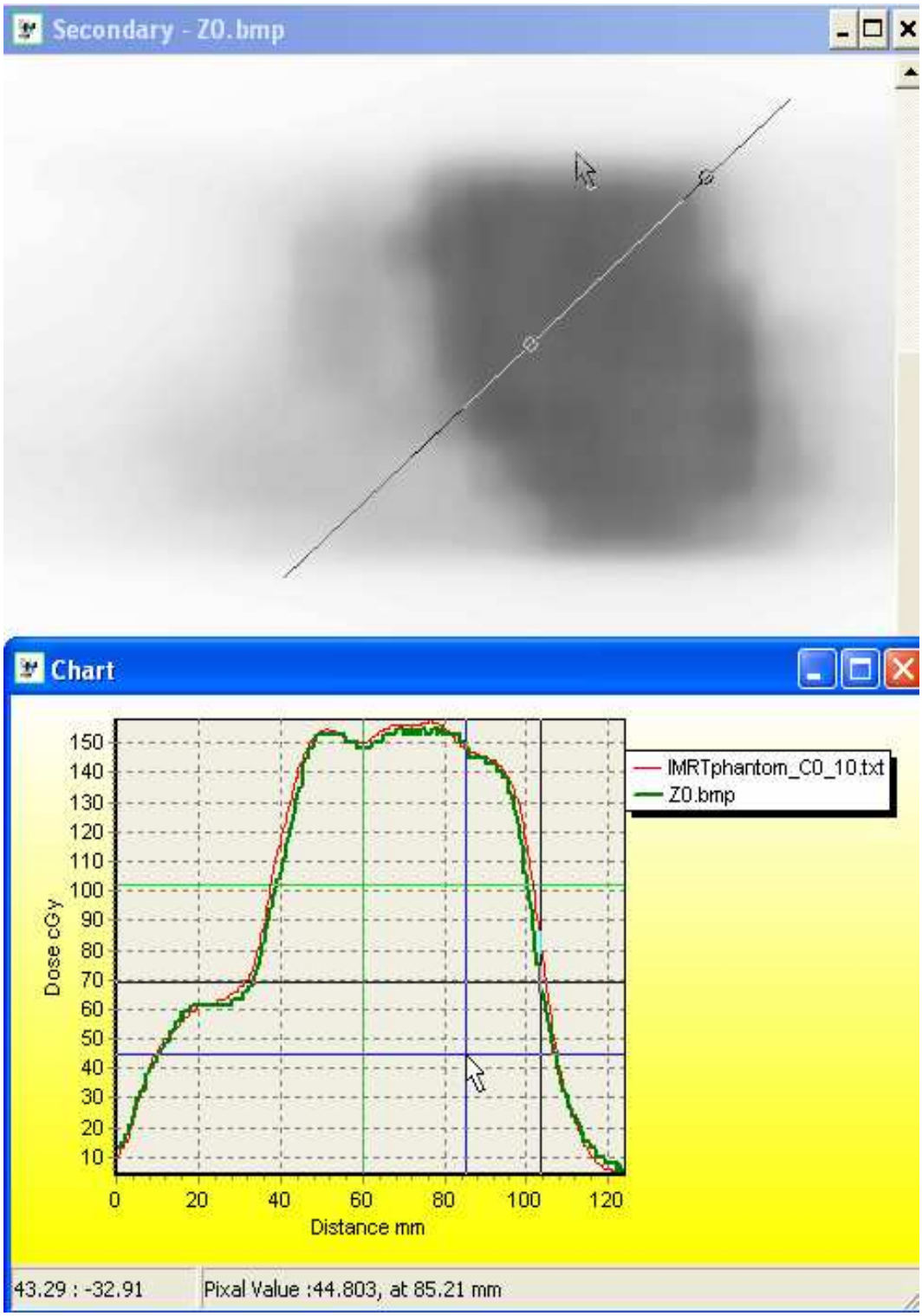

Figure A.3: The upper figure shows an opened film image on which a line was drawn, whereas the lower figure displays the profile along this line in an activated chart window.